AN ABSTRACT OF THE THESIS OF

Austin Dane Wissler for the degree of Master of Science in Water Resources Engineering presented on July 28, 2021.

Title: Assessing the Thermal Sensitivity and Stormflow Response of Headwater Stream Temperatures: A Seasonal and Event-scale Exploration in Northern California, USA.

Abstract approved: _____

Kevin D. Bladon Catalina Segura

Mountainous headwater streams make up ~80 % of stream length globally and are strongly connected with catchment hillslopes and riparian areas, which can influence water quantity, quality, and availability for downstream uses. Accordingly, effective management of headwater streams and riparian zones to maintain desired ecosystem services downstream is critical, particularly in the face of warming climates. Often, a central focus is the protection of stream temperature, which is a critical water quality parameter that influences thermally sensitive species such as salmonid fishes. However, headwater stream temperatures vary depending on characteristics of the stream, catchment, and region. For instance, watershed lithology may control the thermal properties of streamflow during summer baseflow conditions. In addition, there have been few attempts to assess what meteorological or topographic factors control stream temperature change during storm events in forested watersheds and how this response changes seasonally. The goal of this thesis was to improve our understanding of headwater streams by using distributed stream and air temperature monitoring to assess regional differences in summer longitudinal stream temperatures and to determine the factors that influence stream temperature change during storm events in Northern California.

In chapter 2, I collected stream and air temperature data along eight headwater streams in two regions (three in the Cascade Range and five in the Coast Range of Northern California) with distinct lithology, climate, and riparian vegetation. My

objectives were to compare stream thermal regimes and thermal sensitivity—slope of the linear regression relationship between daily stream and air temperature—within and between streams in both study regions. Mean daily stream temperatures were ~4.7 °C warmer in the Coast Range but were less variable (SD = 0.7 °C) compared to the Cascade Range (SD = 2.3 °C). Median thermal sensitivity was 0.33 °C $°C^{-1}$ in the Coast Range and 0.23 °C $°C^{-1}$ in the Cascade Range. I posit that the volcanic lithology underlying the Cascade streams likely supported discrete groundwater discharge locations, which dampened thermal sensitivity. At locations of apparent groundwater discharge in these streams, median stream temperatures rapidly decreased by 2.0 °C, 3.6 °C, and 7.0 °C relative to adjacent locations, approximately 70–90 meters upstream. In contrast, thin friable soils in the Coast Range likely contributed baseflow from shallow subsurface sources, which was more sensitive to air temperature fluctuations and generally warmed downstream (up to 2.1 °C km^{-1}). Overall, my study revealed distinct longitudinal thermal regimes in streams draining contrasting lithology, suggesting that streams in these different regions may respond differentially to forest disturbances or climate change.

In chapter 3, my objective was to use hysteresis metrics to assess the relationship between stream temperature and stormflow across ten forested headwater catchments in the Northern California Coast Range during the 2020 water year. I quantified the magnitude and variability of stream temperature hysteresis during rain events and determined whether catchment topographic metrics could explain the stream temperature response to precipitation inputs. I hypothesized that the direction of hysteresis would vary across seasons due to changes in meteorological conditions and that the stream locations most hydrologically connected to the hillslope (as predicted by topographic indices) would exhibit the greatest hysteresis due to lateral throughflow inputs. My results indicate that the stream temperature response to stormflow is seasonally variable and generally exhibits clockwise hysteresis during the summer and spring when air temperatures are warmer than stream temperatures and anti-clockwise hysteresis during the fall and winter when air temperatures are cooler than stream temperatures. In addition, the stream temperature response to stormflow was the most variable across these 10 catchments during the late summer and early fall (SD = 0.18 and 0.10,

respectively), when catchment-scale wetness conditions and streamflow were low. As the wet season progressed, stream temperature behavior across these 10 catchments became more similar, and remained coupled through the late spring (SD = 0.04). The magnitude and direction of stream temperature hysteresis was well correlated with the gradient between stream and air temperatures at the start of the event (ρ = 0.49), and air temperature change during the storm hydrograph rising limb (ρ = -0.49), indicating the potential role of regional meteorological conditions on stream temperature change. Contrary to my expectations, none of the derived topographic metrics describing the preponderance of saturated areas and lateral inputs to streamflow were correlated with stream temperature change during events, potentially because subsurface topography and seasonally variable catchment wetness conditions could not be properly characterized with static metrics describing surface topography. Overall, these results indicate seasonally variable stream temperature behavior during storm events that become regionally synchronous as catchment moisture conditions increase during the wet season. Collectively, these results indicate that headwater stream thermal regimes are spatiotemporally variable across regions and in response to precipitation inputs, and riparian management should reflect this variable behavior. Using these results to inform headwater stream management can potentially be accomplished by developing regionally-specific riparian buffers that provide additional protection at locations most sensitive to atmospheric energy exchange or along areas with discrete groundwater discharge.

Assessing the Thermal Sensitivity and Stormflow Response of Headwater Stream Temperatures: A Seasonal and Event-scale Exploration in Northern California, USA.

by
Austin Dane Wissler

A THESIS

submitted to

Oregon State University

in partial fulfillment of
the requirements for the
degree of

Master of Science

Presented July 28, 2021
Commencement June 2022

Master of Science thesis of Austin Dane Wissler presented on July 28, 2021

APPROVED:

Co-Major Professor, representing Water Resources Engineering

Co-Major Professor, representing Water Resources Engineering

Director of the Water Resources Graduate Program

Dean of the Graduate School

I understand that my thesis will become part of the permanent collection of Oregon State University libraries. My signature below authorizes release of my thesis to any reader upon request.

Austin Dane Wissler, Author

ACKNOWLEDGEMENTS

First, I would like to sincerely thank both Catalina Segura and Kevin Bladon for advising me over the last two years. I have learned many valuable lessons about conducting sound research and about what it means to generate meaningful research questions from both of you. I will always appreciate your fascination for science and constant positive reinforcement. Thank you to Jason Dunham and Ann Trehu for agreeing to serve on my graduate committee. In addition, thank you to Pat Righter, Matt House, Matt Kluber, and Matt Mannizzi from Green Diamond Resource Company that went above and beyond to help offload data, assist with site selection, and provide constant in-field support. A special thank you for helping us navigate the COVID-19 pandemic to ensure research could continue in a safe and effective manner. In addition, thank you to Drew Coe and Elizabeth Keppeler for assistance with development of research ideas for the Caspar/LaTour study that make up chapter 2 of this thesis. Also, thank you to Wenlong Liu for his help developing R code for chapter 3 of this thesis.

Thank you to Katie Wampler, Sam Zamudio, Ryan Cole, Maddie Maffia, Elle Luedloff, and Clara Eshaghpour for their help in the field. This research would have been much less fun without interactions and laughs with each of you. A special and profound thank you goes to Jonah Nicholas, for his constant help in the field, dealing with my aggressive field schedules that forced us to endure many 10+ hour days, and for always being someone to bounce ideas off of. Also, thank you to all of the friends and future colleagues I've made during my time at OSU, those in the Water Resources Program and elsewhere. Specifically, thank you to Stefan Rose, Elise Mazur, Leah Cromer, and Keaton Schrank for being great friends. A special shout out to those of us who met during GEOG 595, those are some of my most fond memories at OSU. Thank you to my parents, Steve and Deborah Wissler, for being my own personal cheerleading squad. Finally, thank you to my fiancé and soon-to-be wife, Corinne Wagner, for constantly supporting me and assuring me that I could, indeed, finish this thesis. You motivate me to be the best (happiest) version of myself and I will love you always.

TABLE OF CONTENTS

LIST OF FIGURES

Figure Page

LIST OF FIGURES (Continued)

Figure Page

LIST OF TABLES

Table Page

LIST OF APPENDIX FIGURES

Figure Page

LIST OF APPENDIX FIGURES (Continued)

Figure Page

LIST OF APPENDIX FIGURES (Continued)

Figure Page

LIST OF APPENDIX FIGURES (Continued)

Figure Page

LIST OF APPENDIX TABLES

Table Page

Chapter 1: Introduction

Mountainous headwater streams are ubiquitous hydrologic systems that define the uppermost drainages of a watershed. These generally small channels are estimated to drain 70–80 % of catchment area (MacDonald & Coe, 2007; Sidle et al., 2000) and make up about 80 % of total stream length globally (Gomi, Sidle, & Richardon, 2002; Shreve, 1969). Headwater streams are also often strongly connected with the catchments hillslopes and riparian areas (Freeman, Pringle, & Jackson, 2007; Schlosser, 1991), which can influence their sensitivity to fluxes of energy, nutrients, and sediment (Coats & Jackson, 2020; Kiffney, Richardson, & Bull, 2003; Leach, Olson, Anderson, & Eskelson, 2016). As such, headwater streams can have substantial influence on the water quantity, quality, and availability for downstream uses (Bernhardt et al., 2018; MacDonald & Coe, 2007; Olson, Anderson, Frissell, Welsh, & Bradford, 2007; Richardson, 2019; Vannote, Minshall, Cummins, Sedell, & Cushing, 1980). In addition, headwater streams provide vital aquatic and terrestrial habitat for environmentally sensitive species (Brewitt, Danner, & Moore, 2017; Hester & Doyle, 2011; Johnson, Haas, & Fritz, 2010; Olson et al., 2007), as they generally transport cool, highly oxygenated water (Isaak, Luce, Chandler, Horan, & Wollrab, 2018; Maheu, Poff, & St-Hilaire, 2016), provide humid and cool air temperatures (Brosofske, Chen, Naiman, & Franklin, 1997; Rykken, Chan, & Moldenke, 2007), and possess topographic and geomorphic diversity that offers niche habitat availability (Dugdale, Bergeron, & St-Hilaire, 2015; Olson et al., 2007; Steel, Beechie, Torgersen, & Fullerton, 2017).

Recent research indicates the potential for headwater-riparian corridors to act as climate refuges (Isaak et al., 2016; Krosby, Theobald, Norheim, & McRae, 2018; O'Briain, Shephard, & Coghlan, 2017) by providing stable terrestrial and aquatic habitat. Given the projected effects of climate change on summer low flows (Vander Vorste, Obedzinski, Nossaman Pierce, Carlson, & Grantham, 2020), stream and air temperatures (Arismendi, Safeeq, Johnson, Dunham, & Haggerty, 2013; Lisi, Schindler, Cline, Scheuerell, & Walsh, 2015), and habitat provision (MacDonald, Boon, Byrne, Robinson, & Rasmussen, 2014b) it is increasingly critical to improve our understanding of how

headwater streams function (Lowe & Likens, 2005) so they can be appropriately managed.

The exact definition of a headwater stream varies by jurisdiction and scope of inference, but for the purpose of this thesis, we have defined them as fishless mountainous streams that generally have active channel widths less than three meters (Richardson, 2019; Richardson & Danehy, 2007). This definition does not provide a context for the temporal or spatial extent of surface flow in the channel, which is commonly used to characterize different types of headwater channels (Fritz et al., 2020). Accordingly, headwater streams can perennially exhibit surface flow year-round, intermittently flow through the wet season and dry out seasonally, or ephemerally flow only in response to storm events and during the wettest portions of the year (MacDonald & Coe, 2007; Pate, Segura, & Bladon, 2020; van Meerveld et al., 2020).

Regardless of flow duration, headwater channels have historically received less protection than their larger, downstream, fish-bearing counterparts (Olson et al., 2007; Richardson, Naiman, & Bisson, 2012). This protection is commonly applied by limiting activities such as forest harvesting within a certain distance from the channel by implementing riparian buffers. These strips of retained vegetation along one or both sides of a stream are designed to moderate stream and air temperatures, recruit large wood, input organic matter, minimize erosion and mass sediment movement, and maintain cool and moist aquatic and terrestrial habitat (Richardson et al., 2012; Sweeney & Newbold, 2014). However, the historical lack of riparian protection along headwater channels is somewhat at odds with current research signifying the importance of headwaters on water quality and habitat in downstream fish-bearing streams (e.g., Ebersole, Wigington, Leibowitz, Comeleo, & Van Sickle, 2015; MacDonald & Coe, 2007; Wipfli, Richardson, & Naiman, 2007). For this reason, riparian buffer requirements for non-fish bearing headwater streams have become increasingly rigorous across the West of the US to protect downstream aquatic habitat (Groom, Madsen, Jones, & Giovanini, 2018; Kibler, Skaugset, Ganio, & Huso, 2013; Pollock, Beechie, Liermann, & Bigley, 2009; Reiter, Bilby, Beech, & Heffner, 2015), and they continue to change. In California, for example, federal listing of endangered anadromous fish has led to regulations that limit forest

harvesting within the riparian zone of non-fish bearing streams that are greater than 1.5 meters wide (CAL FIRE, 2020). Therefore, additional research is needed to further understand how we can best manage these critical aquatic resources and preserve water quality as regulations change.

One of the key water quality parameters influenced by riparian areas in forested headwater streams is stream temperature. This key physical water quality parameter drives dissolved oxygen solubility (Loperfido, Just, & Schnoor, 2009; Ozaki et al., 2003), nutrient transformations (Morin, Lamoureux, & Busnarda, 1999; Neres-Lima et al., 2017), in-stream primary productivity (Bernhardt et al., 2018), habitat provision (Brewitt et al., 2017), and important life history events for sensitive aquatic species such as salmonids (Caissie, 2006; Hester & Doyle, 2011; MacDonald et al., 2014b).

Stream temperature in headwater streams may be influenced by the rate and magnitude of energy exchange between the water column, atmosphere, and subsurface (Brown, 1969; Webb, Hannah, Moore, Brown, & Nobilis, 2008). The total energy flux to a stream is the sum of radiative, sensible and latent, advective, convective, and conductive heat exchange (Moore, Spittlehouse, & Story, 2005a). Shortwave radiation generally represents the largest and most dominant energy flux to the water surface that controls stream temperature change (Guenther, 2007; Hannah, Malcolm, Soulsby, & Youngson, 2008; Leach & Moore, 2010; MacDonald, Boon, & Byrne, 2014a; Moore et al., 2005a; Roon, Dunham, & Groom, 2021). Longwave radiation, or the thermal energy emitted by riparian vegetation, the atmosphere, and stream banks, commonly provides a relatively small portion of the incoming radiation at a stream surface (Klos & Link, 2018). Incident radiation can be absorbed or released by the water column and adds heat to the water surface during the day when the air is warmer than the stream. Alternatively, heat is generally lost from the stream during the night when air is cooler than the stream.

Sensible heat exchanges can represent heat gained or lost, either through turbulent exchange (heat gained) or convection (heat gained or lost depending on temperature gradient) with air above the stream. Latent heat exchange refers to heat lost from the stream through evaporative cooling or added to the stream via condensation of gaseous water onto the stream surface. The magnitude of sensible and latent heat exchange relies

on the temperature gradient between the stream and air above the stream, as well as wind speed. However, wind speeds along forested riparian corridors are typically low. Thus, the magnitude of sensible and latent heat exchange is typically less than 10 % of radiative energy inputs, and tend to cancel out during summer (Johnson, 2004; Leach & Moore, 2010).

Conductive and advective heat exchange includes groundwater inflow, lateral throughflow from adjacent hillslopes, hyporheic exchange, and bed heat conduction, and represent important heat exchange processes governing stream temperature change in headwaters during both summer and winter (Caissie, 2006; Leach & Moore, 2015). Heat exchange between the water column and the stream bed is driven by the temperature gradient between the two, the thermal conductivity of the stream bed substrates, and the hydraulic gradient between the streambed and subsurface (Guenther, Gomi, & Moore, 2014). Thermally stable groundwater or hyporheic upwelling inputs cool water to the stream in the summer and comparatively warmer water to the stream in the winter (Kelleher et al., 2012). Similarly, heat can be conducted from the water column to the stream bed during summer, but solar radiation inputs may warm the stream bed sufficiently to heat the stream. Bed heat exchanges counteract daytime energy inputs and can minimize downstream warming (Leach & Moore, 2011), and constitute up to 10 % of net radiative exchange in step-pool headwater streams (Moore, Sutherland, Gomi, & Dhakal, 2005b) to less than 1 % in streams with negligible groundwater inputs (Garner, Malcolm, Sadler, & Hannah, 2014).

Riparian forest canopies are critical for preserving stream temperatures by limiting the loading of solar radiation at the stream surface (Bladon, Segura, Cook, Bywater-Reyes, & Reiter, 2018; Garner et al., 2014; Simmons et al., 2014; Wondzell, Diabat, & Haggerty, 2019) and mitigating associated increases in stream temperature (Groom, Dent, Madsen, & Fleuret, 2011; Rex, Maloney, Krauskopf, Beaudry, & Beaudry, 2012). As such, a reduction in riparian canopy cover during forest management activities, or due to forest disturbances, can lead to increased stream temperature sensitivity to atmospheric energy exchanges (Gomi, Moore, & Dhakal, 2006; Moore et al., 2005b; Simmons et al., 2014), compounding the effect on stream temperatures

through space and time. However, in small headwater catchments, stream temperatures may not respond to reductions in canopy cover (Janisch, Wondzell, & Ehinger, 2012; Larson, Larson, & Larson, 2002) and may be more influenced by subsurface hydrology (Leach & Moore, 2011; Macdonald, Boon, Byrne, & Silins, 2014; Wagner et al., 2014), topography (Callahan et al., 2015; Ebersole, Liss, & Frissell, 2003), bed conductive heat transfer (Story, Moore, & Macdonald, 2003), or hyporheic exchange (Magnusson, Jonas, & Kirchner, 2012; Moore et al., 2005b; Poole & Berman, 2001). Thus, these influences on stream temperature are difficult to generalize across diverse regions and additional work is needed to assess the relative importance of riparian shade, subsurface hydrology, and atmospheric controls on stream temperature in headwater catchments.

Heat fluxes dominating stream temperature vary in both time and space, creating a distinct thermal landscape (Steel et al., 2017), that creates thermal variability along a stream. Few studies have characterized the complexities of the longitudinal thermal regime in headwater streams across diverse regions, as many studies have suggested the importance of different factors on stream temperature with one or few point measurements at or near the watershed outlet (e.g., Rex et al., 2012; Kibler et al., 2013) or by focusing study in a single region (Dent, Vick, Abraham, Schoenholtz, & Johnson, 2008; Garner et al., 2014; Leach & Moore, 2011). This has prevented accurate characterization of reach-scale thermal heterogeneity and understanding of the mechanisms governing stream thermal regimes across diverse regions.

Efforts to describe the drivers of longitudinal stream temperature dynamics have illustrated the important roles of stream geomorphology (Leach & Moore, 2011; O'Sullivan, Devito, & Curry, 2019), hyporheic exchange (Kasahara & Wondzell, 2003; Moore & Wondzell, 2005), geology (Briggs et al., 2018b; Johnson, 2004; Tague, Farrell, Grant, Lewis, & Rey, 2007), canopy cover (Garner et al., 2014; Groom et al., 2011; Simmons et al., 2014), atmospheric exchanges (Bond, Stubblefield, & Van Kirk, 2015; Lisi et al., 2015), and discharge (Bond et al., 2015; Hilderbrand, Kashiwagi, & Prochaska, 2014). Geomorphic attributes including channel aspect, width, depth, confinement, and slope can also influence stream temperatures at the reach scale (Garner, Malcolm, Sadler, & Hannah, 2017; O'Briain et al., 2017; Woltemade, 2017) through

bank and topographic shading, frictional heating, and variations in water residence time. Small scale geomorphic elements common in steep headwaters such as step-pools and large wood that drive hyporheic exchange can potentially cool stream temperatures (Kasahara & Wondzell, 2003). However, the relative importance of each of these factors has yet to be fully disentangled across diverse regions.

Of particular interest is underlying watershed lithology—the geologic characteristics of bedrock and soil parent material—which may influence stream temperatures by controlling subsurface hydrological pathways (Nickolas, Segura, & Brooks, 2017; Segura et al., 2019; Tague et al., 2007) and runoff generation processes (Johnson, Snyder, & Hitt, 2017; O'Sullivan et al., 2019; Uchida, Kosugi, & Mizuyama, 2002). For instance, Tague et al., (2007) determined that spring dominated streams in Oregon draining resistant lithology were less thermally sensitive to changing air temperatures than lower elevation shallow sub-surface flow dominated streams due to differences in the magnitude of streamflow sourced from the subsurface. As well, in an Oregon headwater stream, water flowing over bedrock warmed more quickly than water flowing over alluvial substrates, likely due to the low bedrock permeability that lead to limited hyporheic exchange with bed sediments and greater atmospheric control of stream temperature (Johnson, 2004). Watershed lithology may also influence the distribution of instream substrate (Fratkin, Segura, & Bywater-Reyes, 2020; Johnson, 2004) and geomorphic properties of the stream channel (Briggs et al., 2018c), which can influence stream temperature dynamics in headwater catchments and their responsiveness to disturbance such as forest harvesting (Bladon et al., 2018; Janisch et al., 2012). Determining the factors that influence the longitudinal thermal regime in headwater systems is key to improving existing models (Leach et al., 2016) and to facilitate informed water and forest management decisions across diverse regions.

In addition to regional watershed lithology, reach-scale topography may also influence the longitudinal thermal regime (Callahan et al., 2015; Monk, Wilbur, Allen Curry, Gagnon, & Faux, 2013) and may be useful in unraveling runoff production processes during storm events (Hangen, Lindenlaub, Leibundgut, & Von Wilpert, 2001; Jencso et al., 2009). Runoff generation in steep forested headwater catchments is often

controlled by physiographic characteristics, such as geology and topography (Gabrielli, McDonnell, & Jarvis, 2012; Gomi et al., 2010; Hangen et al., 2001; Zimmer & McGlynn, 2017) and by temporal variability in water inputs that drive catchment hydrologic storage (Amatya et al., 2016; Dralle et al., 2018; Sidle et al., 2000). During a storm event, precipitation is partitioned into one of several pathways depending on rainfall intensity (Detty & McGuire, 2010), soil infiltration capacity (Gomi et al., 2010), antecedent moisture conditions (Lange & Haensler, 2012; Radke et al., 2019), and overall catchment storage (Zimmer & McGlynn, 2018, 2017).

Because stream temperature is non-reactive, naturally occurring, and relatively inexpensive to monitor, it has potential utility as a tracer to understand surface water-groundwater interactions and subsurface hydrologic connectivity during storm events (Constantz, Cox, & Su, 2003; Leach et al., 2017; Oware & Peterson, 2020; Ploum, Leach, Kuglerová, & Laudon, 2018; Shanley & Peters, 1988; Uchida et al., 2002). For instance, Uchida et al. (2002) monitored stream and soil temperatures in a steep forested catchment in Japan to differentiate between contributions to stormflow from water at the soil-bedrock interface and shallow bedrock, effectively illustrating the sources of water contributing to streamflow during storms. Similarly, stream temperature and commonly used topographic metrics, such as upslope accumulated area (UAA), topographic wetness index (TWI), and flow weighted slope (FWS), that theoretically describe the location of saturated soil and subsurface water flow paths, have been used successfully to locate areas of strong lateral groundwater influence in boreal regions (Leach et al., 2017) and elucidate topographic control on stream temperature in southern Alaska (Callahan et al., 2015). However, no assessment has been done in the Coast Range of Northern California, where subsurface heterogeneity may prevent accurate characterization of discrete groundwater inflow using metrics derived from the surface (e.g., Gabrielli, McDonnell, & Jarvis, 2012; Genereux, Hemond, & Mulholland, 1993).

In forested catchments along the Northern California Coast, soil hydraulic conductivity is typically high and rainfall intensities low such that overland flow is rare (Keppeler & Brown, 1998), except on bedrock outcrops or areas with extremely shallow soils (e.g., Uchida et al., 2002). Therefore, subsurface flow pathways commonly

dominate during storm events, but the exact partitioning of water inputs into shallow subsurface flow and deeper groundwater flow paths may vary depending on soil characteristics, antecedent moisture conditions, topography, and storm characteristics (Detty & McGuire, 2010; Gomi et al., 2010; Penna et al., 2015; Rinderer, Van Meerveld, & Seibert, 2014; Van Meerveld, Seibert, & Peters, 2015).

Additionally, research assessing stream temperature change during storm events in forested headwaters is limited (Hebert, Caissie, Satish, & El-Jabi, 2011), and there have been few dedicated efforts assessing the influence of storm events on the stream longitudinal thermal regime. During storm events, quickflow from shallow subsurface stormflow or preferential soil channels can strongly influence stream temperatures (Lange & Haensler, 2012; Leach & Moore, 2014; Subehi et al., 2010). But, the response varies depending on seasonally variable antecedent moisture conditions (Lange & Haensler, 2012; Subehi et al., 2010), meteorological conditions (Herb, Janke, Mohseni, & Stefan, 2008; Somers, Bernhardt, Mcglynn, & Urban, 2016), and catchment topography (Leach et al., 2017; Subehi et al., 2010). A better understanding of the variable response to precipitation inputs along headwater channels may provide information into the timing and delivery of runoff, with implications for downstream water quality (Somers et al., 2013; Wilby, Johnson, & Toone, 2015).

Hysteresis analysis has been used to characterize the transport of water quality constituents in catchments during storm events (Aguilera & Melack, 2018; Liu, Birgand, Tian, & Chen, 2021; Mistick & Johnson, 2020; Vaughan et al., 2017). Water quality hysteresis describes the phenomena where a measured constituent has a different relationship with or lags behind discharge during a storm event. This behavior is commonly separated by rising and falling limbs of the hydrograph, where transport behavior of the constituent of interest from the catchment varies between the two. Specifically, hysteresis metrics have recently been developed to easily quantify the direction, slope, and size of hysteretic loops and make comparisons between storms and catchments (Lloyd, Freer, Johnes, & Collins, 2016a, 2016b). During storm events or snowmelt episodes, stream temperature variability with streamflow exhibits hysteresis behavior (Blaen, Hannah, Brown, & Milner, 2013; Kobayashi, Ishii, & Kodama, 1999).

Hysteresis behavior has also been observed in the relationship between stream temperature and precipitation inputs (Kobayashi et al., 1999; Subehi et al., 2010). For instance, clockwise hysteresis behavior during storms when air temperatures are greater than stream temperatures may indicate thermal transfer from shallow quickflow sources that warm the stream water during the rising limb of the hydrograph. In addition, hysteresis loops with a positive slope likely indicate flushing of heat from the catchment that causes stream temperatures to rise towards the hydrograph peak, while loops with a negative slope indicate dilution of heat from the catchment (i.e., from deep-sourced groundwater or direct channel precipitation) (Kobayashi et al., 1999). Quantifying stream temperature hysteresis may provide insights into how headwater streams respond to storm events across seasons and catchment characteristics.

Forested headwaters represent the landscape features with the strongest connection between terrestrial and aquatic elements (Freeman et al., 2007; Schlosser, 1991), and are more reactive to inputs of precipitation than downstream reaches (Wilby et al., 2015). Thus unsurprisingly, there is continued interest in understanding the responsiveness of headwater channels to perturbations at the management-relevant reach scale. For instance, there have been recent calls for riparian forest management practices to consider the spatially variable hydrological connectivity inherent to forested headwaters (Kuglerová, Ågren, Jansson, & Laudon, 2014; Laudon et al., 2016; Tiwari et al., 2016), such as by incorporating wider riparian buffers near variable source areas or permanently saturated areas (Erdozain et al., 2020). Indeed, certain locations along headwater channels in boreal systems have been shown to provide disproportionate contributions of runoff to streamflow given local topography and soil conditions. These so-called discrete riparian inflow points (DRIPS) (Ploum et al., 2018) can have a large influence on stream water chemistry and temperature (Erdozain et al., 2020; Lowry, Walker, Hunt, & Anderson, 2007), and require additional study to determine their influence on stream temperature during storm events. This has important implications for understanding how anthropogenic (forest harvesting activities) or natural (windthrow, debris flows) disturbance influences runoff generation and water quality downstream.

The objective of this thesis is to improve our understanding of headwater stream temperature dynamics by assessing how regional lithology influences the summer thermal regime and how headwater channels respond to seasonally variable precipitation inputs. In chapter 2, I present results from a regional study comparing the summer longitudinal thermal regime and thermal sensitivity of stream temperature to air temperatures between eight headwater catchments draining sedimentary (sandstone) and volcanic (basalt) lithology across Northern California. I hypothesized that streams underlain by coarse, fractured, volcanic lithology would be less thermally sensitive to changing air temperatures than streams draining thin, friable sandstone lithology because of differences in subsurface permeability that yields variable surface water-groundwater interactions between regions.

In chapter 3, I use hysteresis analysis to assess stream temperature change during storm events across seasons in ten headwater catchments in the Northern California Coast Range to better understand how forested headwaters respond to precipitation, and whether local topography influences the stream temperature response to storm events. I hypothesized that the direction of stream temperature hysteresis would vary across seasons due to changes in meteorological conditions and that the stream locations most hydrologically connected to the hillslope (as predicted by topographic indices) would exhibit the greatest hysteresis due to greater hydrologic input via lateral throughflow. In chapter 4, I present a synthesis and discussion of how the results from chapters 2 and 3 may be used to inform riparian forest management along headwater streams and also present questions for future investigation.

Chapter 2: Comparing headwater stream thermal sensitivity across two contrasting lithologies in Northern California

2.1: Abstract

Understanding drivers of thermal regimes in headwater streams is critical for a comprehensive understanding of freshwater ecological condition and habitat resilience to disturbance, and to inform sustainable forest management practices. However, stream temperatures may vary depending on characteristics of the stream, catchment, or region. To improve our knowledge of the key drivers of stream thermal regime, we collected stream and air temperature data along eight headwater streams in two regions with distinct lithology, climate, and riparian vegetation. Five streams were in the Northern California Coast Range at the Caspar Creek Experimental Watershed Study, which is characterized by permeable sandstone lithology. Three streams were in the Cascade Range at the LaTour Demonstration State Forest, which is characterized by fractured and resistant basalt lithology. We instrumented each stream with 12 stream temperature and four air temperature sensors during summer 2018. Our objectives were to compare stream thermal regimes and thermal sensitivity—slope of the linear regression relationship between daily stream and air temperature—within and between both study regions. Mean daily stream temperatures were ~4.7 °C warmer in the Coast Range but were less variable (SD = 0.7 °C) compared to the Cascade Range (SD = 2.3 °C). Median thermal sensitivity was 0.33 °C $°C^{-1}$ in the Coast Range and 0.23 °C $°C^{-1}$ in the Cascade Range. We posit that the volcanic lithology underlying the Cascade streams likely support discrete groundwater discharge locations, which dampened thermal sensitivity. At locations of apparent groundwater discharge in these streams, median stream temperatures rapidly decreased by 2.0 °C, 3.6 °C, and 7.0 °C relative to adjacent locations, approximately 70–90 meters upstream. In contrast, Coast Range streams draining thin friable soils likely had baseflow sourced from shallow subsurface sources, which was more sensitive to air temperature and generally warmed downstream (up to 2.1 °C km^{-1}). Our study revealed distinct longitudinal thermal regimes in streams draining contrasting lithology, suggesting that streams in these different regions may respond differentially to forest disturbances or climate change.

2.2: Introduction

Stream temperature (T_s) is a critical water quality parameter that drives dissolved oxygen solubility (Loperfido et al., 2009; Ozaki et al., 2003), nutrient cycling (Morin et al., 1999; Neres-Lima et al., 2017), in-stream primary productivity (Bernhardt et al., 2018), and habitat suitability for aquatic species (Brewitt et al., 2017). Warming stream temperatures can negatively impact sensitive cold water aquatic species, such as salmonid fishes and amphibians, by reducing habitat suitability for spawning and rearing life stages, and influencing individual metabolism and behavior (Dallas & Ross-Gillespie, 2015; Eaton & Scheller, 1996; Hester & Doyle, 2011; Railsback & Rose, 1999). Recent studies have illustrated that climate change and shifts in forest disturbance regimes have the potential to intensify thermal pollution and increase the risks to anadromous fish and other aquatic vertebrate populations (Benjamin, Connolly, Romine, & Perry, 2013; Ford et al., 2011; Thomas et al., 2004). In Mediterranean climates, the threat to aquatic species is particularly important during the summer low flow period, when precipitation inputs are low and both thermal inputs from solar radiation and convective heat exchange between the warm air and cooler streams are at their maximum (Arismendi et al., 2013; Larsen & Woelfle-Erskine, 2018; Xu, Letcher, & Nislow, 2010).

However, research on longitudinal thermal regimes of streams has revealed substantial complexity and variability in the dominant processes driving the spatial patterns in stream temperature (Fullerton et al., 2015, 2018; Hofmeister, Cianfrani, & Hession, 2015). For many years, the conventional perspective was that stream temperature increased progressively from headwaters to larger downstream river systems (Caissie, 2006; Vannote et al., 1980). Other studies have quantified decreasing stream temperature moving downstream in some headwaters (Dent et al., 2008; Leach & Moore, 2011; Moore et al., 2005b; Story et al., 2003) and larger streams (O'Sullivan et al., 2019). Additionally, recent advances in remote sensing technology and larger scale observations have revealed that many streams cannot be characterized by a simple longitudinal profile pattern in stream temperature (Briggs, Dawson, Holmquist-Johnson, Williams, & Lane, 2018a; Dugdale et al., 2015; Ebersole et al., 2015; Fullerton et al., 2015). This is especially true for non-fish bearing headwaters, where complex geomorphology and

discrete groundwater inputs can produce distinct patterns of flow permanence and network connectivity (Gendaszek et al., 2020; Pate et al., 2020) that influence stream temperature.

Despite recent advances in our knowledge, there is still much uncertainty about the longitudinal patterns in stream temperature due to numerous local and regional controls. One dominant local control on stream temperature is groundwater discharge, which in some systems can provide a stable supply of cool water and promote refugia for sensitive aquatic species during summer (Arscott, Tockner, & Ward, 2001; Briggs et al., 2018b; Griebler & Avramov, 2015; Snyder, Hitt, & Young, 2015). Groundwater contributions are, in part, controlled by regional lithology and are typically greater in more permeable geology (Hale & McDonnell, 2016). The magnitude of groundwater contributions may also be influenced by channel morphology (Johnson, Wilby, & Toone, 2014; Kasahara & Wondzell, 2003; Moore et al., 2005b; Story et al., 2003), the direction of subsurface hydraulic gradients (Peterson & Sickbert, 2006), the available alluvial hydraulic storage (Kelson & Wells, 1989), and the catchment hydraulic conductivity (Morrice, Valett, Dahm, & Campana, 1997). In headwater streams with a predominance of groundwater discharge, stream temperature is often cooler and less variable (Brown & Hannah, 2008; Danehy, Colson, & Duke, 2010; Johnson, 2004). Localized springs (Leach & Moore, 2011) and zones of concentrated upwelling (Moore et al., 2005b) can cause downstream cooling and reduce stream temperature variation, even during the winter (Danehy et al., 2010; Westhoff & Paukert, 2014). As such, streams with substantial groundwater discharge may be less responsive to reductions in canopy cover and subsequent increases in radiative loading (Janisch et al., 2012; Larson et al., 2002) compared to streams with lesser groundwater contributions (Bladon et al., 2018; Dent et al., 2008; Moore et al., 2005a; Story et al., 2003).

Many studies have used air temperature as a predictor of stream temperature (Jackson, Fryer, Hannah, Millar, & Malcolm, 2018; Kelleher et al., 2012; Mayer, 2012; Mohseni & Stefan, 1999; Segura, Caldwell, Sun, Mcnulty, & Zhang, 2015; Snyder et al., 2015; Stefan & Preud'homme, 1993), although convective heat exchange at the water surface often represents a minor portion of the overall stream heat budget (Johnson,

2003). Regardless, air temperature has been used successfully to develop simple, empirical models that predict changes in stream temperature due to climate change (Caldwell et al., 2015) or to identify locations of groundwater discharge (Fullerton et al., 2018; Mayer, 2012; Snyder et al., 2015). Air temperature has often been an effective predictor of stream temperature at coarse temporal scales (e.g., daily, weekly, monthly; Segura et al., 2015) and can act as a surrogate for total heat flux to the stream surface (Arismendi, Safeeq, Dunham, & Johnson, 2014; Gomi et al., 2006; Gu, Anderson, Colby, & Coffey, 2015; Mohseni & Stefan, 1999; Tague et al., 2007).

The relationship between air and stream temperature is often described with a linear regression model in which the slope provides an indicator of the thermal sensitivity of the stream (Lisi et al., 2015; Segura et al., 2015; Snyder et al., 2015). This relationship can also be used to elucidate the spatial extent of different streamflow contributions (Kelleher et al., 2012; Mayer, 2012; Snyder et al., 2015). For example, stream segments dominated by groundwater discharge or substantial hyporheic exchange may be identified by stable stream temperatures or lower thermal sensitivity to diel and seasonal variations in air temperature. Comparatively, stream segments with greater channelized flow, less groundwater or hyporheic contributions may be characterized by greater fluctuations in stream temperature due to greater coupling with atmospheric controls. This observational tool has been used in many broad applications to assess contributions of groundwater and hyporheic flow (Briggs et al., 2018b; Johnson et al., 2014; Mayer, 2012; Selker, van de Giesen, Westhoff, Luxemburg, & Parlange, 2006; Snyder et al., 2015). However, the longitudinal variability in thermal sensitivity along headwater streams remains poorly characterized and the potential implications for headwater stream management in contrasting regions are not known.

In our study, we quantified both stream temperature and air temperature in eight headwater streams draining contrasting lithologies in Northern California. Specifically, we deployed 128 thermistors longitudinally down streams draining volcanic basalt (Cascade Range) and friable sandstone (Coast Range) lithology to characterize local and longitudinal trends in stream warming or cooling. We also sought to quantify the degree of atmospheric control on stream temperature, or thermal sensitivity, to improve our

understanding of the processes driving longitudinal stream temperature variability in headwater streams. Thus, our primary objectives were to: (a) compare stream and air temperatures during the summer low flow period in streams draining contrasting lithology, (b) quantify the reach-scale longitudinal variability in stream and air temperatures in streams draining contrasting lithology, and (c) quantify inter- and intra-regional thermal sensitivity in streams draining contrasting lithology. Our results revealed differences in the likely processes governing the stream thermal regimes across our two study regions. We observed greater longitudinal thermal heterogeneity in streams underlain by basalt than sandstone, which we posit was driven primarily by the presence of discrete groundwater discharge locations that dominated over atmospheric control on stream temperature at these locations. Understanding the dominant controls on the thermal regime of small headwater streams is critical to make informed management decisions in headwater catchments across diverse regions.

2.3: Methodology

2.3.1: Study Locations

Our study occurred in two distinct geological regions of Northern California: the Southern Cascade Range (LaTour Demonstration State Forest) and the North Coast Range (Caspar Creek Experimental Watershed in Jackson Demonstration State Forest) (Figure 2.1). The two regions were selected to represent strongly different climates, geologies, and dominant forest types (Table 2.1).

Our study included three streams in the Cascade Range: Beaver Creek, (BEA), Bullhock Creek (BUL), and Sugar Creek (SUG). All three streams are step-pool systems (Montgomery & Buffington, 1997) with few large cascades—they all have similar slope, canopy cover, and elevation (Table 2.2). Soils are coarse, fast draining loams with depths < 2 meters (McDonald, 1995). The stream channel substrate was coarse gravel (D_{50}: 46–60 mm) except in locations behind debris jams where finer substrate accumulated (Pate et al., 2020). Valleys in the Cascade Range are U-shaped carved by glaciation processes with stream channels typically unconfined, except in some locations along Sugar Creek.

The geology in the Cascade Range contains resistant, fractured basalt and andesite (MacDonald, 1963) characterized by rapid drainage to deep groundwater aquifers with long residence times (Tague et al., 2007; Tague, Grant, Farrell, Choate, & Jefferson, 2008) typical of volcanic geology (Jaeger et al., 2007). The climate is semi-arid, with hot, dry summers, and snowy, cold winters (CAL FIRE, 2013) (Table 2.1). Precipitation is snow dominated with snowpack persisting often into early May (McDonald, 1995; PRISM Climate Group, Oregon State University, http://prism.oregonstate.edu, accessed April 10, 2020), with a snow water equivalent depth on April 1, 2018 of 384 mm (Snow Mountain, CA station, 18 km from study location; NRCS, 2020). The forests in our study catchments were dominated by 10 to 17 m tall sugar pine (*Pinus lambertiana*), lodgepole pine (*Pinus contorta*), and ponderosa pine (*Pinus ponderosa*), with some Douglas-fir (*Pseudotsuga menziesii*) and mountain hemlock (*Tsuga mertensiana*), with a comparatively low to moderate density canopy cover (Oregon State LEMMA Database, 2020) (Table 2.1).

Study streams in the North Coast Range were located in the Caspar Creek Experimental Watershed Study, where research has been ongoing since 1961 addressing questions about forest management effects on forest hydrology and water quality (Cafferata & Reid, 2013; Keppeler, Ziemer, & Cafferata, 1994). We included five streams in the Coast Range: Henningson (HEN), Iverson (IVE), Richards (RIC), Williams (WIL), and Xray (XRA) Creeks, which are step-pool systems (Montgomery & Buffington, 1997) with a few small cascades and similar slope, canopy cover, and elevation (Table 2.2). The channel substrate for all streams was medium gravel (D_{50}: 13–24 mm). Valleys are steep and V-shaped with considerable channel incision, resulting in strong confinement and coupling between the streams and hillslopes. Soils were 1 to 1.5 meters deep, well drained loams underlain by a restrictive clay layer, which results in substantial pipeflow that rapidly transfers shallow subsurface flow laterally to the channel (Amatya et al., 2016; Keppeler & Brown, 1998). Geology of the region is dominated by friable sandstone and mudstone lithology of the Franciscan complex (Amatya et al., 2016). Winter climate is characterized as mild, cool, and wet, with temperatures rarely below 0 °C, while summers are warm and dry (Keppeler et al., 1994) (Table 2.1).

Precipitation is rain dominated, with >1,200 mm falling annually (PRISM Climate Group, Oregon State University, http://prism.oregonstate.edu, accessed April 10, 2020). Riparian vegetation consists of 20 to 30 m tall, dense (canopy cover between 78 to 91 %; Oregon State LEMMA Database, 2020) coast redwood (*Sequoia sempervirens*) forest, with Douglas-fir (*Pseudotsuga menziesii*), grand fir (*Abies grandis*), and western hemlock (*Tsuga heterophylla*) occurring at lower densities (Cafferata & Reid, 2013).

2.3.2: Data Collection

In each of the eight study streams, we installed 16 HOBO TidbiT v2 sensors (Onset, Bourne, MA; accuracy ± 0.21 °C) to measure both air and stream temperature (128 total sensors). Specifically, we installed 12 stream temperature sensors and four air temperature sensors along each stream to collect continuous data (15-minute intervals). The four air temperature sensors were co-located with stream temperature sensors near the top, bottom, and two midpoints of each stream (Figure 2.1, inset). In-stream sensors were placed along the thalweg and secured with rebar driven through the channel bottom. Air temperature sensors were placed adjacent to the channel and suspended from tree branches approximately one meter above the ground. All sensors were enclosed in sections of white PVC tubing with drilled holes to allow fluid exchange and to minimize solar influences. Stream temperature sensors were positioned approximately every 80 m in the Cascade Range streams and every 30 to 60 m in the Coast Range streams (Table 2.2). Sensor spacing was regular and dictated by the available stream length from the point of channel head initiation to the confluence with a higher order stream.

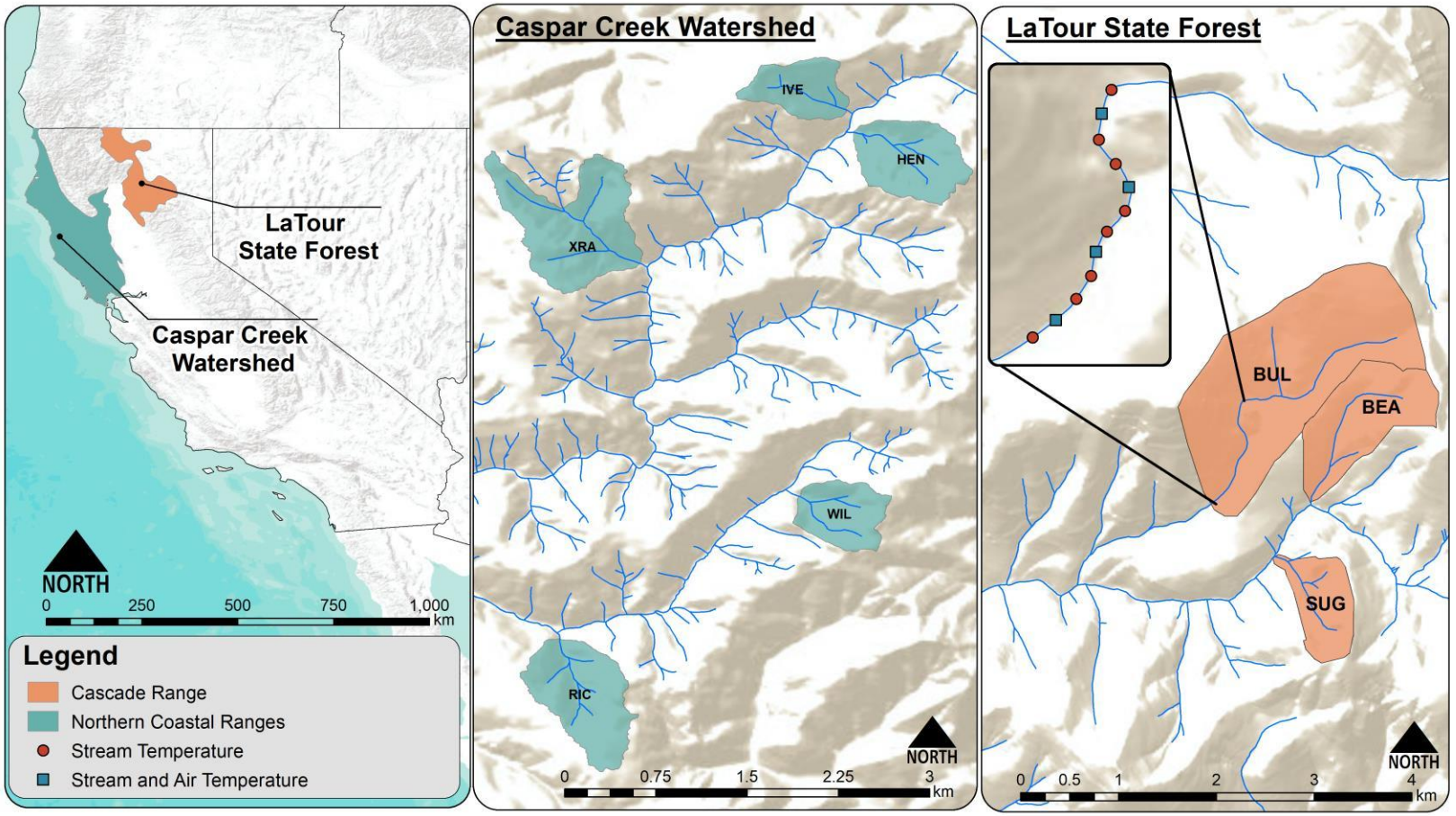

Figure 2.1. Field site locations within California in the LaTour State Forest (Cascade Range) and Caspar Creek (Coast Range). Inset on the right: Schematic of temperature data collection for all 8 study reaches. Spacing between stream temperature sensors varied between streams and study regions (30–80 m).

Table 2.1. Climatic and physical characteristics of the study areas.

Characteristic	Cascade Range	Coast Range	Reference
Mean T_a (°C, range)	10.9 (-6.0–29.2)	13.5 (1.6–28)	Measured herein
Precipitation (mm, Oct 2017–Sept 2018)	1,018	956	PRISM Climate Group, 2020
30-year mean precipitation (mm)	1,350	1,262	PRISM Climate Group, 2020
Mean stream elevation (m, range)	1,741 (1,576–1,912)	124 (52–189)	Measured herein
Mean watershed slope (%)	28	33	Measured herein
Mean canopy cover (%, range)	61 (54–66)	85 (78–91)	Oregon State LEMMA Database, 2020
Dominant forest cover	Sugar, ponderosa, and lodgepole pine	Coast redwood, Douglas-fir, and western hemlock	Observed herein
Dominant lithology	andesite, basalt	sandstone, mudstone	MacDonald, 1963; Amatya et al., 2016

Table 2.2. Individual stream physical characteristics.

Characteristic	Cascade Range			Coast Range				
	BEA	**BUL**	**SUG**	**HEN**	**IVE**	**RIC**	**WIL**	**XRA**
Mean stream slope (%)[†]	19	17	24	21	23	27	19	25
Stream length (m)	880	1,078	902	418	418	550	308	770
Drainage area (km^2)[†]	1.07	3.13	0.58	0.38	0.23	0.47	0.26	0.62
Canopy cover (%)[‡]	66	54	62	92	78	88	80	87
T_s sensor spacing (m)	73	90	75	35	35	45	25	64
D_{50} (mm)[§]	60	51	46	24	13	17	16	21
Stream aspect[†]	S	S	NW	W	SE	SW	NW	SE
Elevation range (m)[†]	1,663–1,777	1,640–1,772	1,637–1,837	104–155	104–164	52–110	135–189	71–178

[†]Derived using ArcMap version 10.7 (ESRI, Redlands, CA)
[‡]Oregon State LEMMA Database (2020)
[§]From Pate et al. (2020)

2.3.3: Data Analysis

Temperature data was first visually explored to remove periods when sensors were not submerged. To do this, we visually assessed and compared the diel temperature range of stream temperature and adjacent air temperature sensors to discern periods when sensors were dry (Campbell et al., 2013; Sowder & Steel, 2012). If sensors were lost during the study, we assumed that any sensor that went dry prior to being lost remained dry throughout the remainder of the monitoring period. Similarly to previous research (Arismendi, Dunham, Heck, Schultz, & Hockman-Wert, 2017), we made this decision by considering data for sensors with complete records, which indicated that once the stream sections went dry, they remained dry for the rest of the summer. We did not make assumptions for sensors that were submerged prior to being lost. As a result, from the total available stream temperature data in the Cascade Range we were able to use 44 % in SUG, 49 % in BUL, and 91 % in BEA. Comparatively, in the Coast Range we were able to use 28 % of the data in HEN, 47 % in IVE, 48 % in WIL, 42 % in XRA, and 69 % in RIC. Data exploration, quality control, and statistical analysis were conducted in R version 3.6.1 (R Core Team, 2020).

We focused our analysis on the summer low flow period (June 1–September 30, 2018), when the warmest stream temperatures are typically recorded in the northern hemisphere (Dent et al., 2008; Groom, Johnson, Seeds, & Ice, 2017; Macdonald et al., 2014). Specifically, we quantified the diel range and daily maximum, minimum, median, and mean temperatures. Statistically, we used one factor ANOVA with Tukey's *post hoc* tests to assess differences in daily mean air temperatures recorded among and within streams in both regions, and among streams in each region. Welch's two-sample *t*-test was used to assess differences in daily stream and air temperature metrics among regions.

2.3.3.1: Assessing longitudinal stream temperature trends

We quantified the rate of downstream warming or cooling for each stream by fitting a linear regression equation with upstream distance (m) as the independent variable and average daily mean stream temperatures at each sensor location (°C) as the

dependent variable (Figure A1). Regression slopes greater than zero indicated net downstream warming, while slopes less than zero indicated net downstream cooling.

We quantified the average incremental temperature difference (AITD) as the absolute value of the difference in the average mean daily stream temperatures between adjacent sensors within each individual stream. Specifically, we calculated AITD to provide an indicator of the site-level variability in stream temperature as:

$$AITD = \frac{\sum_{i=1}^{n-1} |ADM_i - ADM_{i+1}|}{n-1} \quad (2.1)$$

where ADM_i was the average daily mean stream temperature measured at an upstream location, ADM_{i+1} was the average daily mean stream temperature measured at the nearest location downstream, and *n* was the number of stream temperature monitoring locations in each stream (8–12). Large values of AITD, were indicative of high variability in stream temperature magnitude from site to site along each stream. Alternatively, low values of AITD, were indicative of comparatively low site-level variability in stream temperature magnitude. Although the AITD metric captured variability in the central tendency of stream temperature at each monitoring location (average daily mean), it did not consider the variability in stream temperature at each monitoring location. For that reason, we also calculated the average incremental standard deviation difference (AISDD) as the absolute value of the difference between the average daily standard deviation in stream temperatures at each in-stream sensor and the one immediately downstream, using:

$$AISDD = \frac{\sum_{i=1}^{n-1} |ADSD_i - ADSD_{i+1}|}{n-1} \quad (2.2)$$

where $ADSD_i$ was the average of the standard deviation of daily stream temperature at an upstream location, $ADSD_{i+1}$ was the average of the standard deviation of daily stream temperature at the location immediately downstream, and *n* was the number of stream temperature monitoring locations in each stream (8–12). One value of AITD and AISDD was calculated for each stream to assess site-level thermal heterogeneity.

2.3.3.2: Stream thermal sensitivity analysis

To assess relative differences in atmospheric control on stream temperature between and within streams in the Coast and Cascade Ranges, we used the linear relationship between mean daily stream and air temperatures (equation 2.3). Mean daily stream temperatures (T_s) for each in-stream sensor were regressed against mean daily air temperature (T_a) values from the nearest sensor as:

$$T_s = mT_a + b \tag{2.3}$$

where m is the regression slope (hence forth referred to as the thermal sensitivity) and b is the intercept. Thus, our analysis provided up to 12 linear regression equations and corresponding thermal sensitivity values per stream. Prior to analysis, we removed temperature data below 0 °C as linear regression relationships between stream and air temperature were only valid for temperatures above freezing (Mayer, 2012; Mohseni & Stefan, 1999; Morrill, Bales, & Conklin, 2005; Segura et al., 2015). Additionally, we also removed daily mean temperature values derived from less than a complete day of data (i.e., $n < 96$, 15-minute interval data points) prior to fitting linear regression models—this resulted in removal of ~0.2 % of the data (23 days) across all sites. Regression equations where T_a was not significantly correlated with T_s ($p > 0.05$) were not included in the final analysis. Out of 96 stream temperature sensors, 14 were dry at the beginning of monitoring and one was lost during high flows. Four of the remaining 81 models were excluded due to a lack of correlation between T_a and T_s, and were assumed to contain substantial sources of unexplained variation, which was likely due to additional factors that provided greater control on stream temperature than atmospheric conditions. Therefore, 77 model fits were used in the final analysis. The coefficient of determination (R^2) was used to assess individual model fits. Median thermal sensitivity values measured in each region were compared using the non-parametric Wilcoxon Rank Sum test as it was determined that the distribution of thermal sensitivity values measured in the Cascade Range streams were not normally distributed (Shapiro-Wilk test, $p < 0.05$).

2.4: Results

2.4.1: Summer air and stream temperatures

Overall, our data indicated that during summer 2018 air temperatures were warmer and exhibited greater diurnal variability in the Cascade Range than in the Coast Range of California (Table 2.3). Specifically, daily mean air temperatures were 1.63 °C (95 % confidence interval (CI): 1.49–1.75 °C) warmer in the Cascade Range than in the Coast Range (t = -24.67, p < 0.01; Figure 2.2). Air temperatures were also more variable in the Cascade Range—the average diel air temperature range in the Cascade Range was ~2.3-times greater than in the Coast Range (Table 2.3). Daily maximum air temperatures in the Cascade Range (average: 26.2 °C) were also higher than in the Coast Range (average: 17.6 °C; t = -74.52, p < 0.01). Alternatively, daily minimum air temperatures were on average 1.45 °C (95 % CI: 1.33–1.59 °C) warmer in the Coast Range (9.95 °C) than in the Cascade Range (8.48 °C; t = 21.78, p < 0.01).

Table 2.3. Stream (T_s) and air (T_a) temperature statistics during summer 2018 (June 1 to September 30) for streams in the Coast and Cascade Ranges. Avg. = Average, SD = standard deviation.

Type	Region	Avg. Daily Mean (°C)	Avg. Daily SD (°C)	Avg. Daily Max (°C)	Avg. Daily Min (°C)	Avg. diel range (°C)
T_a	Cascade Range	14.73	5.48	26.22	8.49	17.73
	Coast Range	13.11	2.44	17.60	9.95	7.66
T_s	Cascade Range	7.30	0.68	8.77	6.53	2.24
	Coast Range	12.00	0.28	12.46	11.59	0.90

There was strong evidence (F (2, 2620) = 2.11, p < 0.01) that average daily mean air temperatures were different between streams in the Cascade Range. For example, the air temperature at BUL was ~0.31 °C warmer than at BEA and 0.70 °C warmer than at SUG (Figure 2.2). Comparatively, there was suggestive evidence (F (4, 3399) = 2.11, p = 0.08) that average daily mean air temperatures were different between streams in the Coast Range (Figure 2.2). However, there was strong evidence that both the average daily minimum (F (4, 3399) = 16.64, p < 0.01) and maximum (F (4, 3399) = 89.73, p < 0.01)

air temperatures were different across streams in the Coast Range (Table A1). Longitudinally, the average daily mean air temperatures differed between proximate air temperature sensors in the Coast Range by 0.10–0.75 °C and in the Cascade Range by 0.42–2.2 °C (Figure A2). Similarly, in the Coast Range the average daily minimum air temperatures between proximate sensors varied by 0.08–1.45 °C, while the maximum temperatures varied by 0.02–4.0 °C. In the Cascade Range, the average daily minimum air temperatures between proximate sensors varied by 0.10–2.95 °C, while the maximum temperatures varied by 0.90–11.15 °C. Thus, there was greater within-region air temperature variation in Cascade Range streams than in Coast Range streams.

Overall, our data indicated that summer stream temperatures were substantially cooler, but more variable in the Cascade Range streams compared to streams in the Coast Range (Figure 2.2). The average daily mean stream temperature in the Cascade Range streams (7.3 °C) was significantly cooler than in the Coast Range (12.0 °C; $t = 112.4$, $p < 0.01$; Table 2.3). While the streams were cooler, the average diel stream temperature range in the Cascade Range (2.2 °C day^{-1}) was ~2.5-times greater than in the Coast Range (0.9 °C day^{-1}; $t = -45.79$, $p < 0.01$). We also found strong evidence that average daily maximum stream temperatures in the Cascade Range streams (8.8 °C) were less than in the Coast Range streams (12.5 °C; $t = 72.3$, $p < 0.01$). Average daily minimum stream temperatures were also cooler in the Cascade Range streams (6.5 °C) compared to the Coast Range streams (11.6 °C, $t = 134.0$, $p < 0.01$). Site-level stream temperature statistics are available in Table A2. Figure A3 also outlines mean daily temperature time series trends for the entire summer season.

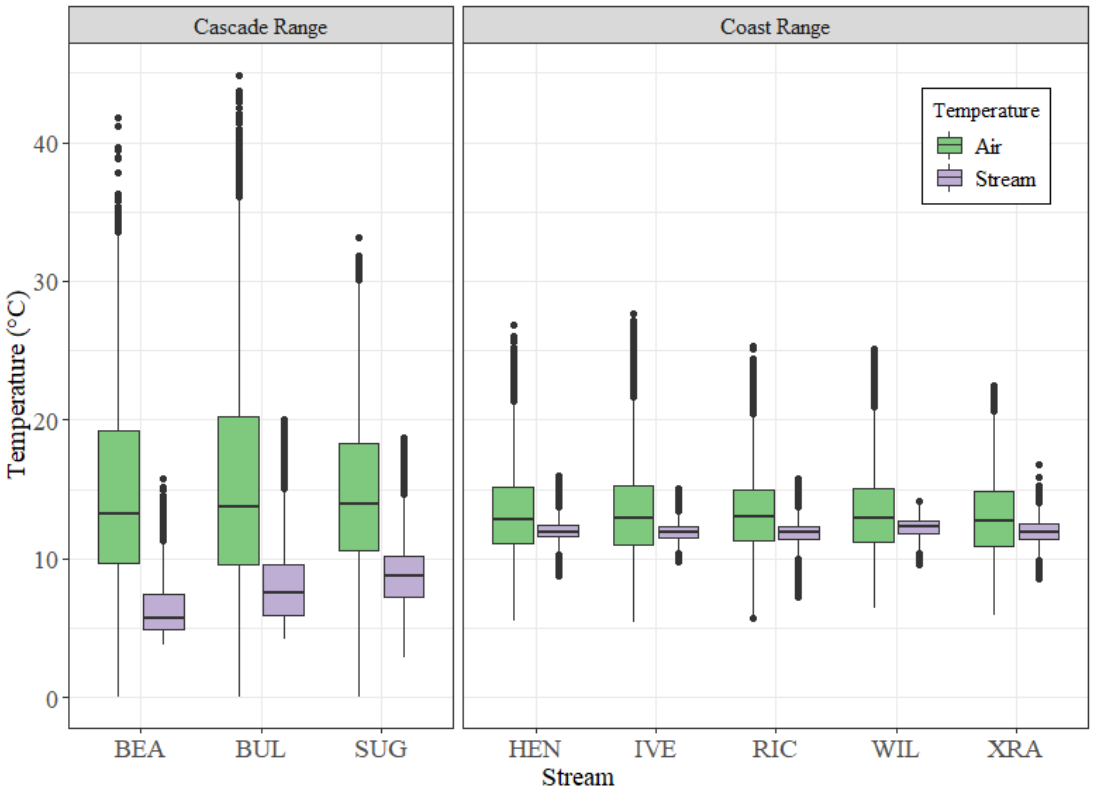

Figure 2.2. Comparison of air and stream temperature distributions among streams in the Coast and Cascade Ranges. Data were pooled from all temperature sensors within each stream. The boxplot central tendency line is the median, shaded boxes represent the interquartile range (IQR), whiskers represent the largest value up to 1.5-times the IQR, and the black dots indicate outliers beyond 1.5-times the IQR.

2.4.2: Longitudinal stream temperatures

Longitudinally down the entire length of our study streams in the Cascade Range, stream temperature generally cooled (-0.66 to -3.9 °C km^{-1}) (Table 2.4). In contrast, four of the five streams in the Coast Range warmed (0.18 to 2.1 °C km^{-1}) in the downstream direction, while HEN displayed moderate cooling (-1.1 °C km^{-1}) (Table 2.4 and Figure 2.3). The average incremental temperature difference (AITD) between each stream temperature sensor and the one immediately downstream was greater in the Cascade streams (1.0 °C) compared to the Coast Range streams (0.29 °C; $t = 3.8$, $p = 0.03$), indicating greater longitudinal variability in stream temperature magnitude in the Cascade Range streams (Table 2.4). AITD values ranged from 0.66 to 1.3 °C in Cascade Range steams and from 0.17 to 0.42 °C in Coast Ranges streams (Table 2.4). The average incremental difference in daily stream temperature standard deviation (AISDD) in the

Cascade Range streams was 0.41 °C, ranging from 0.19 °C (BEA) to 0.61 °C (SUG). Comparatively, the AISDD in the Coast Range streams was 0.19 °C, ranging from 0.15 °C (RIC) to 0.31 °C (HEN). Despite these differences, statistically, we did not find evidence that AISDD values were greater in Cascade Range streams compared to Coast Range streams ($t = 1.73$, $p = 0.11$).

Table 2.4. Longitudinal linear regression modeling results to assess downstream warming or cooling, and longitudinal heterogeneity in stream temperature in each stream. AITD = average difference in average daily mean stream temperature between each stream temperature sensor and the sensor immediately downstream. AISDD = average difference in average daily stream temperature standard deviation between each stream temperature sensor and the sensor immediately downstream.

Region	Stream	Intercept (°C)	Slope (°C km^{-1})	AITD (°C)	AISDD (°C)
Cascade Range	BEA	5.08	-2.74	0.66	0.19
	BUL	6.15	-3.88	1.26	0.44
	SUG	8.42	-0.66	1.16	0.61
	Average	6.55	-2.43	1.03	0.41
Coast Range	HEN	11.79	-1.07	0.30	0.31
	IVE	11.93	0.18	0.21	0.15
	RIC	12.10	0.91	0.17	0.15
	WIL	12.42	2.12	0.36	0.21
	XRA	12.26	0.79	0.42	0.16
	Average	12.10	0.59	0.29	0.19

The three streams in the Cascade Range (underlain by volcanic lithology) exhibited substantial longitudinal variability in stream temperature (Figure 2.3). Overall, the site-level average daily standard deviation (SD) in stream temperature ranged from 0.19–1.84 °C (mean = 0.68 °C). Much of the variability could be attributed to distinct locations where stream temperature decreased markedly in each of the three streams in this region. For example, we observed abrupt declines in average daily mean stream temperatures between two adjacent sensors of 2.0 °C in SUG, 3.5 °C in BEA, and 7.0 °C in BUL (Figure 2.3). Interestingly, stream temperatures generally warmed slightly between stream segments upstream from the locations of dramatic cooling. For example, the average daily mean summer stream temperature at BEA increased from 5.4 to 8.2 °C

between the first (furthest upstream sensor) and sixth temperature sensor (0.55 fractional distance upstream), which represented ~50 % of the monitored distance (~400 m). However, the average daily mean summer stream temperatures abruptly decreased to 4.7 °C (a loss of ~3.5 °C) over the next ~80 meters, between the sixth and seventh stream temperature sensors (between 0.55 and 0.45 fractional distance upstream) (Figure 2.3). We also noted that the variability in daily mean stream temperatures in BEA was generally greater (SD: 1.3 °C) in the upper 400 m of the stream (i.e., above the segment where temperatures cooled rapidly), relative to the lower 480 to 880 m of stream (SD: 0.39 °C). We observed similar patterns in summer stream temperatures in BUL and SUG, although both streams had ephemeral sections, which went dry during portions of the summer.

Comparatively, in the Coast Range, stream temperatures were more stable with no strongly discernible downstream warming or cooling trends (Figure 2.3). Site-level average daily standard deviations in stream temperature in the Coast Range ranged from 0.02–0.95 °C (mean = 0.28 °C). Generally, average daily mean stream temperatures increased moving downstream (Table 2.4), with the exception of the stream temperature at HEN, which cooled by 1.1 °C km^{-1} (Figure A1). There were some sections of localized cooling and reduced stream temperature variability present in HEN, IVE, WIL, and XRA approximately mid-stream. For example, the average daily mean stream temperature decreased 0.67 °C over 38 m between the fifth and sixth sensor location (from 0.64 to 0.55 fractional distance upstream) in HEN with a corresponding decrease in average daily standard deviation of stream temperature of 0.34 °C (Figure 2.3). However, the largest change in average daily mean stream temperatures observed moving downstream between any two adjacent sites along the Coast Range streams was 0.91 °C in XRA (between sensors 9 and 10, from 0.27 to 0.18 fractional distance upstream), which was 13 % of the maximum change observed in the Cascade Range streams (Figure 2.3). The largest observed reductions in average daily mean stream temperature in the remaining three streams in the Coast Range were 0.31 °C in IVE, 0.19 °C in RIC, and 0.64 °C in WIL (Figure 2.3).

Figure 2.3. Longitudinal distribution of stream temperatures measured along Coast Range and Cascade Range streams during summer, 2018. Upstream distance is normalized on the x-axis for comparison. The direction of flow is from left to right. Red arrows indicate likely spring locations in the Cascade Streams. Locations shown without data were either dry (D) throughout the summer or the sensor was missing during data collection (M). Measured stream lengths vary from 300 to 1000 m.

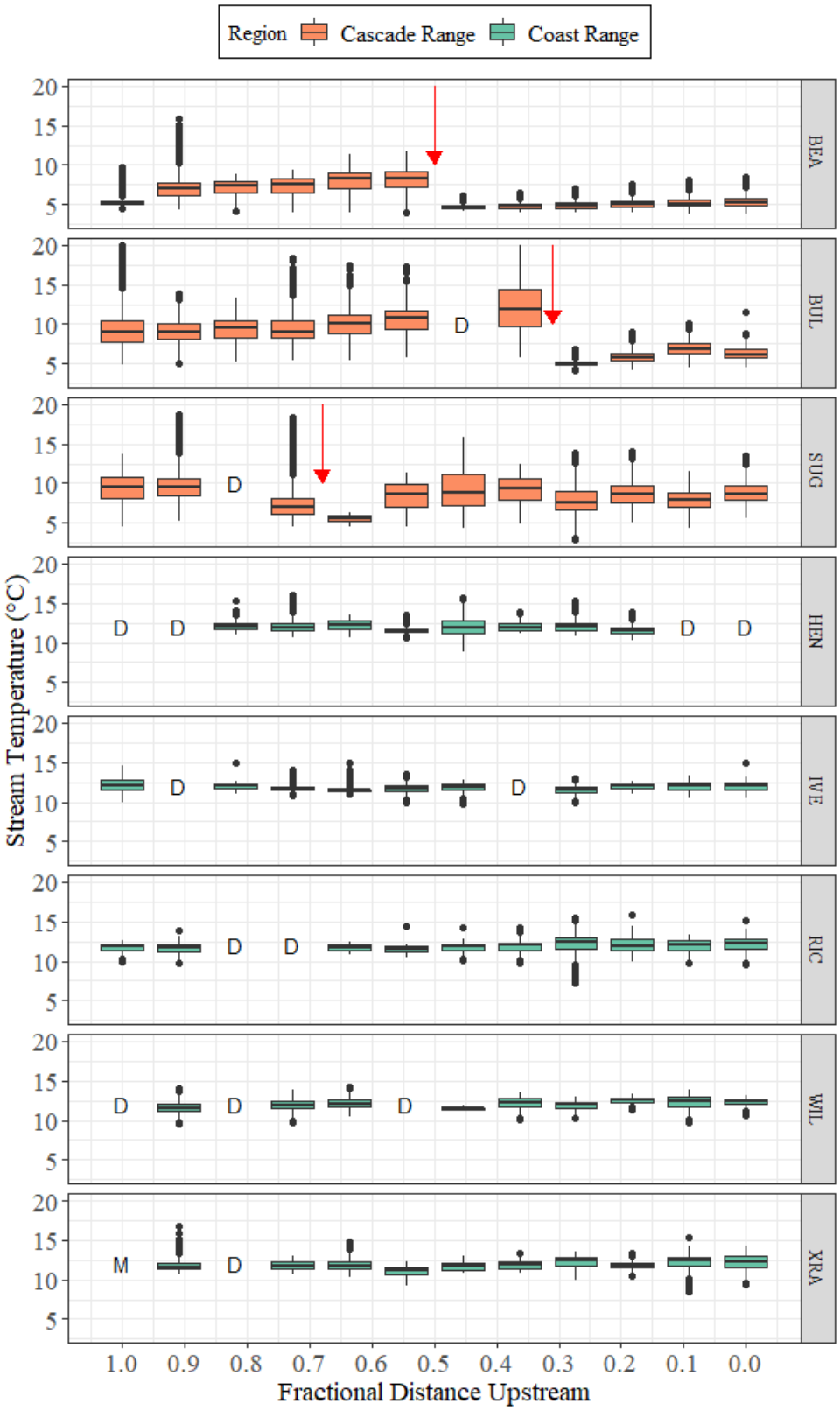

Figure 2.3. (Continued)

2.4.3: Stream thermal sensitivity

Our site-level linear regression models between air and stream temperature revealed fine-scale spatial variability in stream thermal sensitivity to air temperature in both study regions (Figure 2.4). In the Cascade Range streams, the median site-level thermal sensitivity was 0.23 °C °C^{-1}, ranging between 0.04–0.63 °C °C^{-1} (R^2 = 0.11–0.85) (Table 2.5). Interestingly, in BUL, the thermal sensitivity increased consistently from 0.27 °C °C^{-1} at the uppermost sensor to a maximum of 0.63 °C °C^{-1} at the eighth sensor (0.36 fractional distance upstream). However, the thermal sensitivity dramatically decreased to 0.04 °C °C^{-1} at the next sensor downstream and stream temperature generally remained decoupled from atmospheric controls across the bottom ~20 % (starting at 0.27 fractional distance upstream) of the stream reach (Figure 2.4).

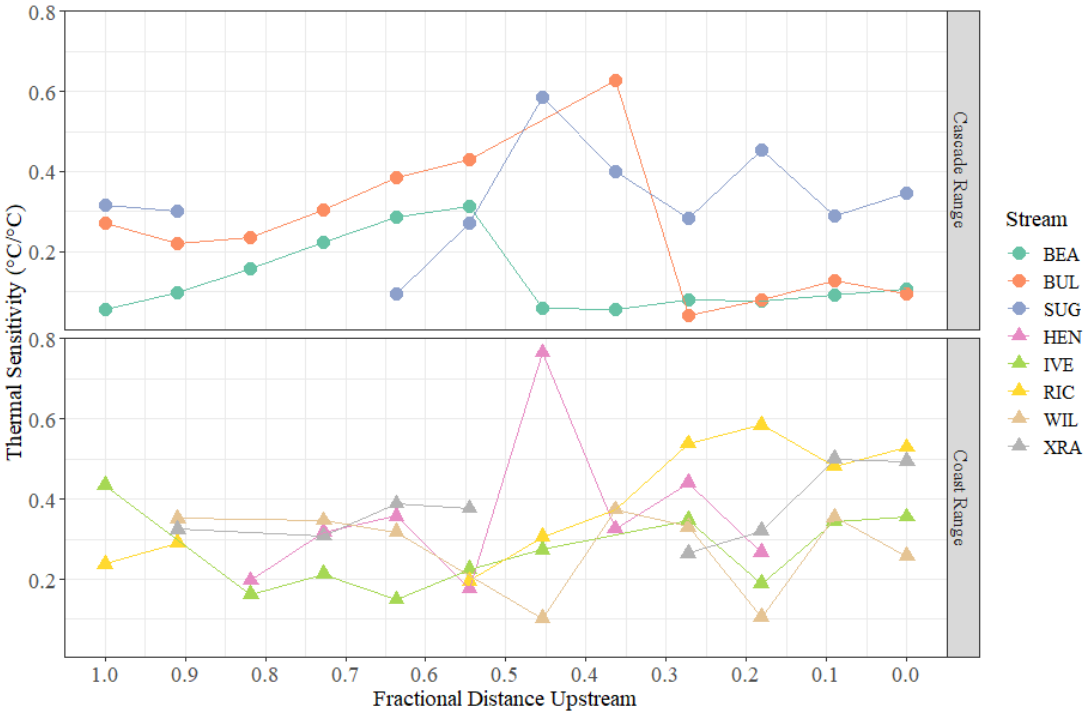

Figure 2.4. Longitudinal trends in thermal sensitivity (linear regression slope, Equation 3) along Cascade Range (BEA, BUL, SUG) and Coast Range (HEN, IVE, RIC, WIL, XRA) streams. Missing data points indicate sensors that went dry or regression models that were not included in the final analysis. The largest value in HEN is characterized by a sensor that went dry after 17 days. The x-axis is normalized for ease of comparison; stream lengths are in Table 2.2.

Similarly, in BEA the thermal sensitivity increased from 0.05 °C °C^{-1} at the uppermost sensor to 0.31 °C °C^{-1} at the sixth sensor (0.55 fractional distance upstream), before also decreasing dramatically to 0.06 °C °C^{-1} at the seventh sensor (0.45 fractional distance upstream) (Figure 2.4). The stream temperature in BEA also generally remained decoupled from air temperature for the remainder of the monitored stream length, which was similar to BUL.

In SUG, site-level thermal sensitivity decreased from 0.32 °C °C^{-1} to 0.10 °C °C^{-1} over the first 328 m (to 0.64 fractional distance upstream). Thermal sensitivity in SUG then increased from 0.10 °C °C^{-1} to 0.59 °C °C^{-1} over 150 m from the fifth to sixth sensor (from 0.64 to 0.45 fractional distance upstream) before alternately decreasing to 0.28 °C °C^{-1} at 0.27 fractional distance upstream then increasing to 0.45 °C °C^{-1} at 0.18 fractional distance upstream. Thermal sensitivity values for each sensor location are included in table A3 in the appendix.

Despite the variability in thermal sensitivity in the Cascade Range, the distribution of thermal sensitivity values was skewed to values less than 0.2 (Figure 2.5A), and these locations generally had the coolest stream temperatures. For instance, across the three Cascade Range streams, there was a strong, positive linear relationship between site-level thermal sensitivity values and the average daily mean stream temperature (R^2 = 0.79). Positive relationships also existed between site-level thermal sensitivities and average daily maximum stream temperatures (R^2 = 0.63), and average diel stream temperature range (R^2 = 0.59) (Figure A4). In other words, warmer stream segments were generally more coupled to air temperature, while cooler stream segments were less coupled with air temperature.

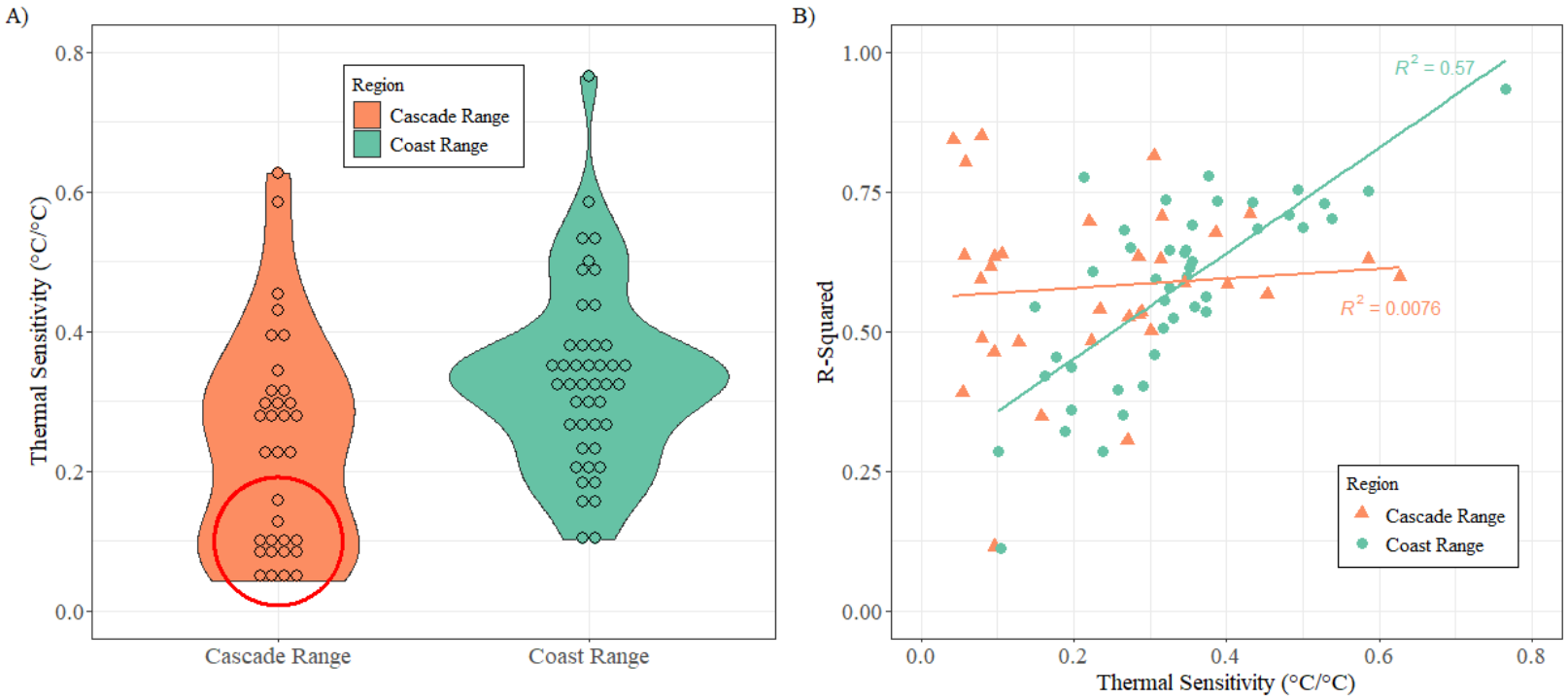

Figure 2.5. (A) Violin plot showing the distribution of thermal sensitivities of streams in the Cascade Range and the Coast Range. (B) The relationship between site-level thermal sensitivity values and model R^2 values. The red circle in (A) indicates likely locations of spring discharge and concentrated groundwater inflow.

In the Coast Range, the median site-level thermal sensitivity was 0.33 °C °C^{-1} and ranged between 0.10–0.77 °C °C^{-1} (R^2 = 0.11–0.93) (Table 2.5). Statistically, the median thermal sensitivity in the Coast Range was greater than in the Cascade Range streams (Wilcoxon Rank Sum test, $p < 0.01$, 95% CI: 0.039 – 0.171) (Table 2.5). Longitudinal patterns in thermal sensitivity varied by stream, but generally increased moving downstream in RIC and XRA (Figure 2.4). For instance, thermal sensitivity increased from 0.20 to 0.53 °C °C^{-1} over 300 meters from mid-reach (0.55 fractional distance upstream) to the bottom of RIC and from 0.26 to 0.49 °C °C^{-1} over 210 m in XRA (from 0.27 fractional distance upstream to the bottom of XRA). Alternatively, longitudinal trends in thermal sensitivity for streams HEN, IVE, and WIL did not show strong increasing or decreasing trends. However, there were some stream segments in those three streams where thermal sensitivity between proximate temperature sensors changed rapidly. For instance, in WIL the thermal sensitivity increased from 0.10 to 0.37 °C °C^{-1} over 28 m (from 0.45 to 0.36 fractional distance upstream), then decreased again to 0.10 °C °C^{-1} over 56 m moving downstream starting at 0.18 fractional distance upstream. The largest change in thermal sensitivity observed in the Coast Range streams occurred mid-reach (0.45 fractional distance upstream) in HEN, where thermal sensitivity increased from 0.18 to 0.77 °C °C^{-1} over 38 m and then decreased to 0.33 °C °C^{-1}; however, this particular stream segment went dry 17 days after the start of monitoring (June 18, 2018). Contrary to results in the Cascade Range, variability in site-level thermal sensitivity values in Coast Range streams was not well explained by the average daily mean stream temperature (R^2 = 0.06), indicating that the most thermally insensitive locations along Coast Range streams were not necessarily the coolest (Figure A4).

Table 2.5. Thermal sensitivity descriptive statistics for each stream and region.

Region	Stream	# of T_s sensors	Mean R^2 (range)	Mean (°C °C^{-1})	Median (°C °C^{-1})	SD (°C °C^{-1})	Minimum (°C °C^{-1})	Max (°C °C^{-1})
Cascade Range	BEA	12	0.55 (0.11–0.85)	0.13	0.09	0.09	0.05	0.31
	BUL	11	0.64 (0.48–0.84)	0.26	0.23	0.18	0.04	0.63
	SUG	10	0.55 (0.30–0.71)	0.33	0.31	0.13	0.10	0.59
	Sub-totals	33	0.58 (0.11–0.85)	0.24	0.23	0.16	0.04	0.63
Coast Range	HEN	8	0.60 (0.44–0.93)	0.36	0.32	0.19	0.18	0.77
	IVE	10	0.60 (0.32–0.78)	0.27	0.25	0.10	0.15	0.44
	RIC	9	0.55 (0.28–0.75)	0.39	0.37	0.14	0.20	0.59
	WIL	9	0.48 (0.11–0.65)	0.28	0.33	0.11	0.10	0.37
	XRA	8	0.66 (0.35–0.78)	0.37	0.35	0.09	0.27	0.50
	Sub-totals	44	0.58 (0.11–0.93)	0.33	0.33	0.13	0.10	0.77

2.5: Discussion

Our study in Northern California provided evidence that stream temperatures during the summer low flow period were generally warmer, but exhibited less diel variation, in Coast Range headwater streams compared to the Cascade Range. Specifically, mean daily stream temperatures were ~4.7 °C warmer in the Coast Range despite greater riparian canopy closure and air temperatures that were ~1.6 °C cooler than in the Cascade Range (Table 2.3). Although stream temperatures were warmer in the Coast Range relative to the Cascades, temperatures remained well within the range found to be tolerable for many anadromous salmonids or amphibians, which inhabit the region (Sloat & Osterback, 2013; Welsh, Hodgson, Harvey, & Roche, 2001).

Our observations in the Coast Range catchments, which occurred in the Caspar Creek Experimental Watershed Study, were also consistent with stream temperature measurements collected over eight years, between 1965–1990, from catchments in the same region (Cafferata, 1990). For example, while we observed summer maximum stream temperatures of 12.5 °C and diel variation of 0.9 °C, Cafferata (1990) reported summer maximums of ~13.3–15.6 °C and diurnal fluctuations of 0.8 °C. Cool summer stream temperatures in Coast Range streams have previously been attributed to the insulating effect of the dense riparian canopy, high humidity, and coastal fog due to the proximity to the Pacific Ocean (Cafferata & Reid, 2013; Lewis et al., 2000; Moore et al., 2005a). In particular, a dense forest canopy cover, as observed in the Coast Range (85 %), has been found to limit energy exchange across the stream-air interface and thus, act as a first order control on the magnitude of stream temperature and thermal sensitivity (Chang & Psaris, 2013; Simmons et al., 2014; Winfree et al., 2018).

Our measurements of the longitudinal variability in stream temperature also indicated that the streams in both the Coast Range and the Cascade Range exhibited complex thermal profiles (Fullerton et al., 2015). In other words, the longitudinal stream temperature profiles across all our study streams included multiple discontinuities, with sections of increasing and decreasing temperatures (Figure 2.3). However, there was greater longitudinal thermal heterogeneity in streams underlain by volcanic lithology (Cascade Range) than in streams underlain by sedimentary lithology (Coast Range). In

the Cascade Range, stream temperatures appeared to warm slightly moving downstream but cooled dramatically—dropping by as much as 2.0 to 7.0 °C, at discrete locations. Overall, this resulted in cooler average stream temperatures, despite warmer summer air temperatures, in the Cascade streams compared to the Coast Range streams. Similar discontinuities have previously been related to discrete groundwater discharge locations, which can thermally buffer streams against daily and seasonal temperature fluctuations (Snyder et al., 2015; Webb et al., 2008). Reduced diel stream temperature variation in the Cascade Range streams was also suggestive of the presence of concentrated groundwater discharge (Harrington, Hayashi, & Kurylyk, 2017; Surfleet & Louen, 2018). In part, this was expected, as the Cascade Range is underlain by highly fractured basalt bedrock, which has previously been shown in the Oregon Cascades to have high water holding capacity and high permeability, resulting in the majority of precipitation draining to groundwater and reemerging as cool springs (Jefferson, Grant, & Rose, 2006; Tague et al., 2007, 2008).

While the thermal buffering from these apparent locations of cool groundwater discharge extended several hundred meters downstream in two of our study streams in the Cascade Range (BEA and BUL), they were less pronounced in our other study stream (SUG). Thus, further research could provide valuable insights into how far downstream the influence of discrete groundwater discharge locations may persist, providing important cold-water refuges (Torgersen, Price, Li, & McIntosh, 1999). For example, in the Shasta River, a tributary to the Klamath in Northern California, Nichols, Willis, Jeffres, and Deas (2014) found that the thermal influence of spring discharge persisted downstream for 23 km, and suggested that understanding similar patterns was critical for managing cold-water fish habitat. Downstream cooling has been observed in other spring dominated systems (Harrington et al., 2017; Leach & Moore, 2011; Roon et al., 2021; Story et al., 2003; Surfleet & Louen, 2018), and has often been associated with the location of fractures or faults along underlying bedrock. Depending on the volume of groundwater discharge at these locations, stream temperatures may be modified for long distances downstream, with potentially important implications for aquatic habitat.

While the thermal profiles in the Coast Range streams were also complex, the downstream temperature variability was less dramatic than in the Cascade streams. The comparatively thin, friable soils in the Coast Range likely contributed to summer baseflow from spatially continuous shallow subsurface sources or perched areas of saturated soil on most of the streams (Keppeler & Brown, 1998), rather than discrete discharge from deep aquifers (Figure 2.6). Lateral inflow from a shallow layer at the base of the soil profile has previously been observed as the primary source of baseflow and a dominant control on stream temperature in a Coast Range watershed in the PNW (Moore et al., 2005b). Additionally, the step-pool geomorphology in the Coast Range streams may have contributed to hyporheic down-welling or sub-surface inter-gravel flow, which can contribute to greater thermal stability (Kasahara & Wondzell, 2003; Peterson & Sickbert, 2006).

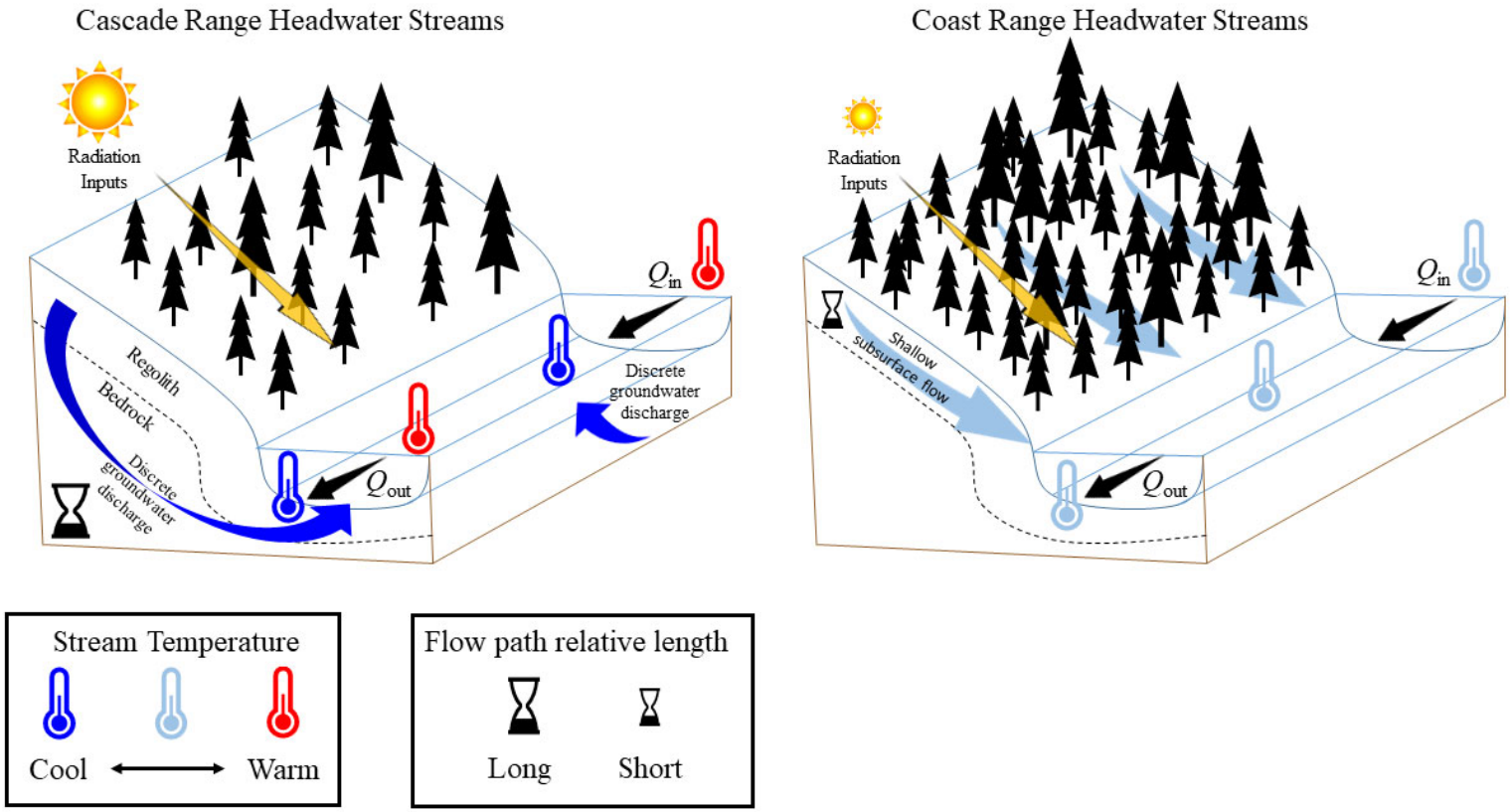

Figure 2.6. Hypothesized mechanisms behind major differences in the longitudinal thermal regimes between the Cascade (volcanic lithology) and Coast Range (sedimentary lithology) headwater streams.

Our results also highlighted the spatial variability in atmospheric control on stream temperature between the Coast Range and Cascade Range streams. Given the regional differences in climate and forest cover, we expected the influence of air temperature on stream temperature (i.e., thermal sensitivity) would be greater in the Cascade Range streams. However, streams were less thermally sensitive in the Cascade Range by 0.039–0.171°C $°C^{-1}$ compared to the Coast Range streams. Indeed, many stream segments along the Cascade Range streams were insensitive to changing air temperatures, despite large diel variability in air temperature. These low thermal sensitivities indicated a decoupling of atmospheric control on stream temperature that was likely due to the concentrated groundwater discharge from deep aquifers. Site level thermal sensitivity values in Cascade Range streams revealed that values less than 0.2 °C $°C^{-1}$ generally corresponded to locations with the coolest and least variable stream temperatures and likely, this threshold separated groundwater dominated versus surface flow dominated portions of the streams (Kelleher et al., 2012; O'Driscoll & DeWalle, 2006).

The importance of lithology as a first order control of groundwater contributions and stream thermal sensitivity was previously illustrated by Tague et al. (2007), who compared stream thermal sensitivities between spring dominated streams draining resistant volcanic lithology in the high Cascades and shallow sub-surface flow dominated streams draining less resistant lithology in the mid-Cascades of Oregon. They determined that spring dominated systems draining resistant lithology were less thermally sensitive than lower elevation shallow sub-surface flow systems due to differences in the magnitude of streamflow sourced from the subsurface. Indeed, headwater streams draining volcanic lithology and deep soils typically have a large proportion of summer baseflow generated from groundwater (Segura et al., 2019) that is derived from prior snowmelt or heavy rains (Tague et al., 2008). These inputs can dampen atmospheric sensitivity at discrete groundwater discharge locations, where the response to atmospheric warming may lag or mute air temperature signals (Briggs et al., 2018b). Briggs et al. (2018c) also determined that the magnitude of groundwater discharge varied longitudinally along a stream with the soil depth to bedrock and influenced the

attenuation of stream temperature signals by groundwater. The authors also determined that shallow aquifer sourced groundwater displayed considerable sensitivity to the downward propagation of heat derived from surficial advective and conductive sources. We posit that we observed similar drivers in our study. It is likely that the Cascade Range streams, characterized by comparatively deeper soils than the Coast Range, were more thermally buffered from atmospheric controls on stream temperature. Alternatively, the stream and air temperature signals were more closely coupled in the Coast Range.

There have been many previous studies that have assessed stream thermal sensitivity; however, the majority have occurred at a regional or larger scale across multiple river basins, rather than a headwater scale (Table 2.6). Despite differences in scale, several of these previous studies have illustrated low thermal sensitivity in groundwater dominated systems (Kanno, Vokoun, & Letcher, 2014; Kelleher et al., 2012; Segura et al., 2015; Tague et al., 2007), similar to our study. Previous studies also found a similar strength (R^2) in their linear regression relationships between stream temperatures and air temperatures (Hilderbrand et al., 2014; Segura et al., 2015; Snyder et al., 2015), as we found in our study, which was indicative that air temperature was only one controlling factor of stream temperature in headwater streams. For instance, baseflow index, a measure of groundwater contributions to flow, and stream size were two variables found to control stream thermal sensitivity in Pennsylvania streams (Kelleher et al., 2012), while drainage area and channel slope exerted the strongest control in regional thermal sensitivity studies (Segura et al., 2015; Winfree et al., 2018). Lisi et al. (2015) observed thermal sensitivity 5–8-times greater in low elevation, low gradient, rain dominated streams compared to high elevation, steep, snowmelt dominated streams due mainly to differences in slope and snowmelt contributions. Others have used measures of accumulated degree days above mean summer air temperature to act as a proxy of groundwater influence with success in stream temperature prediction to generate thermal sensitivity values (Snyder et al., 2015). Similarly, spatially variable groundwater inputs controlled thermal sensitivity magnitude (Kanno et al., 2014; O'Driscoll & DeWalle, 2006) and variability (Trumbo et al., 2014) elsewhere. In the present study, it is likely that site-level differences in riparian vegetation, discharge, and precipitation inputs

explain majority of the remaining variation in stream temperature, but our monitoring did not allow us to consider these factors at a site-level resolution.

Table 2.6. Results from our study and other studies that have quantified stream thermal sensitivity to air temperature at a range of spatial scales.

Thermal Sensitivity Range (°C °C^{-1})	Location	Temporal Resolution	Reference
0.04–0.77	8 streams in Northern California, US	Daily	Present study
0.19–0.67	12 sites in a Pennsylvania watershed	Weekly	O'Driscoll & DeWalle, 2006
0.39–0.61	6 sites across northern latitudes of the US	Daily	Simmons et al., 2014
0.35–1.09	43 streams internationally	Daily, Weekly	Morrill et al., 2005
0.20–0.65	80 boreal streams in SW Alaska	Daily	Lisi et al., 2015
0.02–0.93	57 sites across Pennsylvania	Daily, Weekly	Kelleher et al., 2012
0.10–0.82	78 sites in Shenandoah National Park, Virginia, US	Daily	Snyder et al., 2015
0.10–0.81	74 sites in the Columbia River Basin, US	Daily, Weekly	Chang & Psaris, 2013
0.13–1.25	157 sites across US, Air Temp > 0 °C	Weekly, Monthly	Segura et al., 2015
0.20–1.14	104 sites across US PNW	Weekly	Mayer, 2012
0.02–1.09	43 sites across the Oregon Cascades	Daily	Tague et al., 2007
0.13–0.79	46 sites across Maryland, US	Daily	Hilderbrand et al., 2014
0.01–0.58	43 coastal streams in SW Alaska	Daily	Winfree et al., 2018
0.49–1.08	61 sites across the Southeast US	Monthly	Caldwell et al., 2015

2.6: Conclusions

We compared the longitudinal thermal regimes and thermal sensitivity of eight headwater streams across two distinct regions of Northern California. In general, stream and air temperatures were less coupled in streams underlain by volcanic lithology

compared to streams underlain by sedimentary lithology. We posit that the decoupling of stream temperature from air temperature control in the Cascade Range streams was due to cool groundwater discharge, which occurred predominantly in streams underlain by volcanic lithology. Interestingly, we also observed less variability in longitudinal stream temperatures in the Coast Range streams— underlain by sedimentary lithology—despite a slight warming in the downstream direction. This was likely due to greater sensitivity of the comparatively warmer, shallower subsurface sources in the Coast Range, resulting in a greater coupling to atmospheric temperatures. Our study revealed the complexities in thermal regimes in headwater streams and the potential importance of lithology. Improved understanding of the dominant controls on thermal regimes of small headwater streams will become increasingly critical in the future. This knowledge is necessary to improve projections of aquatic habitat resiliency or vulnerability to pressures from climate change or shifting disturbance regimes, where land management decisions may become increasingly complex. As such, future research should continue to quantify the comparative roles of streamflow, groundwater, and streamside vegetation on fine-scale temperature dynamics and aquatic habitat viability in headwater streams across diverse regions. Additional research is also needed on downstream thermal propagation from spring dominated and shallow subsurface dominated headwater catchments.

Chapter 3: Characterizing stream temperature hysteresis in forested headwater streams: A preliminary investigation.

3.1: Abstract

Stream temperature is a critical water quality parameter that influences many aspects of aquatic systems. However, there have been few attempts to assess how stream temperature changes during storm events and in response to shifts in runoff generation. Thus, our objectives were to use hysteresis metrics to assess the relationship between stream temperature and stormflow across ten forested headwater catchments in Northern California during the 2020 water year. We instrumented each stream with 12 evenly distributed thermistors and four air temperature sensors. Our goal was to quantify the magnitude and variability of stream temperature hysteresis during rain events across seasons within and among catchments. Additionally, we sought to determine whether catchment topographic metrics (upslope accumulated area, topographic wetness index, flow weighted slope) could explain the stream temperature response to precipitation inputs. We hypothesized that the direction of hysteresis would vary across seasons due to changes in meteorological conditions and that the stream locations most hydrologically connected to the hillslope (as predicted by topographic indices) would exhibit the greatest hysteresis due to lateral throughflow inputs. Our results indicate that the stream temperature response to stormflow is seasonally variable and generally exhibits clockwise hysteresis during the summer and spring when air temperatures are warmer than stream temperatures and anti-clockwise hysteresis during the fall and winter when air temperatures are cooler than stream temperatures. In addition, the stream temperature response to stormflow was the most variable across these 10 catchments during the late summer and early fall, when catchment-scale wetness conditions and streamflow were low. As the wet season progressed, stream temperature behavior across these 10 catchments became more similar, and remained coupled through the late spring. The magnitude and direction of stream temperature hysteresis was well correlated with the gradient between stream and air temperatures at the start of the event (ρ = 0.49), and air temperature change during the storm rising limb (ρ = -0.49), indicating the potential role of regional meteorological conditions on stream temperature change during storm events.

None of the derived topographic metrics describing the preponderance of saturated areas and lateral inputs to streamflow were correlated with stream temperature change during events, potentially because subsurface topography and seasonally variable catchment wetness conditions could not be properly characterized with static metrics describing surface topography. Overall, these results indicate seasonally variable stream temperature behavior during storm events that become regionally synchronous as catchment moisture conditions increase during the wet season.

3.2: Introduction

Stream temperature is a critical water quality parameter that drives dissolved oxygen solubility (Fellman, Hood, Dryer, & Pyare, 2015; Loperfido et al., 2009; Ozaki et al., 2003), influences aquatic habitat (Brewitt et al., 2017), and important life history events for sensitive aquatic species such as salmonids (Caissie, 2006; Hester & Doyle, 2011; MacDonald et al., 2014b). In forested headwaters, stream temperature change is the result of energy exchange across the air-water interface, between the stream bed and banks, and through advective transport via groundwater or hyporheic upwelling (Moore, Spittlehouse, & Story, 2005; Webb, Hannah, Moore, Brown, & Nobilis, 2008). Recent literature has elucidated the influence of groundwater inflow (Briggs et al., 2018c; Larsen & Woelfle-Erskine, 2018; Snyder et al., 2015), hyporheic exchange (Briggs, Lautz, McKenzie, Gordon, & Hare, 2012; Surfleet & Louen, 2018; Wondzell & Gooseff, 2013), and hillslope derived throughflow (Leach & Moore, 2015, 2017; Uchida et al., 2002) on stream temperature variability across a range of scales. However, research assessing stream temperature change during storm events in forested headwaters is limited (Hebert et al., 2011), and there have been few dedicated efforts assessing the influence of storm events on the stream longitudinal thermal regime. For instance, during storm events, quickflow from shallow subsurface stormflow or preferential soil channels can strongly influence stream temperatures (Lange & Haensler, 2012; Leach & Moore, 2014; Subehi et al., 2010). This is despite precipitation heat flux often representing only 1–2% of the total heat flux reaching the stream (Hebert et al., 2011; Webb & Zhang, 1997). Others have linked seasonally variable antecedent moisture conditions (Lange & Haensler, 2012; Subehi et al., 2010), meteorological conditions (Herb et al., 2008; Somers et al., 2016),

and catchment topography (Leach et al., 2017; Subehi et al., 2010) to stream temperature dynamics during storm events. This indicates a seasonal response that likely varies with both regional meteorological and catchment-scale topographic characteristics such as local precipitation patterns (Croghan, Van Loon, Sadler, Bradley, & Hannah, 2019) and catchment slope (Subehi et al., 2010).

Because stream temperature is non-reactive, naturally occurring, and relatively inexpensive to monitor, it has potential utility as a tracer to understand surface water-groundwater interactions and subsurface hydrologic connectivity (Constantz et al., 2003; Leach et al., 2017; Oware & Peterson, 2020; Ploum et al., 2018; Shanley & Peters, 1988; Uchida et al., 2002). For instance, Uchida et al. (2002) monitored stream temperatures in a steep forested catchment in Japan to differentiate between contributions to stormflow from water at the soil-bedrock interface and shallow bedrock, effectively illustrating the sources of water contributing to stream flow during storms. Similarly, distributed temperature sensing technology was used to locate discrete areas of groundwater inflow (Leach et al., 2017; Ploum et al., 2018), with the hope of better understanding hydrologic connectivity at the reach scale.

Runoff generation in steep forested headwater catchments is often controlled by physiographic characteristics, such as geology and topography (Gabrielli et al., 2012; Gomi et al., 2010; Hangen et al., 2001; Zimmer & McGlynn, 2017) and by temporal variability in water inputs that drive catchment hydrologic storage (Amatya et al., 2016; Dralle et al., 2018; Sidle et al., 2000). During a storm event, precipitation is partitioned into one of several pathways depending on catchment rainfall intensity (Detty & McGuire, 2010), soil infiltration capacity (Gomi et al., 2010), antecedent moisture conditions (Lange & Haensler, 2012; Radke et al., 2019), and overall catchment storage (Zimmer & McGlynn, 2018, 2017). In forested catchments along the Northern California Coast, soil hydraulic conductivity is typically high and rainfall intensities low such that overland flow is rare (Keppeler & Brown, 1998), except on bedrock outcrops or areas with extremely shallow soils (Uchida et al., 2002). Therefore, subsurface flow pathways commonly dominate during storm events, but the exact partitioning of water inputs into shallow subsurface flow and deeper groundwater flow paths may vary depending on soil

characteristics, topography, and storm characteristics (Detty & McGuire, 2010; Gomi et al., 2010; Rinderer et al., 2014; Van Meerveld et al., 2015).

Hysteresis analysis has been used to characterize the transport of water quality constituents in catchments during storm events (Aguilera & Melack, 2018; Mistick & Johnson, 2020; Vaughan et al., 2017). Water quality hysteresis describes the phenomena where a measured constituent has a different relationship with or lags behind discharge during a storm event. This behavior is commonly separated by rising and falling limbs of the hydrograph, where transport behavior of the constituent of interest from the catchment varies between the two. Specifically, hysteresis metrics have recently been developed to easily quantify the direction, slope, and size of hysteretic loops and make comparisons between storms and catchments (Liu et al., 2021; Lloyd et al., 2016a, 2016b). During storm events or snowmelt episodes, stream temperature variability with streamflow exhibits hysteresis behavior (Blaen et al., 2013; Kobayashi et al., 1999). Hysteresis behavior has also been observed in the relationship between stream temperature and precipitation inputs (Kobayashi et al., 1999; Subehi et al., 2010). For instance, clockwise hysteresis behavior during storms when air temperatures are greater than stream temperatures may indicate thermal transfer from shallow quickflow sources that warm the stream water during the rising limb of the hydrograph. In addition, hysteresis loops with a positive slope likely indicate flushing of heat from the catchment that causes stream temperatures to rise towards the hydrograph peak, while loops with a negative slope indicate dilution of heat from the catchment (i.e., from deep-sourced groundwater or direct channel precipitation) (Kobayashi et al., 1999). Quantifying stream temperature hysteresis may provide insights into how headwater streams respond to storm events across seasons and catchment characteristics.

Forested headwaters represent the landscape features with the strongest connection between terrestrial and aquatic elements (Freeman et al., 2007; Schlosser, 1991), and are more reactive to inputs of precipitation than downstream reaches (Wilby et al., 2015). Thus unsurprisingly, there is continued interest in understanding the responsiveness of headwater channels to perturbations at the management-relevant reach scale. For instance, there have been recent calls for riparian forest management practices

to consider the variable hydrological connectivity inherent to forested headwaters (Kuglerová et al., 2014; Laudon et al., 2016; Tiwari et al., 2016), such as by incorporating wider riparian buffers near variable source areas (Erdozain et al., 2020; Roon et al., 2021). Indeed, certain locations along headwater channels in boreal systems have been measured to provide disproportionate contributions of runoff to streamflow given local topography and soil conditions. These discrete riparian inflow points (DRIPS) (Ploum et al., 2018) can have a large influence on stream water chemistry and temperature (Erdozain et al., 2020; Lowry et al., 2007), and require additional study to determine their influence on stream temperature during storm events. Topographic metrics, such as upslope accumulated area (UAA), topographic wetness index (TWI), and flow weighted slope (FWS) that theoretically describe the location of saturated soil and subsurface water flow paths have been used successfully to locate areas of strong lateral groundwater influence in boreal regions (Leach et al., 2017) and elucidate topographic control on stream temperature in southern Alaska (Callahan et al., 2015). However, such an analysis has not been undertaken in steep, temperate conifer forests like the coast redwood (*Sequoia sempervirens*) dominated North Coast range of California, USA. These metrics could potentially provide insight into whether some areas respond differently than others to precipitation inputs along headwater streams. This has important implications for quantifying available habitat and refugia to aquatic ecosystems and in understanding how forest harvesting activities or natural disturbance (windthrow, debris flows) influence runoff generation and the potential influence on water quality downstream.

Our objectives were to improve understanding of how forested headwaters respond to storm events by analyzing data collected from an array of distributed temperature sensors across ten catchments. To achieve our objectives, we addressed the following questions:

1. How does stream temperature hysteresis vary in forested headwater streams across seasons?
2. What storm, topography, or meteorological characteristics influence stream temperature hysteresis during storm events?

We used recently developed metrics to quantify the magnitude and direction of hysteresis in the streamflow-stream temperature relationship and topographic metrics of hydrological connectivity to compare the response to 23 storm events paired across ten headwater catchments across the Northern coast range of California, USA during the 2020 water year. Our intent was not to use this analysis to infer variable runoff generation mechanisms across these ten catchments, but to provide a preliminary exploration into how stream temperature hysteresis varies across headwater catchments, storm characteristics, and season.

3.3: Methodology

3.3.1: Study Locations

We collected data along ten headwater streams, which all drain to the Klamath River in the Northern California Coast Range, USA (Figure 3.1). The catchments ranged in area from 21 to 63 ha and were located in two distinct elevation ranges (Table 3.1). Five study streams (1 to 5) were located along the west fork of Tectah Creek between 425–500 m elevation. The other group of five streams (11, 13, 14, 15, 18) were located along McGarvey Creek at elevations below 190 m. The two groups of study catchments were separated by approximately 25 km. Stream valleys are V-shaped with considerable channel incision and steep slopes (19–31°) (Woodward, Lamphear, & House, 2011). The streams also have narrow riparian areas, resulting in strong confinement and coupling between the streams and hillslopes. All ten streams are characterized as perennial, step-pool systems (Fritz et al., 2020; Montgomery & Buffington, 1997) with a few small cascades. As such, most of the monitored stream lengths were perennial during the study, with the exception of mid-reach in streams 1, 3, and 14, and the most upstream portion of streams 11 and 13, which were dry during the late summer months. The monitored portions of these streams have average active widths less than two meters, with average stream channel slopes along studied reach lengths ranging from 8-15° (Table 3.1).

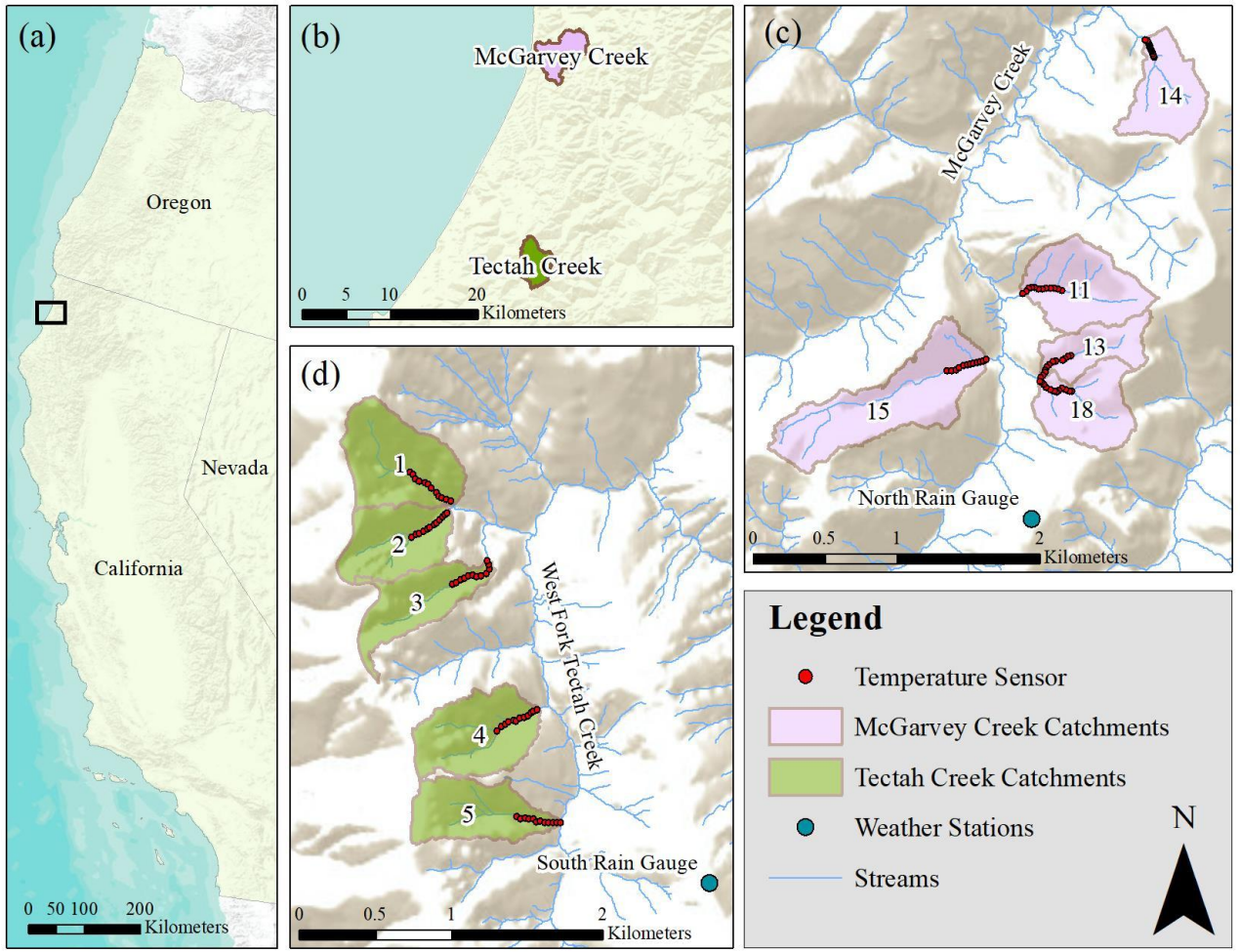

Figure 3.1. Map of study area locations, with (a) denoting general study location in Northern California, USA, (b) showing the catchment locations relative to each other, (c) detailing the McGarvey Creek catchments, and (d) outlining the Tectah Creek catchments.

Climate is characterized as temperate and maritime with a distinct wet-dry seasonality and considerable influence from coastal fog (Dawson, 1998). Summers are warm and dry and winters are mild and wet, with average annual air temperatures between 11 and 12 °C (PRISM Climate Group, 2021). The majority of precipitation occurs as rainfall between October and May, with an average annual rainfall of 2,900 mm in Tectah Creek and 2,000 mm in McGarvey Creek (PRISM Climate Group, 2021) (Figure 3.2). Accordingly, streamflow reaches an annual peak during mid-winter and an annual low during late summer. Vegetation consists primarily of 30–60-year-old second-growth Douglas-fir (*Pseudotsuga menziesii*) and coast redwood (*Sequoia sempervirens*), with western red cedar (*Thuja plicata*), and western hemlock (*Tsuga heterophylla*) occurring at lower densities, and red alder (*Alnus rubra*) and tanoak (*Notholithocarpus densiflorus*) becoming frequent in riparian areas. Riparian canopy closure along the streams is very high (above 90%) and similar across streams (Table 3.1). Soils are well-drained gravelly clay loams of the Coppercreek and Sasquatch series, with depths typically between 70 and 100 cm (Soil Survey Staff, NRCS, 2016). Field observations indicate increasing soil clay content with soil depth, and the uppermost soil layers are composed of extremely well drained organic detritus, likely leading to the presence of soil macropores and pipes that quickly transmit runoff as shallow subsurface stormflow to the stream (Amatya et al., 2016; Keppeler & Brown, 1998). The lithology consists of marine-derived sedimentary and metasedimentary rock of the Franciscan Complex (Woodward et al., 2011).

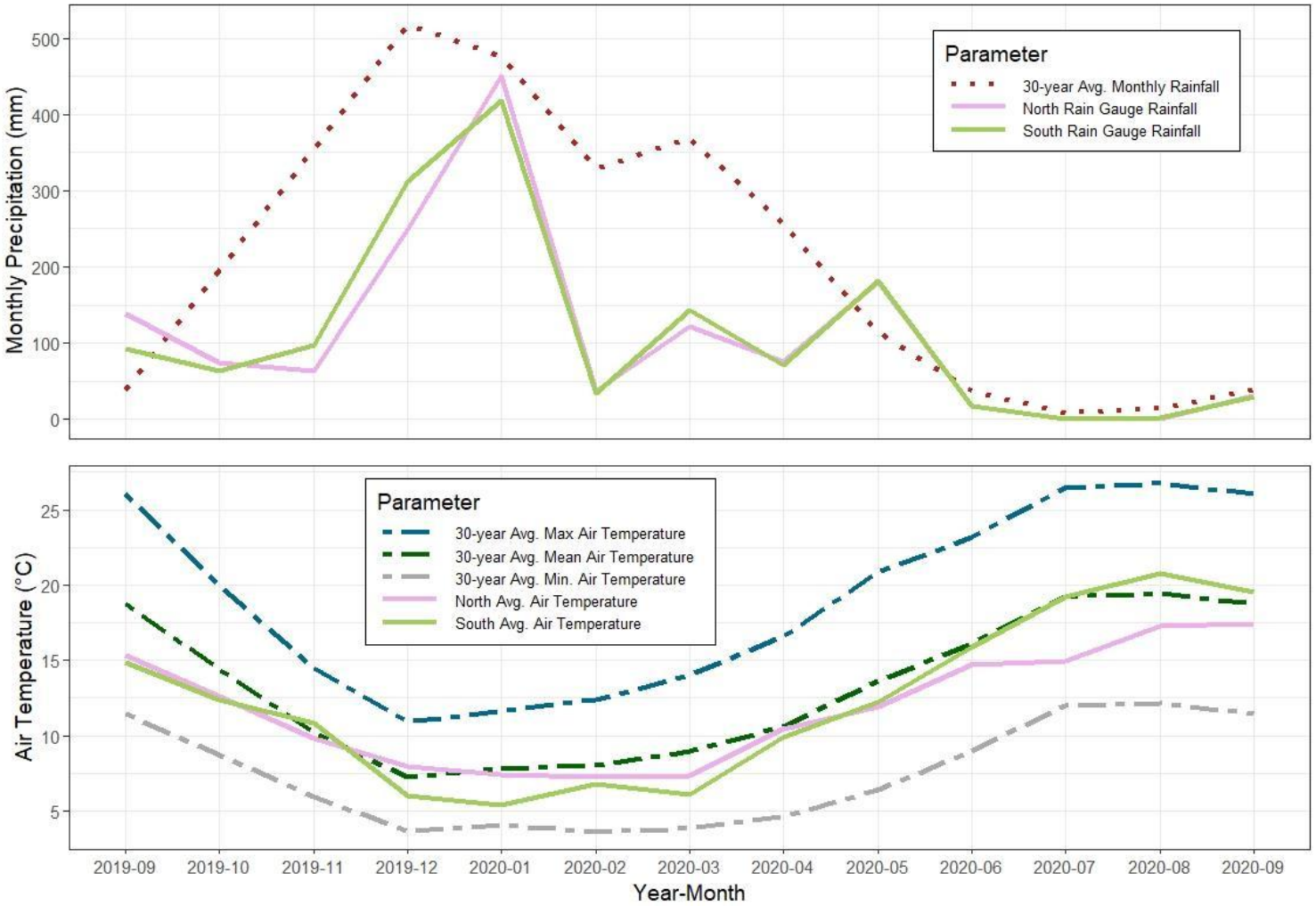

Figure 3.2. Monthly rainfall measured at the north and south rain gauge over the 2020 water year (top) and average monthly air temperatures (bottom) measured at the north and south rain gauge, compared to the 30-year average. (PRISM Climate Group, 2021).

Table 3.1. Study catchment characteristics. T_s = stream temperature.

Catchment	Watershed	Catchment Area (ha)	Average Elevation (m)	Monitored Length (m)	T_s Sensor Spacing (m)	Average Catchment Slope (°)*	Average Stream Slope (°)*	Riparian Canopy Closure (%)**	Average Active Width (m)
1	Tectah	38	462	305	28	25	12	97.4	1.7
2	Tectah	30	450	305	28	25	8	92.4	1.9
3	Tectah	28	452	305	28	24	9	93.6	2.0
4	Tectah	37	450	305	28	24	11	96.4	1.8
5	Tectah	30	463	305	28	19	10	98.1	1.4
11	McGarvey	40	114	305	28	31	12	97.6	1.7
13	McGarvey	21	153	305	28	25	15	97.2	1.9
14	McGarvey	30	82	202	18	30	11	94.2	2.0
15	McGarvey	63	85	305	28	27	12	99.6	1.8
18	McGarvey	32	133	305	28	26	9	97.0	1.4

* Derived from 1-meter DEM in ArcMap 10.8.1

** Measured as the average value computed for six hemispherical photos taken evenly throughout the riparian area adjacent to each monitored stream. Photos were analyzed using Hemi-View software (Delta-T Devices, Ltd., Cambridge, UK).

3.3.2: Data Collection

To quantify stream and air temperature, we installed 16 thermistors (Onset HOBO TidbiT v2, Bourne, MA; accuracy ± 0.21 °C) in each study stream. This included 12 in-stream sensors and four air temperature sensors, which were spaced approximately every 28 meters (except in stream 14, see Table 3.1) along each stream (Figure 3.1). Data was collected at a 15-minute resolution. Stream thermistors were affixed along the thalweg of the stream in sections of white PVC to minimize solar influences. We also drilled holes in the PVC to allow adequate mixing of stream water across the sensor. The four air temperature sensors were also enclosed in sections of white PVC and affixed either to rebar or trees adjacent to the stream channel at the top, bottom, and two midpoints of each stream. Stream and air sensor locations were recorded in Avenza Pro (version 3.14) on a Samsung Galaxy Tab Active2 Tablet (estimated accuracy ± 10 meters in closed canopy).

We also measured stream stage at the downstream end of each stream with a pressure transducer (Levelogger Edge, Model 3001. Accuracy: ± 0.05%, Solinst Canada Ltd., Georgetown, ON, Canada) housed in a PVC stilling well. A barometer (Barologger Edge, Model 3001. Accuracy: ± 0.05 kPa. Solinst Canada Ltd., Georgetown, ON, Canada) was placed at the outlet of streams 1 and 11 to quantify atmospheric pressure for compensation of stream stage. Manual measurements of stream stage were taken with a ruler at the base of each stilling well to the nearest half centimeter during 5 field visits (approximately every 2 months) to derive continuous stage data from the pressure transducers.

Discharge was estimated during a range of flow conditions using salt dilution gauging (Moore, 2005) to develop a stage-discharge relationship and calculate a timeseries of discharge. However, only a few salt dilution measurements (five to seven) were conducted at the time of this analysis, mainly during low flows, and prevented development of a robust rating curve for each of the ten catchments in our study. For this reason, we focused our analysis on relationships between stage and stream temperature. However, we also completed a supplementary analysis with discharge from the single most reliable rating curve (Figure A5) to assess the sensitivity of the hysteresis indices

we calculated. Statistically, there was no evidence that the hysteresis indices derived using a time series of discharge were different than those derived from a timeseries of stage (Figure A6, A7).

We also installed two weather stations (Onset HOBO U30 Data Logger, Bourne, MA) in central locations during summer 2019 to quantify precipitation, air temperature, solar radiation, relative humidity, soil moisture, air pressure, and wind speed direction. The weather stations were located in central locations—within 3 km of all study steams—to each of the two major groups of catchments (Figure 3.1). Precipitation data was collected via an Onset tipping bucket rain gauge (model S-RGB-M002, Onset, Bourne, MA). Solar radiation data was collected with an Onset pyranometer (model S-LIB-M003, Onset, Bourne, MA). Air temperature and relative humidity were collected via an Onset Temp/RH probe (model S-THB-M002, Onset, Bourne, MA). Soil moisture was monitored at 10, 30, and 60 cm depths at both weather stations with Onset soil moisture probes (model S-SMD-M005, Onset, Bourn, MA). Wind speed and wind direction were monitored using Onset sensors (model S-WSB-M003 and S-WDA-M003, respectively, Onset, Bourne, MA). Air pressure was monitored with an Onset barometer (model S-BPB-CM50, Onset, Bourne, MA). All data were collected at a 15-minute resolution.

3.3.3: Data Analysis

We focused our analysis of stream temperature change during storm events on events that occurred during the wet season of the 2020 water year (October 1, 2019–June 15, 2020), but also included the first significant summer storms, which occurred in September 2019. Individual storm events were identified if there was at least 6-hours between event tips in the precipitation data (Driscoll, 1989). Initial analysis was limited to storm events with a minimum depth of 10 mm, as this depth of rainfall was visually determined as the threshold of rainfall necessary to achieve an in-stream response (i.e., a change in stream stage). This yielded 40 storm events for the Tectah Creek study area and 38 events for the McGarvey Creek study area.

Prior to storm event separation, stream and air temperature data were visually inspected to remove periods when sensors were not submerged or behaving abnormally. To do this, we visually assessed and compared the diel temperature range of stream temperature and adjacent air temperature sensors to discern periods when sensors were dry or removed from flow (Campbell et al., 2013; Sowder & Steel, 2012). We also relied on visual inspection and field notes from routine field visits to help identify periods when stream segments may have been dry. Periods of data during the study period when evidence suggested stream drying were removed.

Hydrograph recession was assumed to end when stream stage reached the stage value closest to what it was at the beginning of rainfall by minimizing the difference between the initial stage value and each subsequent stage value, within twice the storm duration following the end of each storm event. Therefore, storm duration was defined as the time from the onset of the first tip in the precipitation data to the time of hydrograph recession. Any storm event where stream stage did not recede to less than half the maximum stage before the onset of the next storm was excluded to constrain our analysis to storms with hydrographs that are not influenced by succeeding events. This resulted in between 13 and 32 storms in McGarvey streams, and 17 and 27 storms in Tectah streams being carried forward for initial analysis (Figures A7 to A16). Due to equipment failure, stage data was only available in stream 13 for storms prior to January 24, 2020.

3.3.3.1: Storm hysteresis behavior

We used hysteresis analysis to quantify the event-based temporal relationship between stream temperature and stream stage. We also used the analysis to provide a means to quantitatively assess how stream temperature in headwater catchments responds to precipitation inputs and changes in streamflow across seasons (Subehi et al., 2010). Hysteresis loops can be used to describe the shape, magnitude, direction, and slope of the stream temperature-stage relationship during storm events, where the slope of the loop and rotational direction (clockwise or anti-clockwise) may be used to detect different flow pathways that contribute runoff during events (Aguilera & Melack, 2018; Evans & Davies, 1998). The hysteresis index (HI) proposed by Lloyd, Freer, Johnes, & Collins (2016) was used to assess variable stream temperature responses to precipitation events

among streams and through seasons. This HI is attractive for hysteresis analysis because it is constrained between 1 and -1, with positive values associated to clockwise hysteresis and negative values denoting anti-clockwise hysteresis. Clockwise (Anti-clockwise) direction indicates stream temperatures are warmer (cooler) on the rising limb than the falling limb of the storm hydrograph. The magnitude of the HI corresponds to the 'fatness' of the loop, where hysteresis loops with HI values close to |1| have a greater area than those with HI values close to |0|. This index requires normalizing flow (stage) (Equation 3.1) and temperature (Equation 3.2) values for each storm to make comparisons possible among storms and catchments:

$$Normalized\ Q_i(stage) = \frac{Q_i - Q_{min}}{Q_{max} - Q_{min}} \tag{3.1}$$

$$Normalized\ T_i = \frac{T_i - T_{min}}{T_{max} - T_{min}} \tag{3.2}$$

where Q_i is the stream stage at time i, Q_{min} and Q_{max} are the minimum and maximum stage measured over the storm event, T_i is the stream temperature measured at time i, and T_{min} and T_{max} are the minimum and maximum stream temperature measured over the storm event.

The HI (Equation 3.3) is computed by finding the difference between temperature values on the rising and falling limb of the hydrograph for even intervals of the change in stage. This involves splitting the time series of stage and stream temperature for each storm into two sections, one prior to the peak stage, and one after the peak stage value. We used 2% intervals of normalized stage to compute differences in stream temperature on the rising and falling limb for each storm (as in Vaughan et al., 2017). The average of these differences for each storm event is the HI.

$$HI = \frac{\sum(T_{RL\_normalized} - T_{FL\_normalized})}{n} \tag{3.3}$$

where $T_{RL\_normalized}$ is the normalized temperature value at an interval of normalized stage on the rising limb of the hydrograph, $T_{FL\_normalized}$ is the normalized temperature value at the same interval of normalized stage on the falling limb, and n is

the number of rising limb-falling limb pairs. An HI value was calculated for every stream temperature monitoring location that was submerged at the start of the event along each stream.

We also calculated the flushing index (FI) to quantify whether stream temperature increased or decreases during the rising limb of the storm hydrograph (Butturini, Alvarez, Bernał, Vazquez, & Sabater, 2008; Vaughan et al., 2017) (Equation 3.4):

$$FI = T_{peak\_normalized} - T_{i\_normalized} \quad (3.4)$$

where $T_{peak\_normalized}$ is the normalized temperature value at the hydrograph peak, and $T_{i\_normalized}$ is the normalized temperature value at the onset of precipitation. Similar to the HI, FI is also constrained between -1 and 1. A positive FI indicates stream temperatures increase on the rising limb of the event and heat is delivered (or flushed) to the stream. When FI is negative, stream temperatures decrease during the rising limb, indicating heat is lost (or diluted) from the stream. A FI value of 1 indicates that peak stream temperatures coincide with the peak stage value during an event. For analysis of HI and FI values, any storm event that had computed HI and FI values from less than six of the ten catchments was removed from the analysis to prevent our results from being biased towards certain catchments. This resulted in up to 23 paired storm events across six or more of the ten catchments being analyzed (Table A4).

3.3.3.2: Topographic analysis

Topographic metrics including upslope accumulated area (UAA), topographic wetness index (TWI), and flow weighted slope (FWS) were calculated for each stream temperature monitoring location. This was done to assess whether the magnitude and direction of hysteresis metrics describing the stream temperature response to storm events could be explained by indices that relate surface topography to runoff generation processes (Callahan et al., 2015; Leach et al., 2017). A primary assumption of all three metrics is that subsurface hydrologic flow pathways reflect surface topography. This may not be a valid assumption in areas with lithology characterized by extensive bedrock fractures, complex soil structure, or where bedrock and surface topography are dissimilar (Freer et al., 2002; Gabrielli et al., 2012; Genereux et al., 1993).

UAA is defined as the area of land draining to a single point on the stream channel from either side of the stream. For this analysis, we calculated UAA as the sum of the area draining from both sides of the stream (e.g., the drainage area at each stream temperature sensor location). TWI relates flow accumulation values and local slope for each DEM cell as (Equation 3.5):

$$TWI_i = \ln(\frac{UAA_i}{Tan(\beta_i)}) \quad (3.5)$$

where TWI_i is the topographic wetness index at each DEM grid cell, UAA_i is the flow accumulation area per unit contour width (cell width; m), and β_i is the grid cell slope (°) (Beven & Kirkby, 1979). Values with a high TWI are topographically predicted to remain saturated longer than those areas with low values of TWI, and thus may represent areas where groundwater levels are higher and therefore more responsive to precipitation inputs. We computed two values of TWI for each stream temperature monitoring location: the point value and an average value for the entire upslope accumulated area (as in Rinderer, Van Meerveld, & Seibert, 2014).

Flow weighted slope (FWS) is an alternative metric to the TWI that integrates local slope and flow accumulation values for each DEM cell. FWS is the sum of the product of the slope and flow accumulation value for each pixel in the area of interest divided by the sum of the flow accumulation of all pixels in the area of interest (Callahan et al., 2015; Walker, King, Whigham, & Baird, 2012). FWS is calculated as (Equation 3.6):

$$FWS = \sum(\beta_i * FA_i) \,/\, \sum(FA_i) \quad (3.6)$$

where FWS is the flow weighted slope, FA_i is the flow accumulation value for each cell in the area of interest (m^2), and β_i is the grid cell slope (°). FWS values reported herein correspond to each stream temperature monitoring location. Low FWS values indicate an upslope area with a lower gradient and higher topographically predicted wetness than locations with higher FWS values (Callahan et al., 2015; Walker et al., 2012).

Calculations were carried out using 0.25-meter resolution digital elevation models (DEMs) for both study areas in ArcMap 10.8.1 (ESRI®, Redlands, CA). The DEMs were first preprocessed by coarsening to 1-meter resolution to remove minor topographic discrepancies and by filling sinks (Wang & Liu, 2006). The Deterministic 8 method was used to calculate a flow accumulation grid and compute UAA (O'Callaghan & Mark, 1984), and TWI was calculated using the Topographic Wetness Index tool within the TauDEM toolbox for ArcMap (Tarboton, 1997). To resolve differences between GPS-recorded locations of stream temperature sensors and their actual location in the field, we first assessed the distribution of differences between GPS-derived sensor locations and the flow accumulation derived stream channel (average difference = 2.1 meters, SD = 2.0 meters). Then, we snapped GPS-derived sensor locations to the nearest location on the DEM derived stream channel. We assumed that because, on average, the difference between GPS-derived sensor locations and snapped sensor locations to the channel were much less than the stated GPS accuracy (± 10 meters), these snapped locations represented the best estimate for the actual sensor locations on the DEMs we utilized. To provide an upper and lower bound on the potential true value of each topographic metric at each sensor location, we calculated average values of UAA, TWI, and FWS for all cell locations on the stream channel within a three-meter radius of each snapped sensor location. Values of all three topographic metrics from within this three-meter radius were used to compute average point values for UAA, TWI, and FWS that were used as predictors in a correlation analysis. Locations along each stream with greater values of UAA and TWI are predicted to have greater subsurface lateral inflow and remain wet longer based on their topographic position and local slope.

3.3.3.3: Statistical Analysis

We analyzed the hysteresis metrics (HI and FI) between seasons using a Welch's F-test. This approach was selected because a Levene's test indicated that the distribution of seasonal hysteresis metrics had unequal variances. The assumption of normality for both hysteresis metrics was assessed visually using Q-Q plots and were reasonably satisfied. To account for unequal variance, seasonal differences in both HI and FI were assessed using the Games-Howell post-hoc multiple comparisons method in the *rstatix*

package (Kassambara, 2021). Differences in mean storm characteristics measured at both weather stations were assessed using paired t-tests.

To assess potential drivers of either HI and FI, we included 30 predictor variables in a correlation matrix, including variables describing storm, hydrologic, and topographic characteristics (Table A5). We chose the variables *a priori* based on knowledge of potential drivers of stream temperature behavior during storm events. To assess the relationships between the variables and the hysteresis metrics, we created a correlation matrix using the R package *corrplot* (Wei et al., 2017). As part of this correlation, we included both the HI and FI values, and the absolute value of HI and FI values to assess what variables may drive the direction (positive or negative) and magnitude (absolute value) of stream temperature hysteresis. We calculated the Spearman's rank correlation coefficient, ρ, because the distribution of many predictor variables were non-normally distributed (Spearman, 1904). The Benjamini & Hochberg *p*-value adjustment for multiple comparisons was used to minimize the false discovery rate (Benjamini & Hochberg, 1995). All data exploration, quality control, and statistical analysis were conducted in R version 3.6.1 (R Core Team, 2020).

3.4: Results

3.4.1: Storm Characteristics

During the 2020 water year, ~1,431 mm of rain fell in the Tectah Creek catchments and ~1,402 mm fell in the McGarvey Creek catchments. Relative to the 30-year average annual rainfall, precipitation during this year in these catchments represented only 50% in Tectah Creek and 70% in McGarvey Creek, respectively (Oregon State PRISM, 2021).

In total, we selected up to 23 storm events across the 10 catchments to analyze the stream temperature response. The storm events ranged in magnitude from 10.6 to 79.2 mm (35.4 ± 17.5 [SD] mm), with storm durations between 5.8 and 76.8 hours (24.4 ± 14.5 hr), and average intensities from 0.57 to 4.37 mm hr^{-1} (1.7 ± 0.83 mm hr^{-1}) (Table A4). Two of the 23 events occurred during the late summer when antecedent moisture conditions and baseflow were at their annual low. Four events occurred during early fall (October–November), that represents a transitional period where average soil moisture increased from 0.17 m^3/m^3 to 0.25 m^3/m^3 and average air temperatures decreased from 14.8 °C to 11.6 °C compared to September (Figure 3.3). December and January were the wettest and coldest months over the study period (average soil moisture = 0.30 m^3/m^3, average air temperature = 5.7 °C) containing nine of the 23 analyzed storms and half of the total rainfall (50% at the North rain gauge and 51% at the South rain gauge). February was uncommonly dry, with only ~35 mm total precipitation, which represents ~15% of the 30-yr average. Despite how dry it was, we still captured one storm event during this time, which represented a period of low antecedent precipitation conditions (Table A4). The seven remaining events occurred during spring in April and May, when soil moisture remained elevated but air temperatures warmed (average soil moisture = 0.29 m^3/m^3, average air temperature = 11.1 °C).

The 14-day antecedent precipitation conditions prior to the storm events followed a seasonal pattern across both the Tectah and McGarvey catchments. Specifically, the lowest antecedent precipitation occurred during the summer and early fall and highest antecedent precipitation occurred during mid-winter (Figure 3.4B). Volumetric soil water

content data from soil moisture probes installed at three depths adjacent to the south weather station confirmed this trend in subsurface moisture, with the annual high occurring during mid-January (0.33 m^3/m^3), and low occurring prior to the first significant rain event in September 2019 (0.11 m^3/m^3) (Figure 3.3). In general, the average rainfall intensities and maximum rainfall intensities were greatest during early season storms and decreased through the wet season (Figure 3.4C and 3.4D). Statistically, there was no evidence that mean storm depth ($t = 0.79$, $p = 0.43$), 14-day antecedent rainfall ($t = -0.26$, $p = 0.80$), or average rainfall intensity ($t = -0.31$, $p = 0.76$) were different between the two meteorological stations. There was weak statistical evidence that maximum 1-hr rainfall intensities ($t = 1.75$, $p = 0.09$) were different between our two meteorological stations, however the mean difference between stations was small (1.05 mm/hr) and likely not substantial. Therefore, storm characteristics did not meaningfully differ across the study area.

3.4.2: Catchment Scale Analysis of Hysteresis Metrics

Hysteresis analysis yielded up to 12 HI values per stream for each storm, corresponding to each stream temperature measurement location. HI values varied in direction and magnitude between season, storm, and catchment. Positive HI values, indicating clockwise hysteresis, generally occurred during summer and spring events. Negative HI values, or anti-clockwise hysteresis, mainly occurred during fall and winter events (Figure 3.5).

The average HI value for summer events across all 10 catchments was 0.15 ± 0.25 (SD), but decreased during fall events to -0.06 ± 0.36. The average HI value for winter events was also negative at -0.18 ± 0.27, but was positive for spring events at 0.05 ± 0.26 (Table 3.2). Statistically, the Games-Howell post-hoc multiple comparisons tests indicated strong evidence that mean HI values across all 10 catchments were different among all seasonal combinations. The largest difference in mean HI values were between summer and winter events ($p < 0.001$, difference: 0.34, 95% CI: 0.29–0.39), and smallest between summer and spring events ($p < 0.001$, difference: 0.11, 95% CI: 0.05–0.16).

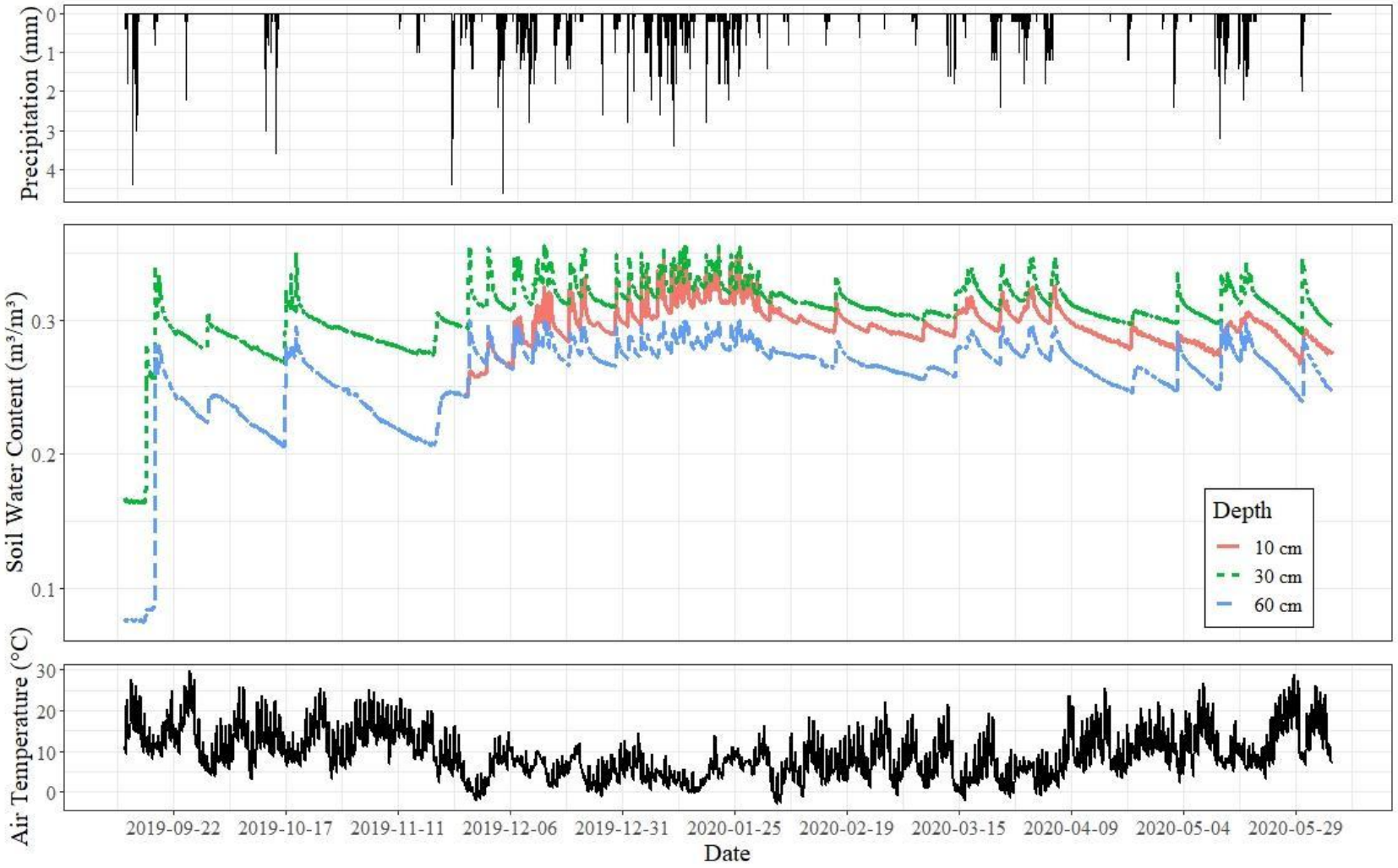

Figure 3.3. Precipitation, volumetric soil water content, and air temperature at the South meteorological station in the Tectah study area.

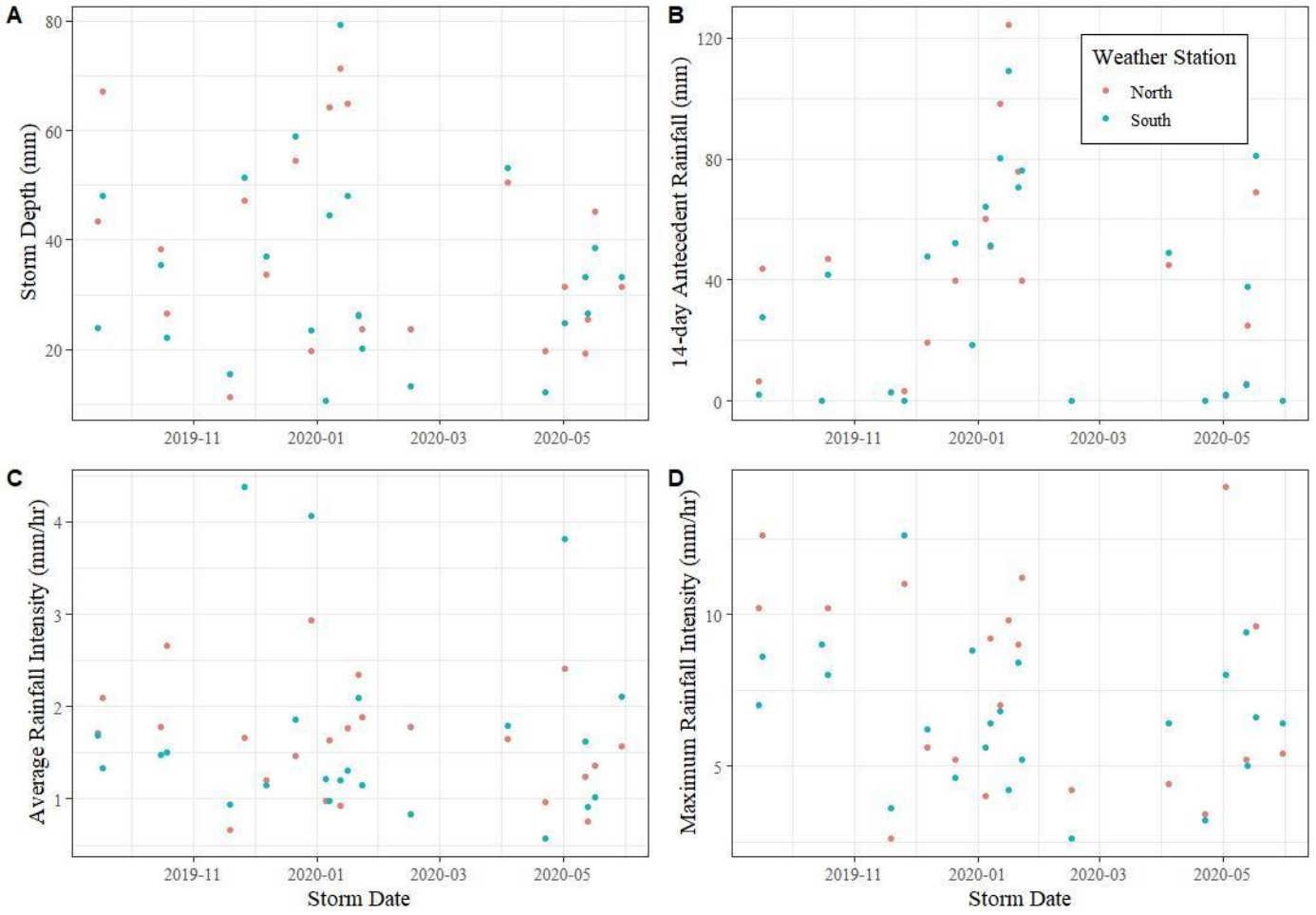

Figure 3.4. Storm event descriptive statistics between September 15th, 2019 and May 30th, 2020 by storm date for both the North (McGarvey) and South (Tectah) meteorological stations. (A) storm depth (mm), (B) 14-day antecedent rainfall (mm), (C) average rainfall intensity (mm hr^{-1}), and (D) maximum one-hour rainfall intensity (mm hr^{-1}).

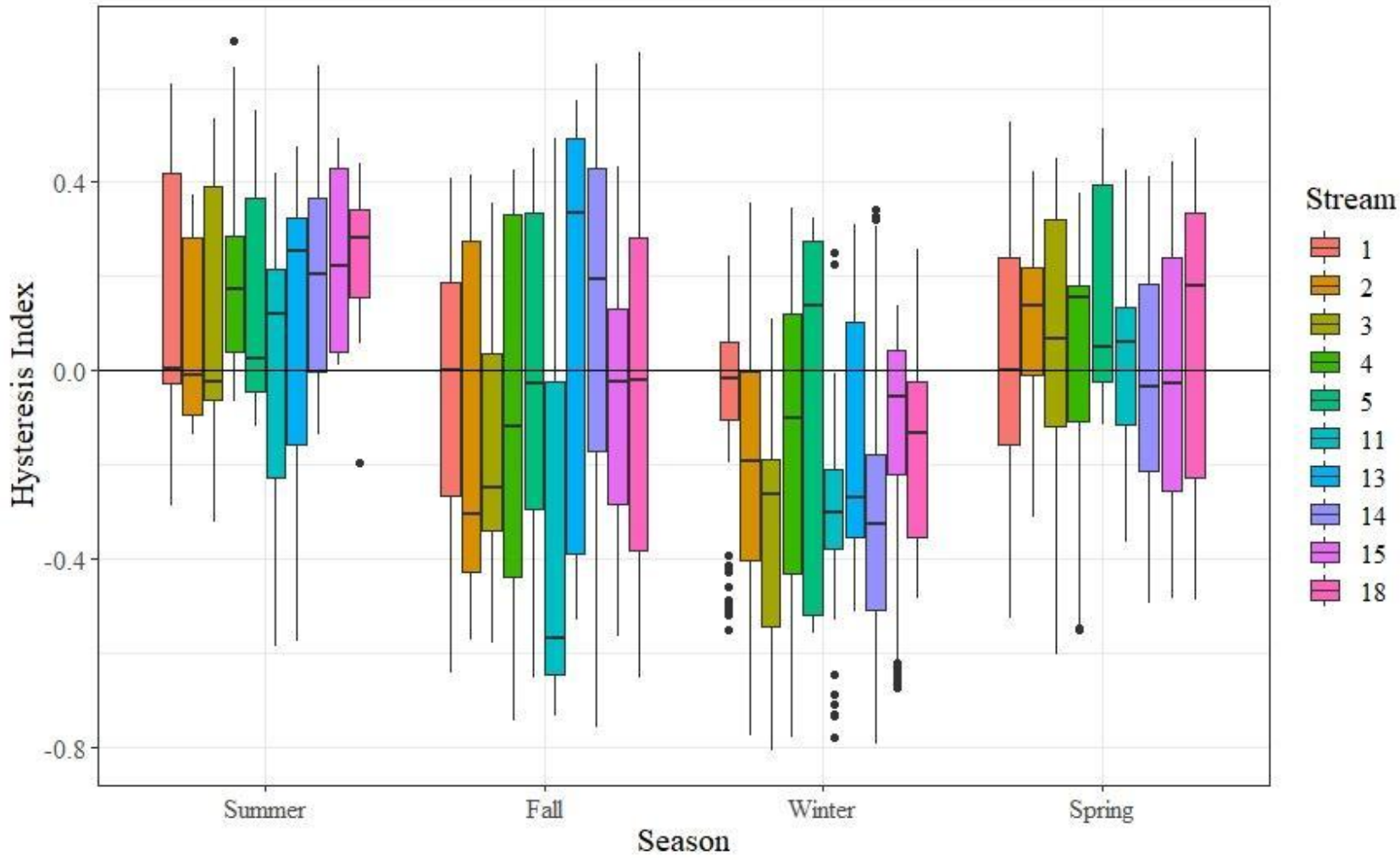

Figure 3.5. Distribution of hysteresis index (HI) values measured for each stream, grouped by season. The number of storms analyzed in each season varied: summer $n = 2$; fall $n = 6$; winter $n = 8$; spring $n = 7$.

These general seasonal trends were subject to variability from stream to stream. As an example, HI values during fall storms were the most variable among the 10 catchments (SD: 0.36). During these events, streams 13 and 14 had average HI values greater than zero (0.11 and 0.09, respectively), indicating weak clockwise hysteresis, while nearby stream 11 had an average HI value of -0.32, indicating anti-clockwise hysteresis behavior. For the remaining seasons, stream-average HI values were either all positive (for summer and spring, except streams 14 and 15 in spring) or all negative (winter) (Table 3.2).

In contrast to HI values, season-average flushing index (FI) values were consistently positive across seasons, with the exception of streams 13 and 18 (Figure 3.6). This indicates that stream temperatures in these catchments most commonly increased on the rising limb of the storm hydrograph, likely indicating a weak flushing of heat from the catchment. Season-average FI values were highest during summer events (0.30 ± 0.35) and decreased through fall and winter to a seasonal low in spring (0.10 ± 0.33) (Table 3.2). FI values in stream 13 were consistently negative across seasons, with the exception of spring, when data could not be collected due to equipment failure. Statistically, the results of the Games-Howell multiple comparisons test indicated that there was no evidence that season-averaged FI values were different between fall and winter ($p = 0.15$). However, there was suggestive evidence that season average FI values were different between summer and fall ($p = 0.07$) and strong evidence that they differed between summer and spring ($p < 0.001$, estimate: 0.21, 95% CI: 0.14–0.28).

Table 3.2. Seasonal hysteresis statistics for the study period. Avg.: Average, Std.: Standard Deviation, HI: Hysteresis Index, FI: Flushing Index.

		Stream										
Metric	**Season**	**1**	**2**	**3**	**4**	**5**	**11**	**13**	**14**	**15**	**18**	**Overall Average**
Avg. HI	Summer	0.13	0.09	0.12	0.21	0.15	0.00	0.08	0.19	0.24	0.24	0.15
	Fall	-0.05	-0.14	-0.11	-0.10	-0.02	-0.32	0.11	0.09	-0.04	0.00	-0.06
	Winter	-0.08	-0.20	-0.33	-0.15	-0.04	-0.30	-0.15	-0.28	-0.14	-0.14	-0.18
	Spring	0.03	0.09	0.05	0.03	0.17	0.04	-	-0.02	-0.02	0.08	0.05
Std. HI	Summer	0.27	0.20	0.27	0.22	0.24	0.33	0.41	0.22	0.21	0.14	0.25
	Fall	0.28	0.35	0.29	0.38	0.32	0.45	0.44	0.40	0.29	0.42	0.36
	Winter	0.20	0.31	0.24	0.31	0.36	0.20	0.27	0.37	0.24	0.20	0.27
	Spring	0.27	0.23	0.30	0.29	0.23	0.23	-	0.24	0.26	0.29	0.26
Avg. FI	Summer	0.38	0.28	0.36	0.41	0.24	0.46	-0.20	0.42	0.18	0.23	0.28
	Fall	0.26	0.39	0.26	0.29	0.33	0.28	-0.13	0.01	0.26	-0.05	0.19
	Winter	0.28	0.36	0.35	0.31	0.19	0.04	-0.09	0.06	0.15	-0.04	0.16
	Spring	0.06	0.05	0.02	0.15	0.19	0.17	-	0.10	0.11	0.08	0.10
Std. FI	Summer	0.28	0.11	0.30	0.24	0.32	0.27	0.66	0.59	0.24	0.44	0.34
	Fall	0.44	0.41	0.47	0.34	0.42	0.34	0.46	0.52	0.18	0.38	0.40
	Winter	0.45	0.46	0.27	0.48	0.13	0.54	0.52	0.23	0.42	0.49	0.40
	Spring	0.32	0.37	0.30	0.35	0.40	0.32	-	0.25	0.26	0.35	0.33

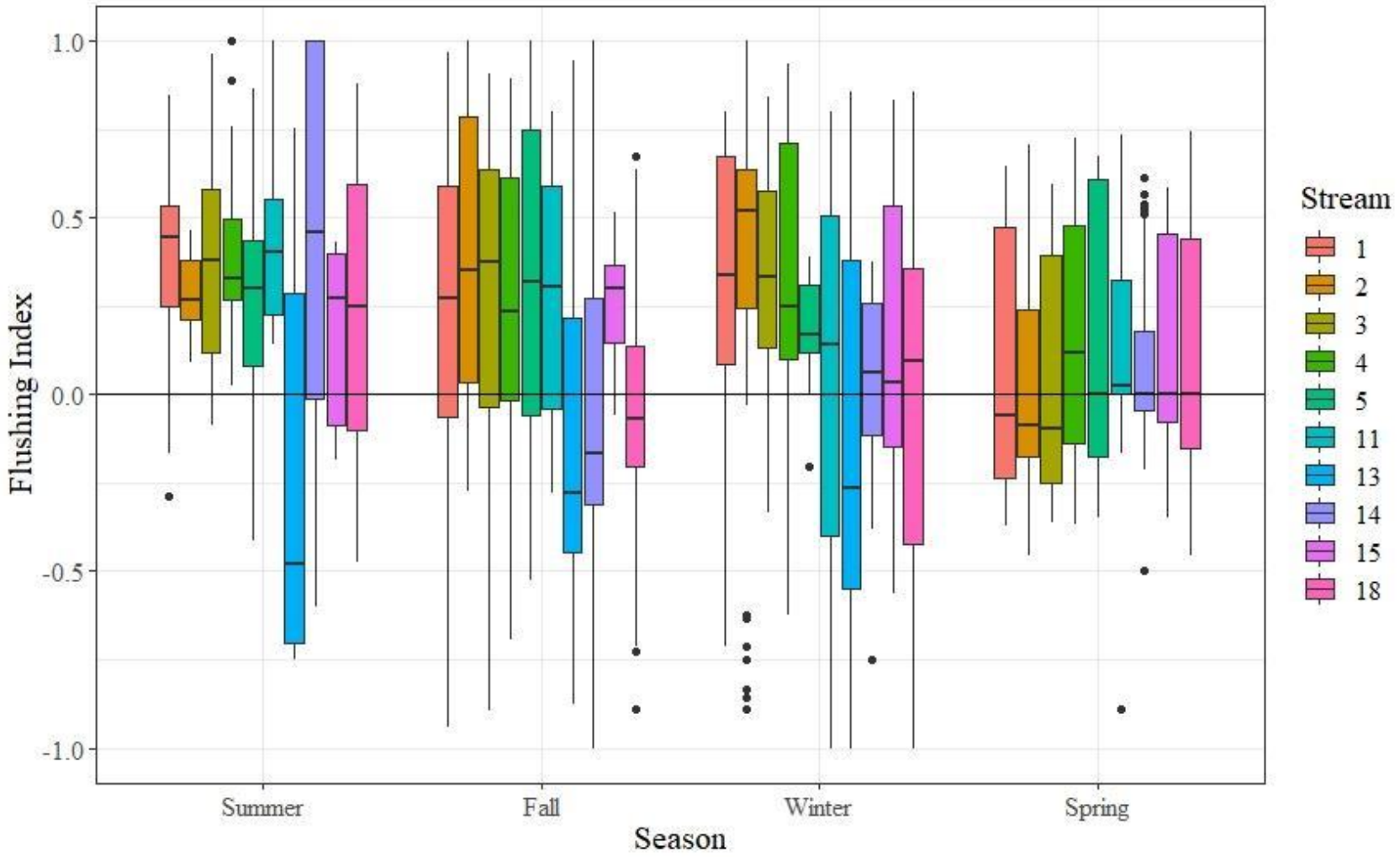

Figure 3.6. Distribution of flushing index (FI) values measured for each stream, grouped by season. The number of storms analyzed in each season varies: summer $n = 2$; fall $n = 6$; winter $n = 8$; spring $n = 7$.

For 12 of the 23 storms analyzed (52%), all catchments exhibited a similar stream temperature hysteresis pattern across both the Tectah and McGarvey watersheds (Table 3.3). As well, for seven of the 23 events, all but one or two streams exhibited the same hysteresis pattern (82% of storms total). As an example of this consistent intra-catchment behavior, for the summer 24 mm storm on 2019-09-15 (43 mm measured at the North weather station) with low antecedent moisture (~8 mm 14-day antecedent rainfall), the average HI value was 0.25 across all 10 catchments, with a standard deviation value of just 0.12 (Figure 3.7). Similarly, the winter 48 mm event (65 mm at the North weather station) on 2020-01-16 with high antecedent moisture (~190 mm 14-day antecedent rainfall) had an average HI values of -0.42 and standard deviation of only 0.08. These events represent different storm characteristics but were expressed similarly across the 10 study catchments, which was common for the storms analyzed herein (Figure 3.7). The remaining four (18%) events exhibited both positive and negative hysteresis across all catchments, resulting in average HI values near 0.

For majority (82%) of events, hysteretic behavior was similar across all the catchments, however there were storm events occurring close in time that had very different hysteresis behavior, indicating deviations from the seasonal trend described above (Figure 3.7). For example, two of six (33%) fall events and one of eight (13%) winter events had average HI values greater than 0, while the remainder had average HI values less than 0. As an example, the 59 mm late fall event on 2019-12-21 (54 mm measured at the North weather station) with high antecedent moisture (~150 mm 14-day antecedent rainfall), had an average HI value of 0.37 ± 0.10. Only a week later, during the high-intensity 23 mm (19 mm at the North weather station) winter event on 2019-12-29 with intermediate antecedent moisture (~76 mm 14-day antecedent rainfall), the direction of hysteresis changed to anti-clockwise with an average HI value of -0.66 ± 0.08. Interestingly, average air temperatures during the events were similar (5.14 and 5.55 °C for the 2019-12-21 and 2019-12-29 events, respectively), and average stream temperatures were only marginally lower during the 2019-12-29 event (8.39 versus 9.48 °C). These events reflect the variability in stream temperature behavior during storm events, even during subsequent storms.

Storm-average FI values averaged across all streams were greater than zero for 14 of 16 events (88%) during the summer, fall, and winter, with the exception of one storm during the fall (2019-12-21, average value = -0.12) and one storm during the winter (2020-01-21, average value = -0.42) (Table 3.4). Four of the five (80%) late spring events had negative average FI values (range from -0.03 to -0.27), indicating a loss of heat from the catchment during the storm hydrograph rising limb (Figure 3.7). FI values were more consistent across events than HI values; however, FI values also shifted rapidly from positive to negative during the wettest portion of the mid-winter. During the 48 mm event (65 mm at the North weather station) on 2020-01-16, the average FI value was 0.06 ± 0.49, four days later it was -0.42 ± 0.37 during the 26 mm event on 2020-01-21, 2 days after that it was positive again with a value of 0.35 ± 0.45 during the 20 mm storm on 2020-01-23. The events on 2020-01-21 and 2020-01-23 had very similar storm characteristics, but different stream temperature behavior during the initial input of precipitation (Table 3.4).

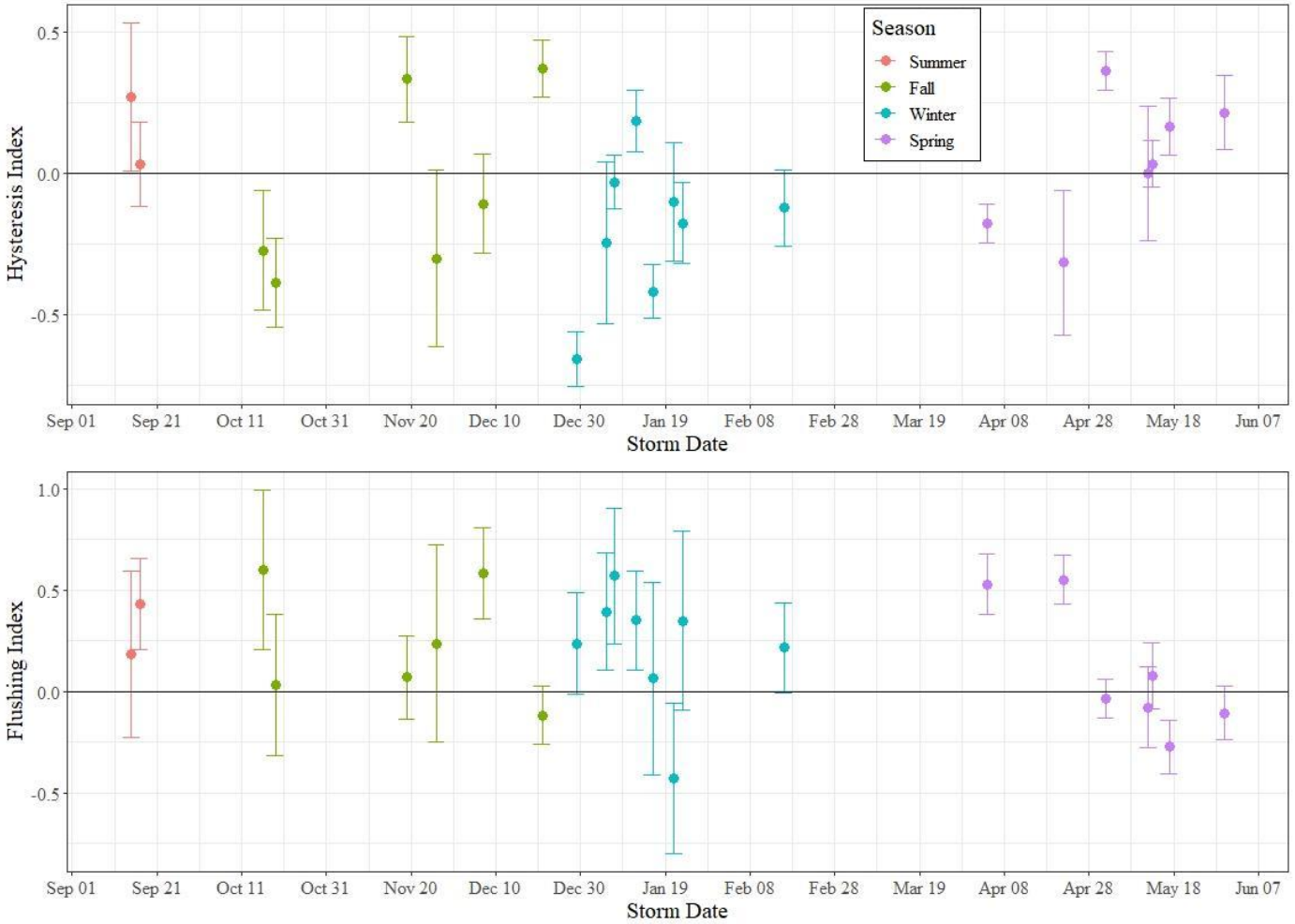

Figure 3.7. Seasonal variability in hysteresis index (HI) values (top) and flushing index (FI) values (bottom) measured across the 10 studied headwater catchments. Points indicate mean values measured across all catchments for an individual storm event, and whiskers indicate the standard deviation. The number of streams included for each storm varies, but all storms include at least 6 of the 10 streams. See Tables 3.3 and 3.4 for more information.

Table 3.3. Stream-average hysteresis index (HI) values for each monitored storm.

	Stream											
Storm Start Date	**1**	**2**	**3**	**4**	**5**	**11**	**13**	**14**	**15**	**18**	**Average**	**SD**
2019-09-15	0.29	0.28	0.29	0.31	0.33	0.01	0.08	0.24	0.44	0.24	0.25	0.12
2019-09-17	-0.03	-0.09	-0.05	0.11	-0.02	-0.01	-	0.14	0.04	0.24	0.04	0.11
2019-10-16	-0.17	-0.22	-0.22	-0.25	-0.16	-0.62	-	-0.34	-0.29	-0.32	-0.29	0.14
2019-10-19	-0.28	-0.33	-0.29	-0.46	-0.30	-0.65	-	-0.32	-0.48	-0.44	-0.40	0.12
2019-11-19	0.16	0.38	-	0.36	0.37	-	-	0.40	0.15	0.60	0.34	0.16
2019-11-26	-0.24	-0.51	-0.39	-0.59	-0.36	-0.65	-0.29	0.15	-0.02	-0.15	-0.31	0.25
2019-12-07	-0.08	-0.43	-0.03	-0.04	0.02	-0.23	-	-0.05	-0.03	-	-0.11	0.15
2019-12-21	0.30	0.27	0.34	0.34	0.35	0.43	0.47	0.57	0.42	0.25	0.37	0.10
2019-12-29	-	-0.72	-0.51	-0.71	-	-0.64	-	-0.73	-0.63	-	-0.66	0.08
2020-01-05	-	0.08	-0.64	-	-0.53	-0.29	-0.39	-	0.06	-0.04	-0.25	0.29
2020-01-07	-0.11	-0.06	-	0.09	-	-	0.00	-	-0.01	-0.10	-0.03	0.08
2020-01-12	0.06	0.33	0.08	0.12	-	-	0.29	0.30	0.08	0.23	0.19	0.11
2020-01-16	-0.47	-0.49	-0.57	-0.45	-	-0.32	-0.37	-0.31	-0.42	-0.37	-0.42	0.08
2020-01-21	0.03	-0.20	-0.17	0.17	0.30	-0.30	-0.29	-0.33	0.02	-0.20	-0.10	0.21
2020-01-23	0.10	-0.20	-0.25	-0.18	-	-0.26	-	-	-0.10	-0.35	-0.18	0.14
2020-02-16	-0.06	-0.33	-0.26	-0.10	0.12	-0.04	-	-	-0.13	-0.14	-0.12	0.14
2020-04-04	-0.19	-0.28	-0.13	-0.12	-0.10	-	-	-	-0.20	-0.25	-0.18	0.07
2020-04-22	-0.44	-	-0.55	-0.52	0.31	-0.28	-	-0.32	-0.29	-0.38	-0.31	0.27
2020-05-02	0.36	0.40	0.42	0.37	0.47	0.38	-	0.30	0.24	0.35	0.36	0.07
2020-05-12	-0.04	0.20	0.02	-	-	-0.09	-	-0.17	-0.35	0.41	-0.01	0.25
2020-05-13	0.01	0.00	0.06	0.17	-	0.12	-	-0.03	-0.02	-0.03	0.04	0.08
2020-05-17	0.17	0.14	0.15	0.13	0.02	-	-	-	0.37	0.17	0.17	0.10
2020-05-30	0.32	-	0.36	0.17	-	0.08	-	0.13	0.12	0.28	0.21	0.11

Table 3.4. Stream-average flushing index (FI) values for each monitored storm.

	Stream											
Storm Start Date	**1**	**2**	**3**	**4**	**5**	**11**	**13**	**14**	**15**	**18**	**Average**	**Std. Dev.**
2019-09-15	0.30	0.22	0.21	0.48	0.17	0.53	-0.20	0.17	-0.04	-0.09	0.18	0.24
2019-09-17	0.47	0.34	0.51	0.33	0.31	0.38	-	0.66	0.40	0.53	0.44	0.11
2019-10-16	0.83	0.91	0.60	0.66	0.81	0.58	-	-0.03	0.50	0.32	0.58	0.29
2019-10-19	0.15	0.14	-0.03	0.17	0.19	0.25	-	-0.54	0.14	-0.34	0.01	0.27
2019-11-19	0.00	0.05	-	0.05	0.05	-	-	0.18	0.35	-0.26	0.06	0.18
2019-11-26	0.01	0.73	0.34	0.57	0.31	0.13	0.04	-0.37	0.32	0.12	0.22	0.31
2019-12-07	0.62	0.69	0.43	0.36	0.77	0.61	-	0.90	0.31	-	0.59	0.21
2019-12-21	-0.08	-0.17	-0.03	-0.06	-0.16	-0.17	-0.29	-0.12	-0.05	-0.07	-0.12	0.08
2019-12-29	-	0.29	0.06	0.12	-	0.68	-	0.00	0.38	-	0.25	0.25
2020-01-05	-	0.57	0.45	-	0.33	0.62	0.40	-	0.00	0.42	0.40	0.20
2020-01-07	0.68	0.52	-	0.91	-	-	0.00	-	0.78	0.53	0.57	0.32
2020-01-12	0.23	0.21	0.74	0.13	-	-	0.33	0.31	0.73	0.12	0.35	0.25
2020-01-16	0.71	0.52	0.36	0.64	-	-0.28	-0.53	-0.21	-0.17	-0.45	0.06	0.49
2020-01-21	-0.56	-0.74	0.02	-0.55	0.08	-0.73	-0.63	0.18	-0.47	-0.85	-0.42	0.37
2020-01-23	0.55	0.84	0.59	0.76	-	0.12	-	-	-0.11	-0.32	0.35	0.45
2020-02-16	0.08	0.66	0.21	0.16	0.15	0.11	-	-	0.07	0.26	0.21	0.19
2020-04-04	0.45	0.66	0.40	0.47	0.54	-	-	-	0.56	0.63	0.53	0.09
2020-04-22	0.56	-	0.51	0.68	0.60	0.68	-	0.48	0.46	0.45	0.55	0.09
2020-05-02	-0.03	-0.08	-0.10	-0.13	-0.04	0.01	-	0.05	0.06	-0.04	-0.03	0.07
2020-05-12	-0.24	-0.14	-0.33	-	-	-0.03	-	0.11	0.01	0.10	-0.07	0.17
2020-05-13	0.10	0.23	0.08	0.19	-	0.31	-	-0.11	-0.11	-0.04	0.08	0.16
2020-05-17	-0.27	-0.43	-0.26	-0.29	-0.29	-	-	-	-0.01	-0.37	-0.27	0.13
2020-05-30	-0.13	-	-0.13	-0.03	-	-0.09	-	-0.08	-0.13	-0.14	-0.11	0.04

3.4.3: Reach-Scale Analysis of Hysteresis Metrics

Along each of the 10 study streams, HI and FI values varied considerably from sensor location to sensor location, leading to variable longitudinal behavior at the reach scale between streams. The greatest reach-wide variability in both hysteresis metrics occurred during the summer and early fall and decreased into the wet season across the 10 streams (Figure 3.8). During the two summer events, two streams had stream-level standard deviation in HI values greater than 0.4 (mean SD = 0.18), while six had variability less than 0.1. Variability in longitudinal HI behavior across the 10 streams decreased during fall (mean SD = 0.10) and winter (mean SD = 0.05), and remained below 0.15 through the spring events (mean SD = 0.04), indicating stream temperature hysteresis behavior along each stream was more similar during winter and spring events than those in summer and fall. The reach-scale variability in FI was similar to the variability observed in HI, with higher variability in the summer (mean SD = 0.27) and fall (mean SD = 0.19) than winter (mean SD = 0.11) and spring (mean SD = 0.08) (Figure 3.8).

Figure 3.9 displays the longitudinal variability in stream temperature HI values during all monitored storm events and provides additional evidence of seasonal variation in hysteresis behavior. HI values along each stream generally became more similar as the wet season progressed within and across streams, with the greatest variability during summer and early fall. During summer and fall events, certain locations along streams had positive hysteresis while others had negative hysteresis. For instance, during the 2019-09-15 storm, stream 1 exhibited clockwise hysteresis along the upper 150 meters of the reach (first 4 data points) and anti-clockwise hysteresis for two locations downstream between 100 and 50 meters upstream, and then clockwise hysteresis at the two most downstream sensor locations over 50 meters. Later in the fall, during the 2019-11-26 storm, stream 1 exhibited the opposite behavior: anti-clockwise hysteresis in the upstream 150 meters of the monitored reach, and positive hysteresis in the downstream 150 meters of the reach. However, other streams showed little or no longitudinal variability in hysteresis behavior during any storms, even during summer and early fall. Stream 15, the largest catchment included in the study (drainage area = 60 ha) exhibited the least

longitudinal variability in HI, as measured by the mean longitudinal standard deviation in hysteresis metrics across all storm events, in either HI values (mean SD = 0.03) or FI values (mean SD = 0.05). Stream 2, one of the smallest catchments in the study (drainage area = 30 ha) exhibited similar behavior, with mean standard deviation values of 0.04 for HI values and 0.07 for FI values. Every location along these streams responded similarly to precipitation inputs during events. This is in contrast to streams 13 and 14 (drainage areas of 21 and 29 ha, respectively), which had the greatest overall longitudinal variability, with mean standard deviation values of 0.14 and 0.13 for HI values and 0.34 and 0.20 for FI values, respectively.

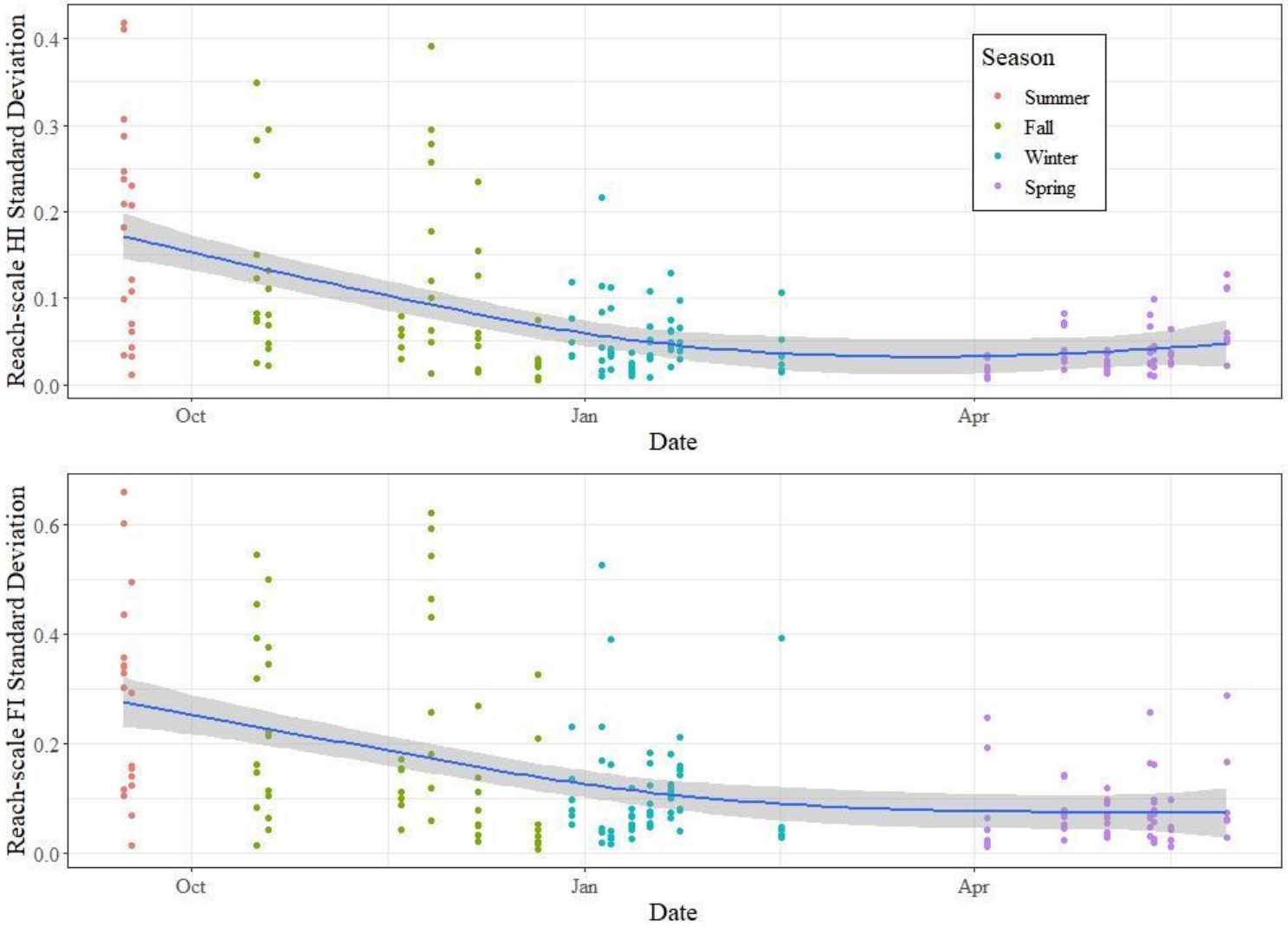

Figure 3.8. Seasonal changes in the longitudinal variability in stream temperature hysteresis metrics measured at all 10 catchments. Each point represents the standard deviation of HI (top) and FI (bottom) values measured along each stream for each storm. The blue line represents a general additive model fit to illustrate the seasonal trend.

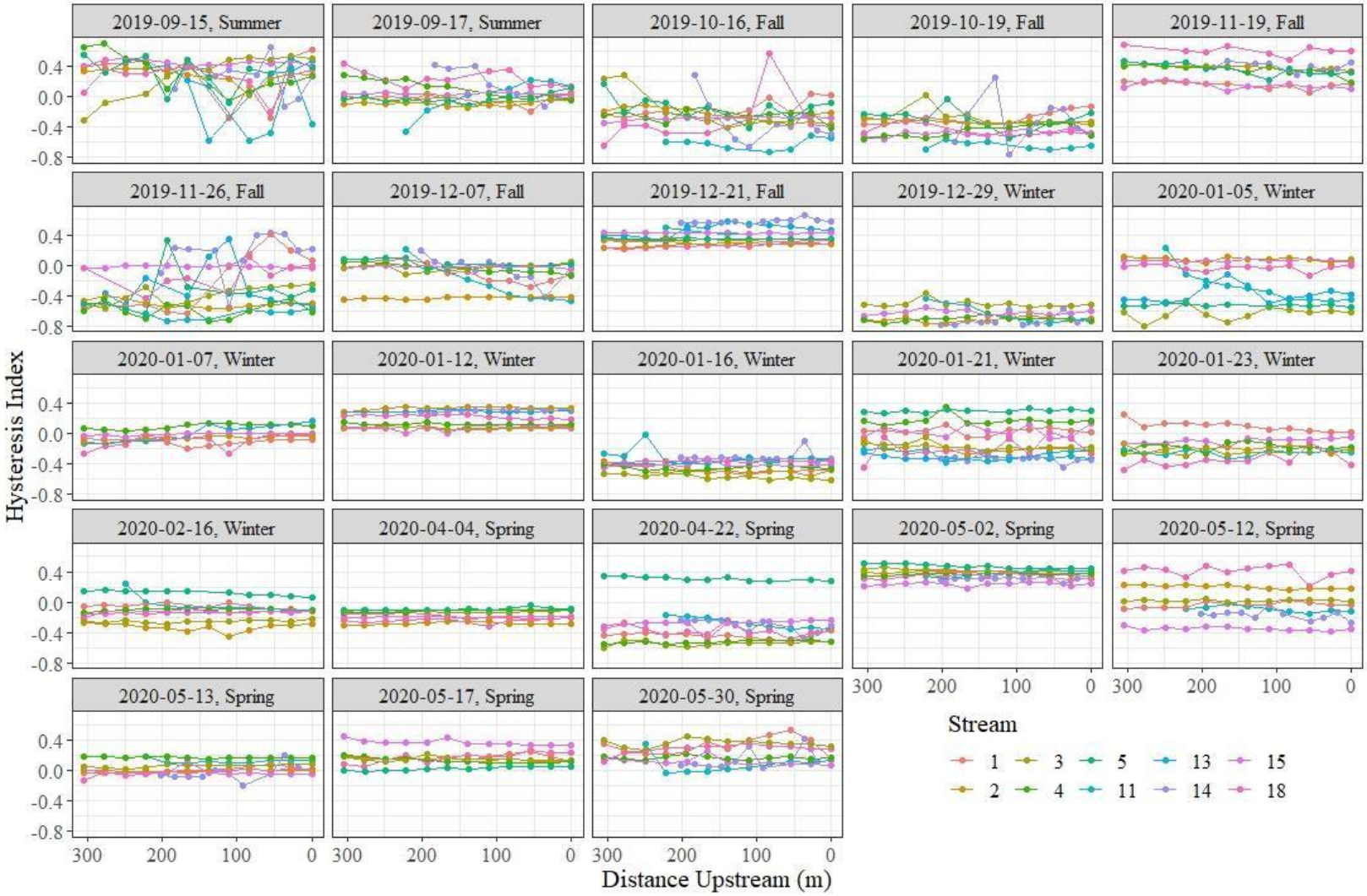

Figure 3.9. Longitudinal trends in HI values for each storm event. Direction of stream flow is from left to right.

3.4.4: Comparison of Hysteresis Metrics to Meteorological and Topographic Characteristics

Results of the Spearman rank correlation matrix revealed strong linear correlations between hysteresis metrics and storm and meteorological conditions (Table 3.5). HI values were most strongly correlated with predictors describing the magnitude and variation of air temperature before and during storm events. The strongest predictors of the hysteresis index direction were the air temperature change during the rising limb of the storm event ($\rho = -0.49$), indicating that hysteresis was generally anti-clockwise (indicating stream warming) when air temperatures warmed during the event and clockwise (indicating stream cooling) when air temperatures decreased during the event (Figure 3.10B). HI values were also negatively correlated with flushing index ($\rho = -0.35$), initial stream stage ($\rho = -0.15$), and peak stream stage ($\rho = -0.15$). HI values were positively correlated with the initial difference between stream and air temperatures ($\rho = 0.49$), initial air temperature ($\rho = 0.48$), initial stream temperature ($\rho = 0.34$), and peak air temperature ($\rho = 0.19$). Comparatively, FI values were positively correlated with the air temperature change during the rising limb of the storm event ($\rho = 0.54$) indicating that stream temperatures generally increased during the rising limb of the hydrograph when air temperatures also increased (Figure 3.10E). FI values were negatively correlated with HI index values ($\rho = -0.35$), initial stream temperature ($\rho = -0.35$), initial air temperature ($\rho = -0.30$), average rainfall intensity ($\rho = -0.27$), and the difference between stream and air temperatures at the start of the event ($\rho = -0.23$).

For events with clockwise hysteresis (HI > 0), initial air temperatures were 2.4–3.0 °C warmer on average, than those exhibiting anti-clockwise hysteresis ($t = -19.2$, $p < 0.001$) (Figure 3.10A). Similarly, for events with anti-clockwise hysteresis, air temperatures on average increased by 1 °C during the event, while those with clockwise hysteresis decreased on average by 0.8 °C ($t = 22.9$, $p < 0.001$). This indicated a reliance of hysteresis behavior during storm events on meteorological conditions both prior to and during the storm event.

Initial air temperatures were 1.7–2.3 °C cooler for events with positive FI values (indicating warming during the event), than for events with negative FI values ($t = 13.4$, p

< 0.001) (Figure 3.10D). This indicates that stream temperatures decreased during storm events more often during warmer parts of the year (summer and spring) than during cooler portions of the year (fall and winter), potentially due to cold frontal events or fog during the summer and early fall that bring cooler air temperatures. Unsurprisingly, stream temperatures increased during storm events when air temperatures increased through the event. On average, air temperatures increased by 1.1 °C when FI was positive and decreased by 1.1 °C when FI was negative (t = -29.1, $p < 0.001$) (Figure 3.10E). Average rainfall intensity was also marginally higher (0.26–0.40 mm hr^{-1}; t = 9.02, $p <$ 0.001,) during events with negative FI values than positive FI values (Figure 3.10F).

Interestingly, we did not find correlations between topographic metrics and the hysteresis indices (HI or FI). Even when hysteresis metrics were split into seasonal groups, there were no strong correlations between UAA, TWI, FWS, or other computed topographic metrics and either of the hysteresis metrics. This indicated either a lack of linear dependence of HI or FI values on the derived topographic metrics, a failure of the derived metrics to properly characterize subsurface hydrological processes influencing stream temperature change in the study catchments, or that stream temperature change during events is influenced primarily by other factors.

Table 3.5. Spearman Rank correlation coefficients (ρ) for hydrological, meteorological, and topographic predictor variables and hysteresis metrics. Values in bold are statistically significant at the α = 0.05 level. Missing values had ρ values less than 0.10 and were considered inconsequential predictor variables.

			Direction		**Magnitude**	
Category	**Predictor Description**	**Predictor**	**HI**	**FI**	**|HI|**	**|FI|**
-	Flushing index absolute value	FI_abs	**-0.38**	**0.54**	-	**1.00**
-	Flushing index	FI_index	**-0.35**	**1.00**	-	**0.54**
-	Hysteresis index absolute value	HI_abs	-0.23	-	**1.00**	-
-	Hysteresis index	HI_index	**1.00**	**-0.35**	-0.23	**-0.38**
Hydrological	Intial stream stage	ql_initial	**-0.15**	-	-	-
Hydrological	Peak stream stage	ql_peak	**-0.15**	-	-0.11	-
Hydrological	Difference between peak and initial stream stage	ql_response	-	-	-	-
Meteorological	Air temperature change during rising limb	air_tempC_risinglimb_response	**-0.49**	**0.54**	-0.10	**0.29**
Meteorological	Maximum 1-hour rainfall intensity	max1hr_intens	-0.10	-0.17	-	-
Meteorological	Storm depth	depth_mm	0.15	-	-0.12	0.13
Meteorological	Three-day average solar radiation prior to storm	three_day_solrad	0.17	-	-	**-0.17**
Meteorological	Average air temperature	avg_air_temp	**0.18**	-	-0.12	**-0.10**
Meteorological	Air Temperature at hydrograph peak	air_tempC_at_peak	**0.19**	-	-0.11	**-0.13**
Meteorological	Storm duration	dur_hours	0.20	0.12	-0.31	0.15
Meteorological	Initial stream temperature	tempC_initial	**0.34**	**-0.35**	-	**-0.26**
Meteorological	Initial air temperature	air_tempC_initial	**0.48**	**-0.30**	-	**-0.31**
Meteorological	Difference between stream and air temperature at event start	stream_air_tempdif_initial	**0.49**	**-0.23**	-	**-0.30**
Meteorological	14-day antecedent rainfall	antecedent_14day	-	-0.20	-	-

Table 3.6. continued

Meteorological	Average rainfall intensity	avgintensity	-	**-0.27**	**0.30**	-
Topographic	Stream average elevation	ele	-	0.12	-	-
Topographic	Stream temperature sensor elevation	sensor_elevation	-	0.11	-	0.10
Topographic	Average topographic wetness index of upslope area draining to each monitoring location	avg_TWI	-	-	-	-
Topographic	Average flow weighted slope at each monitoring location	avg_FWS	-	-	-	-
Topographic	Lateral upslope accumulated area draining to each monitoring location	lateral_uaa_ha	-	-	-	-
Topographic	Topographic wetness index point value at each monitoring location	twi_point	-	-	-	-
Topographic	Average upslope accumulated area measured at each monitoring location	avg_UAA_m2	-	-	-0.10	-0.10
Topographic	Average stream channel slope	reach_wide_stream_slope	-	-	-	-
Topographic	Stream average watershed slope	average_watershed_slope	-	-0.12	-	-0.10
Topographic	Drainage area of catchment	drainage_area_ac	-	-	-0.11	-0.11
Topographic	Mean slope of upslope are draining to each monitoring location	mean_slope_deg	-	-	-	-
Topographic	Wetted width at each monitoring location	average_active_width_ft	-	-	-	-
Topographic	Flow weighted slope at each monitoring location scaled by lateral UAA	fws_point_uaa	-	-	-	-

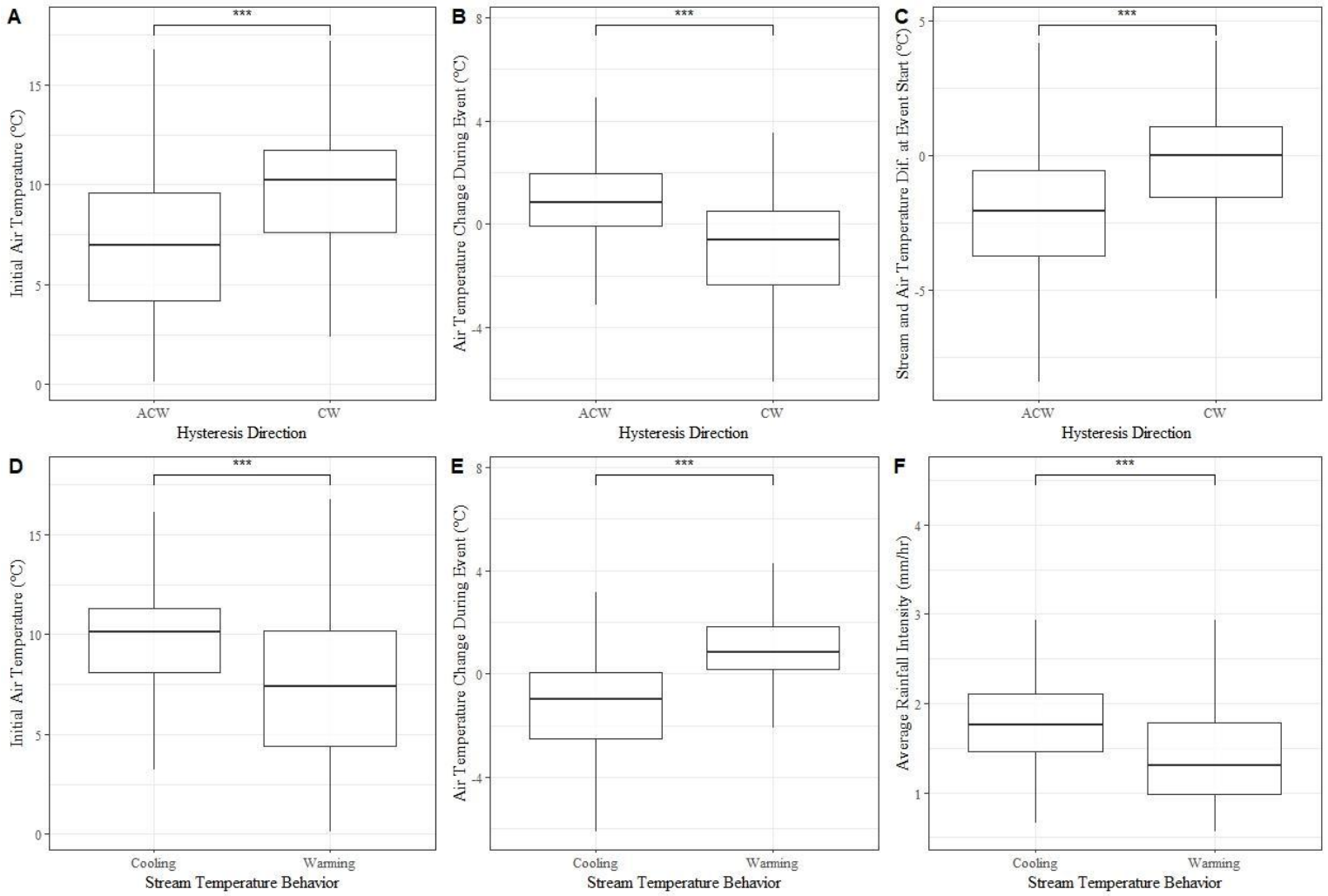

Figure 3.10. Influence of select correlated predictor variables on the direction of stream temperature hysteresis (A, B, C), and the direction of stream temperature change during storm events (D, E, F). Direction of hysteresis is given as: HI >0, clockwise (CW), HI<0, anti-clockwise (ACW). In D, E, and F, cooling corresponds to FI values less than 0, and warming corresponds to FI values greater than 0. Stars indicate statistical significance at the $\alpha = 0.001$ level ($p < 0.001$).

3.5: Discussion

We observed a seasonally variable relationship between stream temperature and stormflow, with clockwise hysteresis occurring during summer and spring and anti-clockwise hysteresis occurring during fall and winter storm events. This indicates that during summer and spring, when stream temperatures are generally cooler than air temperatures, stream temperatures warm on the rising limb and cool on the falling limb of the storm hydrograph, potentially due to accumulated heat in the catchment during preceding days that is flushed to the stream during the initial onset of precipitation (Kobayashi et al., 1999; Wilby, Johnson, & Toone, 2014) or subsequent reconnections with groundwater flow paths on the falling limb that input cool ground water (Lange & Haensler, 2012). This initial warming during summer and spring storm events may also be due to accumulated warm water within the narrow riparian zone or permanent saturated areas that gets pushed into the stream via groundwater ridging (e.g., Sklash & Farvolden, 1979). Alternatively, flushing index values were generally positive, indicating that storm events input heat to the stream during the rising limb. FI values did not show a clear seasonal trend; however, on average, FI values were highest in summer and decreased through the wet season, to reach a low during spring.

During fall and winter when hydrologic connectivity is greatest and air temperatures are cooler than stream temperatures, the observed anti-clockwise hysteresis indicates that stream temperatures are cooler on the rising limb and warmer on the falling limb of the storm hydrograph, potentially due to the reconnection of deep groundwater flow paths that input comparatively warm groundwater (Kobayashi et al., 1999; Lange & Haensler, 2012). If we assume that deep groundwater temperatures can be approximated by adding 1-2 °C to mean annual air temperatures (Ficklin, Luo, Stewart, & Maurer, 2012, but see Leach & Moore, 2015), then deep groundwater temperatures should be within the range of 12-13 °C for this region. Input of groundwater in this temperature range during the falling limb of all the observed fall and winter storm events would cause stream warming, and confirm the anti-clockwise behavior observed herein. This behavior may also be due to a combination of direct rainfall into the channel and throughflow from adjacent hillslopes, such as those derived from longer flow paths that do not activate until

later in the storm event when full hillslope-riparian-stream connectivity is reached (Penna et al., 2015; Uchida et al., 2002; Van Meerveld et al., 2015). Indeed, during times of maximum hydrologic connectivity preferential flow paths can deliver groundwater from upper hillslopes that influence stream temperatures (Uchida et al., 2002). It is likely that for storms during the wettest part of the year, subsurface water is sufficiently mixed prior to emerging in the stream that these lateral inputs can cause localized warming.

Other studies have observed similar stream temperature hysteresis behavior. (Kobayashi et al., 1999) paired stream temperature and specific conductance measurements and observed clockwise stream temperature hysteresis during an early fall storm, while specific conductance exhibited anti-clockwise hysteresis. The authors suggest that increasing inputs of shallow subsurface flow on the rising limb warmed through the soil, increasing stream temperatures, and simultaneously diluted specific conductance in the stream. After the storm peak, specific conductance increased and stream temperature decreased, indicating that the contributions from shallow sources decreased and inputs from deeper groundwater cooled the stream. This may have been the mechanism causing stream warming (positive FI values) during summer and spring events in this study, however it does not explain why temperatures increased on the rising limb during fall and winter. Subehi et al., (2010) observed seasonally variable stream temperature hysteresis across 16 forested watersheds (0.5 to 100 ha) in Japan, with clockwise hysteresis during spring and summer seasons and anti-clockwise hysteresis during fall and winter, which is similar to the trend observed herein. The authors conclude that watershed slope and the magnitude of streamflow change during storm events had a greater effect on stream temperature change during storm events than air temperature change by influencing shallow subsurface flow paths. However, this is contrary to our study, which did not find watershed slope or the magnitude of the stream stage response to be a meaningful predictor of hysteresis direction or magnitude.

During both warm and cool seasons, the direction of hysteresis appears to be driven partly by the gradient between stream and air temperatures and direction of air temperature change during events (Figure 3.10). This is similar to recent work, where Oware & Peterson, (2020) measured seasonally variable thermal gradients during storm

events, with stream and hyporheic substrate temperatures increasing during summer storms and decreasing during winter storms. During warm season storm events when the direction of the thermal gradient is from the air to the stream, stream temperatures initially increased during events, resulting in clockwise hysteresis. This was true for our study. For instance, the pre-storm thermal gradient between stream and air temperatures was positively correlated with HI values (ρ = 0.49), indicating that the magnitude of stream temperature hysteresis was largest during events with the largest temperature gradient between the stream and overlying air. If we assume air temperatures approximate rainfall temperatures (Gerecht, 2012; Shanley & Peters, 1988), this indicates transfer of heat from rainfall to soil to stream, likely through shallow subsurface inputs and direct channel interception, driven primarily by the gradient between stream and air (rainfall) temperatures. In addition, stream temperature hysteresis was negatively correlated with air temperature change during the event (ρ = -0.49), indicating that stream temperatures generally reflected the direction of air temperature change during storm events (e.g., stream temperatures warmed (cooled) when air temperatures warmed (cooled)).

Our results also indicate that the stream temperature response to precipitation inputs is the most variable along streams during the driest period of the year. Longitudinal variability in HI and FI values was greatest during the summer and decreased through the fall and winter. This is likely because low flows in the late summer lead to greater longitudinal thermal heterogeneity than during wetter portions of the year (Leach et al., 2016), where stream temperature may be dominated by discrete groundwater sources or hyporheic exchange that buffers the response to storm flow (Leach et al., 2017; Lowry et al., 2007). Once groundwater levels began to rise during the onset of the wet season and watershed storage thresholds became satisfied (e.g., Detty & McGuire, 2010), stream temperatures along these streams became more homogeneous, and more synchronous in their response to storm flow. At the same time, runoff generation during events likely shifts from shallow subsurface sources to deeper, longer groundwater flow paths that are now connected (Lange & Haensler, 2012). This behavior could also be explained by differences in the dominant energy exchanges influencing

stream temperature change between summer and winter. During summer, when flows are low and solar radiation dominates the stream temperature energy budget (Hebert et al., 2011; Leach & Moore, 2010), small discrepancies in canopy cover and variable stream geomorphology can lead to localized warming and cooling that influences the stream temperature response to storm flow (e.g., some areas along these streams warm during storms while others cool). Alternatively, during winter, energy exchange primarily occurs through hillslope advection, not solar radiation, because of persistent cloud cover and low solar angles (Leach & Moore, 2014). In addition, streamflow is higher during winter and spring, which leads to greater water depths and velocities. This increases the energy required to alter stream temperatures, and because less energy is available and residence times are reduced, stream temperatures become more homogeneous along each stream.

Topographic metrics derived herein may not have been able to explain variability in seasonal stream temperature hysteresis behavior for a number of reasons. First, GPS-derived sensor locations may have been incorrectly recorded and adjusted to the derived channel network and thus do not provide a meaningful comparison to the actual behavior at each monitoring location. However, our methodology included an assessment of variability for each metric upstream and downstream of the assumed location of each temperature sensor, so we feel confident that this represents our best estimate of the true sensor location on the derived stream channel. It may have also been because during many of monitored storm events (during winter and spring) HI and FI values measured at each stream temperature monitoring location were too similar within and among streams to find a link to site-level topographic metrics that were more variable (e.g., Figure 3.9, storms on 2020-04-04 and 2020-05-02). It may also have been because hysteresis behavior was so variable from storm to storm due to the overriding effects of changing meteorological and storm characteristics that it prevented properly detecting a topographic influence. This is important considering these topographic metrics (UAA, TWI, and FWS) are static in time (Grabs, Seibert, Bishop, & Laudon, 2009; Leach et al., 2017), and do not change with temporally variable catchment scale wetness conditions and hydraulic gradients that influence stormflow generation and thus stream temperature behavior during storms. Another option is that stream temperature behavior during storm

events in this region simply are not an expression of local surface topography at the scales we investigated, and may rely more on regional meteorological conditions such as air temperature changes and cloud cover (Wilby et al., 2015) or subsurface bedrock topography (Tromp-Van Meerveld & McDonnell, 2006). For instance, in a steep forested watershed in Georgia, USA, Freer et al., (2002) found values of UAA and TWI calculated for bedrock topography to be better predictors of subsurface flow during storm events than metrics derived for surface topography. It is likely that for this region, the overriding effects of seasonally variable meteorological conditions and complex subsurface topography limited the usefulness of temporally static, topographically derived metrics at explaining the stream temperature response to stormflow.

This study also has a few important limitations. The use of single point precipitation measurements on two adjacent ridges likely resulted in under characterization of the in-stream temperature response to precipitation, as single point precipitation measurements are known to cause error when extrapolated across entire catchments (Croghan et al., 2019). Although storm characteristics were not found to be meaningfully different between rain gauge locations, catchment-scale differences in vegetation likely influence the amount of hydrologic input driving stormflow that was not accounted for. In addition, measurement of rainfall water temperature would have been valuable to better understand whether the observed hysteresis is due to variable subsurface flow paths or whether stream temperature change during storm events is simply a reflection of rainfall temperature, especially for events early in the wet season when shallow subsurface pathways likely dominated. As well, hysteresis metrics for each stream temperature monitoring location within each stream were calculated using the same time series of stream stage, measured at the downstream catchment outlet. Although this likely provides a reasonable estimate of the streamflow response at each stream temperature measurement point, installation of additional level loggers and additional measurements of stream discharge along each study reach would have provided more accurate calculation of these metrics, and likely provided a better explanation of the variable hysteresis behavior observed along each stream. Future work should include spatially distributed measurements of soil temperature at a range of depths and

groundwater levels to further elucidate variable runoff generation mechanisms using stream temperature as a tracer and provide additional evidence that metrics describing the hysteresis of stream temperature during storm events correlates well to measurements upslope. Additional analysis is required to determine whether hysteresis metrics using stream temperature and stormflow could be used to assess the influence of forest harvesting or other disturbances on stream flow response, potentially providing an additional method of quantifying the effects of reach scale perturbations on hydrologic processes in forested headwaters (e.g., Mistick & Johnson, 2020).

3.6: Conclusions

We evaluated the seasonal stream temperature response to stormflow across 23 storm events and 10 forested headwater catchments outfitted with spatially distributed stream temperature sensors in the Northern California coast range during the 2020 water year. We used hysteresis metrics to quantify the magnitude and direction of stream temperature change and used correlation analysis to assess what meteorological, hydrological, and topographic characteristics influence stream temperature change during storm events. Our results indicate that the stream temperature response to stormflow is seasonally variable and exhibits clockwise hysteresis during the summer and spring when air temperatures are warmer than stream temperatures and anti-clockwise hysteresis during the fall and winter when air temperatures are cooler than air temperatures. In addition, the stream temperature response to stormflow was the most variable across these 10 catchments during the late summer and early fall, when catchment-scale wetness conditions and streamflow were at the annual low. As the wet season progressed, stream temperature behavior across these 10 catchments became more similar, and remained coupled through the late spring. The magnitude and direction of stream temperature hysteresis was well correlated with the gradient between stream and air temperatures at the start of the event, and air temperature change during the storm rising limb, indicating the role of regional meteorological conditions on stream temperature change during storm events. None of the derived topographic metrics describing the preponderance of saturated areas and lateral inputs to streamflow were correlated with stream temperature change during events, potentially because subsurface topography and seasonally variable

catchment wetness conditions could not be properly characterized with these static metrics describing surface topography. Future research should develop temporally-dynamic topographic metrics that consider seasonally variable stormflow generation processes and hydrologic connectivity, and use subsurface temperature and groundwater level measurements across contributing hillslopes to better understand the runoff production mechanisms that cause stream temperature change during storm events.

Chapter 4: Synthesis

My results show that headwater streams exhibit distinct summer thermal regimes and patterns of thermal sensitivity that vary regionally with underlying lithology likely due to differences in the spatial extent and magnitude of groundwater flow. In addition, during periods of low stream flow and soil moisture, the stream temperature response to stormflow is the most longitudinally variable along headwater streams. This period of large longitudinal variability often coincides with the warmest annual stream and air temperatures, and lowest flows, and therefore the largest threat to aquatic species downstream (Arismendi et al., 2013). Overall, headwater stream sensitivity to atmospheric energy exchanges and responsiveness to precipitation inputs varies longitudinally, and riparian forest management should reflect this variable behavior. This may be considered in the context of riparian management prescriptions, to reduce the impact of contemporary forest harvest, or to use riparian corridors as climate refuges in the face of climate change. This chapter focuses on the question: how can we use these results in the context of riparian forest management to improve the way we manage headwater stream thermal regimes?

Across the US, riparian protections implemented to limit changes to headwater stream thermal regimes and preserve aquatic habitat are homogeneous across diverse regions managed by centralized (i.e., state level) organizations (Broadmeadow & Nisbet, 2004; Lee, Smyth, & Boutin, 2004). For instance, riparian buffer prescriptions may be of fixed width and identical for two similarly sized streams located in contrasting regions with diverse lithology, climate, and vegetation. This “one size fits all” approach is often variably effective at protecting stream temperatures (Bowler, Mant, Orr, Hannah, & Pullin, 2012; Martin, Kroll, & Knoth, 2021; Sweeney & Newbold, 2014), and does not consider the heterogeneity in thermal sensitivity or streamflow generation processes that exist along headwater streams (Kuglerová et al., 2014; Martin et al., 2021). Recent work has also highlighted that headwater stream thermal regimes are influenced by land area much larger than that commonly protected by riparian buffers, limiting their effectiveness across seasons and with changes in hydrological connectivity to adjacent hillslopes (Dick, Tetzlaff, & Soulsby, 2018). For these reasons, there is a need to improve upon the fixed-

width buffers commonly implemented similarly across diverse regions to tailor headwater riparian management to individual streams. Alternative riparian management strategies will become critical to minimize the influence of future climate warming on headwater resources (Krosby et al., 2018; O'Briain et al., 2017).

A land-management perspective based on the theory of 'hydrologic landscapes' has been proposed to consider regional heterogeneity in climate, soils, geology, topography, and vegetation that influences catchment-scale hydrology (Cowood et al., 2017; Leibowitz et al., 2014; Tague et al., 2007; Winter, 2001). This concept can be used to tailor research or management actions to account for spatial heterogeneity in hydrology across regions (Winter, 2001). For example, there have been recommendations to guide riparian forest management along headwater streams by considering spatially variable hydrologic behavior such as groundwater inflow (Kuglerová et al., 2014; Story et al., 2003; Tiwari et al., 2016) and by basing buffer design on geophysical factors known to influence stream temperature, such as lithology, topography, and stream azimuth (Dugdale, Malcolm, Kantola, & Hannah, 2018; Martin et al., 2021). Land managers interested in preserving areas of cold water habitat in mountainous headwater streams could adopt riparian management schemes that consider the hydrologic source of this habitat and adjust operations and management along the most thermally sensitive and responsive areas (Laudon et al., 2016).

One way to tailor riparian management across hydrologic landscapes may be by installing variable-width riparian buffers (Kuglerová et al., 2014; Laudon et al., 2016; Tiwari et al., 2016) to increase riparian protection at locations along streams most susceptible to atmospheric energy exchange. Variable-width buffers can be designed to expand along areas that require additional protection via shading or by excluding equipment because of their unique hydrological character or potential to influence water quality. This may include permanently saturated areas, steep slopes, locations with riparian forest features, and topographically predicted groundwater discharge zones (Anderson & Poage, 2014; Kuglerová et al., 2014; Laudon et al., 2016; Olson & Rugger, 2007). On the other hand, variable-width buffers could be designed to contract at locations less sensitivity to atmospheric energy exchange (i.e., where topographic and

bank shading is sufficient to limit radiative loading and increases in summertime stream temperatures). This is one reason variable-width buffers have been considered more cost effective than fixed-width buffers, considering protection is focused in certain locations, such as wet areas of relatively low forest productivity (Tiwari et al., 2016) or areas that grow primarily non-merchantable species. Therefore, variable-width buffers can potentially help balance the economic demands of forest land managers and the environmental demands of protecting aquatic resources.

However, areas of strong hydrological connectivity may not be topographically predictable in all regions, such as shown in chapter three of this thesis and other literature (e.g., Freer et al., 2002). This will require new methods to properly identify locations of discrete groundwater inflow or thermal refuges in regions with steep, complex bedrock and surface topography, or where shallow subsurface flow dominates streamflow (i.e., the Northern California Coast Range). One method may be to use field measurements of longitudinal thermal sensitivity combined with site-level covariates to develop regionally specific reach-scale models to help guide the placement of variable-width riparian buffers. These models could incorporate data collected during the summer when incoming thermal energy is greatest and stream temperature protection is most critical, but also incorporate data on the spatial extent of catchment wetness during other seasons. This approach has been used at the watershed-scale, to aid in the design of spatially variable riparian buffers based on the extent of hydrologically sensitive areas (Gorsevski, Boll, Gomezdelcampo, & Brooks, 2008). The authors used spatiotemporal soil-moisture routing to assess seasonal changes in catchment wet areas to guide buffer width. However, this effort did not focus on protecting stream temperatures. Others have used similar methods to define machine exclusion zones in near-stream areas to minimize sediment pollution during forestry operations (Arp, 2009). Another emerging application that could be used to guide riparian management are spatially distributed models that predict radiative loading to the stream under different riparian vegetation scenarios, such as Penumbra (Halama et al., 2018). In addition, thermal satellite imagery and thermal infrared remote sensing technology can be used across a range of spatial scales to assess locations of groundwater discharge to aid in protection of thermal refugia (Sass, Creed,

Riddell, & Bayley, 2014; Wawrzyniak et al., 2016). Future efforts to optimize the width and placement of riparian buffers should focus on developing models and tools that can be used across hydrologic landscapes and incorporate easily accessible topographic and atmospheric data.

Others contend that riparian buffers should provide additional shading along areas with the most critical cold-water habitat even if stream temperatures are less sensitive to changing atmospheric conditions at these locations (Kanno et al., 2014). This can involve implementing buffers containing gaps that simultaneously fuel primary production and provide shade where it is most needed (Benda, Litschert, Reeves, & Pabst, 2016; Coats & Jackson, 2020; Newton & Ice, 2016; Swartz, Roon, Reiter, & Warren, 2020). Site-specific prescriptions will depend on management goals (e.g., prescriptions targeting large wood recruitment and shade provision, Benda, Litschert, Reeves, & Pabst, 2016). However, the effects of site-specific or variable width regulations on longitudinal headwater stream temperature dynamics and the response to precipitation require additional study (Martin et al., 2021). This is because most variable-width buffer work has focused on boreal regions (Kuglerová et al., 2014; Laudon et al., 2016; Tiwari et al., 2016), with limited consideration of stream temperature. However, the very limited results in forested headwater streams are promising. In western Oregon, Anderson & Poage (2014) determined that variable-width buffers designed to encompass the extent of riparian forest features (20.2-29.5 m wide) were suitable to maintain streambed temperatures similar to unharvested reference streams.

As forest harvesting has been measured to increase air temperatures 3-6 °C and soil temperatures 10-15 °C (Moore et al., 2005a), the potential for increases in stream temperature related to forest harvest is greatest for thermally sensitive locations and geomorphic features within streams. Indeed, higher thermal sensitivities have been measured in streams with open versus forested canopy, indicating the effect of radiative and convective warming are cumulative (Simmons et al., 2014). Thus, the impact to shallow subsurface sourced streams such as those in the Northern California Coast Range will likely be greater than to those sourced from deeper groundwater sources or snowmelt (Mayer, 2012) such as those draining the Cascade Range. Overall, there is a critical need

for more effective, dynamic riparian protections that are specific to a given hydrologic landscape, considering the spatial heterogeneity in hydrological and atmospheric processes that influence stream temperature. Riparian regulations should consider the dynamic vegetation, lithology, and soil characteristics present in the riparian zone (Kuglerová et al., 2014) and represent the gradient of riparian forest composition such that exists on a landscape unaffected by anthropogenic disturbances (Kreutzweiser, Sibley, Richardson, & Gordon, 2012).

There is also potential for the hysteresis indices used in chapter three to be used to analyze the effects of forest harvest on streamflow generation processes using stream temperature as a tracer. Monitoring the instream response of stream temperature and quantifying the post-harvest change in temperature-discharge hysteresis behavior may provide insight into the influence of forest harvesting and effectiveness of riparian buffers on minimizing changes to stormflow generation and stream temperature dynamics. After forest harvest, hillslopes denude of vegetation can transmit precipitation more quickly to the receiving stream as canopy interception and evapotranspiration are drastically reduced across the harvested area (Moore & Wondzell, 2005). The influence may be even greater in situations where topographic slope allow ground-based operations to compact soils on hillslopes or in the near stream zone, potentially increasing the proportion of runoff entering the stream as overland flow (Zemke, Enderling, Klein, & Skubski, 2019).

It is expected that compared to pre-harvest conditions, hysteresis index and flushing index values measured during similar events would be greater in magnitude post-harvest. This is likely due to a combination of 1) faster transmission of rainfall to the channel via direct channel interception as hillslopes and potentially riparian areas have less overhead vegetation (Moore & Wondzell, 2005), 2) greater shallow soil temperatures due to adsorption of solar radiation (Anderson, Larson, & Chan, 2007; Moore et al., 2005a), 3) alteration of subsurface flow pathways due to the removal or modification of macropores and preferential flow pathways (Moore & Wondzell, 2005; Puntenney-Desmond, Bladon, & Silins, 2020), and 4) increased proportion of overland flow if soil compaction results in decreased infiltration capacity (Zemke et al., 2019). These factors may also coalesce and cause potentially biologically significant increases in stream

temperature during storm events, especially during summer events when air temperatures are high and catchment wetness is low (Lange & Haensler, 2012; Wilby et al., 2015) and runoff is primarily sourced from the shallow subsurface and near stream areas (Penna et al., 2015). Although the stream temperature response to storm events measured in chapter three were not likely biologically meaningful, it is expected that following forest harvest, increases in shallow throughflow temperatures due to accumulated solar radiation could potentially cause short-term changes in stream temperature during storm events that could cause acute stress to aquatic macroinvertebrates and fish (Hester & Doyle, 2011; Somers et al., 2013).

The in-stream response to storm events for other water quality constituents, such as dissolved organic carbon, has been measured to occur faster and be larger in magnitude in a harvested catchment compared to an unharvested catchment using hysteresis analysis (Mistick & Johnson, 2020). These authors attributed the increase in response magnitude post-harvest to changes in the dominate flow paths, which could alter both chemical and thermal water quality. For studies assessing stream temperature change or the effectiveness of riparian buffer prescriptions following forest harvest, this could be achieved by comparing hysteresis metrics between harvested and unharvested catchments over a range of storm events. This is similar to the before-after-control-impact design commonly deployed in studies assessing the influence of forest harvesting activities on stream water quality (e.g., Groom, Johnson, Seeds, & Ice, 2017; Roon, Dunham, & Groom, 2021).

Overall, future investigations into headwater stream temperature dynamics, the response to storm flow, and the influence of alternative riparian management strategies should address the following questions:

- How effective are variable-width riparian buffers that are designed to protect locations along headwater streams with higher thermal sensitivity to changing atmospheric conditions?

- Can we develop reach scale models to predict longitudinal thermal sensitivity with easily accessible data on topography and meteorological conditions to inform alternative riparian management?
- How can regional lithology be incorporated into the design of alternative riparian management strategies?
- How does stream temperature hysteresis during storm events change after forest harvest?
- Can stream temperature hysteresis analysis be used to assess the influence of forest harvest on stream temperature or the effectiveness of riparian buffers?
- Can stream temperature hysteresis analysis during storm events be used to assess changes in runoff production pathways after forest harvest?

Bibliography

Aguilera, R., & Melack, J. M. (2018). Concentration-Discharge Responses to Storm Events in Coastal California Watersheds. *Water Resources Research*, *54*(1), 407–424. doi:10.1002/2017WR021578

Amatya, D. M., Campbell, J. L., Wohlgemuth, P., Elder, K. J., Sebestyen, S., Johnson, S. L., … Misra, D. (2016). Hydrological processes of reference watersheds in experimental forests, USA. In D. M. Amatya, T. M. Williams, L. Bren, & C. Jong (Eds.), *Forest hydrology: processes, management and assessment* (pp. 227–227). doi:10.1079/9781780646602.0000

Anderson, P. D., Larson, D. J., & Chan, S. S. (2007). Riparian buffer and density management influences on microclimate of young headwater forests of western Oregon. *Forest Science*, *53*(2), 254–269. doi:10.1093/forestscience/53.2.254

Anderson, P. D., & Poage, N. J. (2014). The Density Management and Riparian Buffer Study: A large-scale silviculture experiment informing riparian management in the Pacific Northwest, USA. *Forest Ecology and Management*, *316*, 90–99. doi:10.1016/j.foreco.2013.06.055

Arismendi, I., Dunham, J. B., Heck, M. P., Schultz, L. D., & Hockman-Wert, D. (2017). A statistical method to predict flow permanence in dryland streams from time series of stream Temperature. *Water (Switzerland)*, *9*(12), 1–13. doi:10.3390/w9120946

Arismendi, I., Safeeq, M., Dunham, J. B., & Johnson, S. L. (2014). Can air temperature be used to project influences of climate change on stream temperature? *Environmental Research Letters*, *9*(8), 1–12. doi:10.1088/1748-9326/9/8/084015

Arismendi, I., Safeeq, M., Johnson, S. L., Dunham, J. B., & Haggerty, R. (2013). Increasing synchrony of high temperature and low flow in western North American streams: Double trouble for coldwater biota? *Hydrobiologia*, *712*(1), 61–70. doi:10.1007/s10750-012-1327-2

Arp, P. (2009). Wet-Areas Maps : a Tool for Better Forest Operations Planning. SFM Network Research Note Series No. 55. In *Network*. Fredericton.

Arscott, D., Tockner, K., & Ward, J. V. (2001). Thermal heterogeneity along a braided floodplain river (Tagliamento River, northeastern Italy). *Canadian Journal of Fisheries and Aquatic Sciences*, *58*(12), 2359–2373. doi:10.1139/cjfas-58-12-2359

Benda, L. E., Litschert, S. E., Reeves, G., & Pabst, R. (2016). Thinning and in-stream wood recruitment in riparian second growth forests in coastal Oregon and the use of buffers and tree tipping as mitigation. *Journal of Forestry Research*, *27*(4), 821–836. doi:10.1007/s11676-015-0173-2

Benjamin, J. R., Connolly, P. J., Romine, J. G., & Perry, R. M. (2013). Potential effects of changes in temperature and food resources on life history trajectories of juvenile oncorhynchus mykiss. *Transactions of the American Fisheries Society*, *142*(1), 208–220. doi:10.1080/00028487.2012.728162

Benjamini, Y., & Hochberg, Y. (1995). Controlling the False Discovery Rate : A Practical and Powerful Approach to Multiple Testing. *Journal of the Royal Statistical Society*, *57*(1), 289–300.

Bernhardt, E. S., Heffernan, J. B., Grimm, N. B., Stanley, E. H., Harvey, J. W., Arroita, M., … Yackulic, C. B. (2018). The metabolic regimes of flowing waters. *Limnology and Oceanography*, *63*, 99–118. doi:10.1002/lno.10726

Beven, K. J., & Kirkby, M. J. (1979). A physically based, variable contributing area model of basin hydrology. *Hydrological Sciences Bulletin*, *24*(1), 43–69. doi:10.1080/02626667909491834

Bladon, K. D., Segura, C., Cook, N. A., Bywater-Reyes, S., & Reiter, M. (2018). A multicatchment analysis of headwater and downstream temperature effects from contemporary forest harvesting. *Hydrological Processes*, *32*(2), 293–304. doi:10.1002/hyp.11415

Blaen, P. J., Hannah, D. M., Brown, L. E., & Milner, A. M. (2013). Water temperature dynamics in High Arctic river basins. *Hydrological Processes*, *27*(20), 2958–2972. doi:10.1002/hyp.9431

Bond, R. M., Stubblefield, A. P., & Van Kirk, R. W. (2015). Sensitivity of summer stream temperatures to climate variability and riparian reforestation strategies. *Journal of Hydrology: Regional Studies*, *4*, 267–279. doi:10.1016/j.ejrh.2015.07.002

Bowler, D. E., Mant, R., Orr, H., Hannah, D. M., & Pullin, A. S. (2012). What are the effects of wooded riparian zones on stream temperature? *Environmental Evidence*, *1*(1). doi:10.1186/2047-2382-1-3

Brewitt, K. S., Danner, E. M., & Moore, J. W. (2017). Hot eats and cool creeks: Juvenile pacific Salmonids use mainstem prey while in thermal refuges. *Canadian Journal of Fisheries and Aquatic Sciences*, *74*(10), 1588–1602. doi:10.1139/cjfas-2016-0395

Briggs, M. A., Dawson, C. B., Holmquist-Johnson, C. L., Williams, K. H., & Lane, J. W. (2018a). Efficient hydrogeological characterization of remote stream corridors using drones. *Hydrological Processes*, *33*(2), 316–319. doi:10.1002/hyp.13332

Briggs, M. A., Johnson, Z. C., Snyder, C. D., Hitt, N. P., Kurylyk, B. L., Lautz, L., … Lane, J. W. (2018b). Inferring watershed hydraulics and cold-water habitat persistence using multi-year air and stream temperature signals. *Science of the Total Environment*, *636*, 1117–1127. doi:10.1016/j.scitotenv.2018.04.344

Briggs, M. A., Lane, J. W., Snyder, C. D., White, E. A., Johnson, Z. C., Nelms, D. L., & Hitt, N. P. (2018c). Shallow bedrock limits groundwater seepage-based headwater climate refugia. *Limnologica*, *68*, 142–156. doi:10.1016/j.limno.2017.02.005

Briggs, M. A., Lautz, L. K., McKenzie, J. M., Gordon, R. P., & Hare, D. K. (2012). Using high-resolution distributed temperature sensing to quantify spatial and temporal variability in vertical hyporheic flux. *Water Resources Research*, *48*(2), 1–16. doi:10.1029/2011WR011227

Broadmeadow, S., & Nisbet, T. R. (2004). The effects of riparian forest management on the freshwater environment: a literature review of best management practice. *Hydrology and Earth System Sciences*, *8*(3), 286–305. doi:10.5194/hess-8-286-2004

Brosofske, K. D., Chen, J., Naiman, R. J. ., & Franklin, J. F. . (1997). Harvesting Effects on Microclimatic Gradients from Small Streams to Uplands in Western Washington. *Ecological Applications*, *7*(4), 1188–1200. doi:10.1890/1051-0761(1997)007[1188:HEOMGF]2.0.CO;2

Brown, G. W. (1969). Predicting Temperatures of Small Streams. *Water Resources Research*, *5*(1), 68–75. doi:10.1029/WR005i001p00068

Brown, L. E., & Hannah, D. M. (2008). Spatial heterogeneity of water temperature across an alpine river basin. *Hydrological Processes*, *22*, 954–967. doi:10.1002/hyp.6982

Butturini, A., Alvarez, M., Bernał, S., Vazquez, E., & Sabater, F. (2008). Diversity and temporal sequences of forms of DOC and NO3- discharge responses in an intermittent stream: Predictable or random succession? *Journal of Geophysical Research: Biogeosciences*, *113*(3), 1–10. doi:10.1029/2008JG000721

Cafferata, P. H. (1990). Temperature regimes of small streams along the Mendocino coast. In *JDSF Newsletter* (Vol. 39). Fort Bragg, CA.

Cafferata, P. H., & Reid, L. M. (2013). *Applications of long-term watershed research to forest management in California: 50 years of learning from the Caspar Creek experimental watersheds*. California Forestry Report No. 5. The State of California Board of Forestry and Fire Protection, Sacramento, CA.

Caissie, D. (2006). The thermal regime of rivers: A review. *Freshwater Biology*, *51*(8), 1389–1406. doi:10.1111/j.1365-2427.2006.01597.x

CAL FIRE. (2013). *Initial study for the proposed LaTour Demonstration State Forest 2013 management plan*. The State of California Board of Forestry and Fire Protection, Sacramento, CA.

CAL FIRE. (2020). *California Forest Practice Rules*.

Caldwell, P., Segura, C., Gull Laird, S., Sun, G., Mcnulty, S. G., Sandercock, M., … Vose, J. M. (2015). Short-term stream water temperature observations permit rapid assessment of potential climate change impacts. *Hydrological Processes*, *29*(9), 2196–2211. doi:10.1002/hyp.10358

Callahan, M. K., Rains, M. C., Bellino, J. C., Walker, C. M., Baird, S. J., Whigham, D. F., & King, R. S. (2015). Controls on temperature in salmonid-bearing headwater streams in two common hydrogeologic settings, Kenai Peninsula, Alaska. *Journal of the American Water Resources Association*, *51*(1), 84–98. doi:10.1111/jawr.12235

Campbell, J. L., Rustad, L. E., Porter, J. H., Taylor, J. R., Dereszynski, E. W., Shanley, J. B., … Boose, E. R. (2013). Quantity is nothing without quality: Automated QA/QC for streaming environmental sensor data. *BioScience*, *63*(7), 574–585. doi:10.1525/bio.2013.63.7.10

Chang, H., & Psaris, M. (2013). Local landscape predictors of maximum stream temperature and thermal sensitivity in the Columbia River Basin, USA. *Science of the Total Environment*, *461–462*, 587–600. doi:10.1016/j.scitotenv.2013.05.033

Coats, W. A., & Jackson, C. R. (2020). Riparian canopy openings on mountain streams: Landscape controls upon temperature increases within openings and cooling downstream. *Hydrological Processes*, (March 2019), 1966–1980. doi:10.1002/hyp.13706

Constantz, J., Cox, M. H., & Su, G. W. (2003). Comparison of Heat and Bromide as Ground Water Tracers Near Streams. *Ground Water*, *41*(5), 647–656. doi:10.1111/j.1745-6584.2003.tb02403.x

Cowood, A. L., Moore, C. L., Cracknell, M. J., Young, J., Muller, R., Nicholson, A. T., … Cook, W. (2017). Expansion of landscape characterisation methods within the Hydrogeological Landscape Framework: application in the Australian Capital Territory. *Australian Journal of Earth Sciences*, *64*(8), 1073–1084. doi:10.1080/08120099.2017.1255656

Croghan, D., Van Loon, A. F., Sadler, J. P., Bradley, C., & Hannah, D. M. (2019). Prediction of river temperature surges is dependent on precipitation method. *Hydrological Processes*, *33*(1), 144–159. doi:10.1002/hyp.13317

Dallas, H. F., & Ross-Gillespie, V. (2015). Sublethal effects of temperature on freshwater organisms, with special reference to aquatic insects. *Water SA*, *41*(5), 712–726. doi:10.4314/wsa.v41i5.15

Danehy, R. J., Colson, C. G., & Duke, S. D. (2010). Winter longitudinal thermal regime in four mountain streams. *Northwest Science*, *84*(2), 151–158. doi:10.3955/046.084.0204

Dawson, T. E. (1998). Fog in the California redwood forest: ecosystem inputs and use by plants. *Oecologia*, *117*, 476–485. doi:10.1007/s004420050683

Dent, L., Vick, D., Abraham, K., Schoenholtz, S., & Johnson, S. L. (2008). Summer temperature patterns in headwater streams of the Oregon Coast Range. *Journal of the American Water Resources Association*, *44*(4), 803–813. doi:10.1111/j.1752-1688.2008.00204.x

Detty, J. M., & McGuire, K. J. (2010). Threshold changes in storm runoff generation at a till-mantled headwater catchment. *Water Resources Research*, *46*(7), 1–15. doi:10.1029/2009WR008102

Dick, J. J., Tetzlaff, D., & Soulsby, C. (2018). Role of riparian wetlands and hydrological connectivity in the dynamics of stream thermal regimes. *Hydrology Research*, *49*(3), 634–647. doi:10.2166/nh.2017.066

Dralle, D. N., Hahm, W. J., Rempe, D. M., Karst, N. J., Thompson, S. E., & Dietrich, W. E. (2018). Quantification of the seasonal hillslope water storage that does not drive streamflow. *Hydrological Processes*, *32*(13), 1978–1992. doi:10.1002/hyp.11627

Dugdale, S. J., Bergeron, N. E., & St-Hilaire, A. (2015). Spatial distribution of thermal refuges analysed in relation to riverscape hydromorphology using airborne thermal infrared imagery. *Remote Sensing of Environment*, *160*, 43–55. doi:10.1016/j.rse.2014.12.021

Dugdale, S. J., Malcolm, I. A., Kantola, K., & Hannah, D. M. (2018). Stream temperature under contrasting riparian forest cover: Understanding thermal dynamics and heat exchange processes. *Science of the Total Environment*, *610–611*, 1375–1389. doi:10.1016/j.scitotenv.2017.08.198

Eaton, J. G., & Scheller, R. M. (1996). Effects of climate warming on fish thermal habitat in streams of the United States. *Limnology and Oceanography*, *41*(5), 1109–1115. doi:10.4319/lo.1996.41.5.1109

Ebersole, J. L., Liss, W. J., & Frissell, C. A. (2003). Cold water patches in warm streams: Physicochemical characteristics and the influence of shading. *Journal of the American Water Resources Association*, *39*(2), 355–368. doi:10.1111/j.1752-1688.2003.tb04390.x

Ebersole, J. L., Wigington, P. J., Leibowitz, S. G., Comeleo, R. L., & Van Sickle, J. (2015). Predicting the occurrence of cold-water patches at intermittent and ephemeral tributary confluences with warm rivers. *Freshwater Science*, *34*(1), 111–124. doi:10.1086/678127

Erdozain, M., Emilson, C. E., Kreutzweiser, D. P., Kidd, K. A., Mykytczuk, N., & Sibley, P. K. (2020). Forest management influences the effects of streamside wet areas on stream ecosystems. *Ecological Applications*, *30*(4), 1–16. doi:10.1002/eap.2077

Evans, C., & Davies, T. D. (1998). Causes of concentration/discharge hysteresis and its potential as a tool for analysis of episode hydrochemistry. *Water Resources Research*, *34*(1), 129–137. doi:10.1029/97WR01881

Fellman, J. B., Hood, E., Dryer, W., & Pyare, S. (2015). Stream physical characteristics impact habitat quality for pacific salmon in two temperate coastal watersheds. *PLoS ONE*, *10*(7), 1–16. doi:10.1371/journal.pone.0132652

Ficklin, D. L., Luo, Y., Stewart, I. T., & Maurer, E. P. (2012). Development and application of a hydroclimatological stream temperature model within the Soil and Water Assessment Tool. *Water Resources Research*, *48*(1), 1511. doi:10.1029/2011WR011256

Ford, M. J., Albaugh, A., Barnas, K., Cooney, T., Cowen, J., Hard, J. J., … Weitkamp, L. A. (2011). *Status review update for Pacific Salmon and steelhead listed under the Endangered Species Act: Pacific Northwest*. U.S. Dept. Commer. NOAA Technical Memorandum NMFS-NWFSC-113, Seattle, WA.

Fratkin, M. M., Segura, C., & Bywater-Reyes, S. (2020). The influence of lithology on channel geometry and bed sediment organization in mountainous hillslope-coupled streams. *Earth Surface Processes and Landforms*, *45*(10), 2365–2379. doi:10.1002/esp.4885

Freeman, M. C., Pringle, C. M., & Jackson, C. R. (2007). Hydrologic connectivity and the contribution of stream headwaters to ecological integrity at regional scales. *Journal of the American Water Resources Association*, *43*(1), 5–14. doi:10.1111/j.1752-1688.2007.00002.x

Freer, J., McDonnell, J. J., Beven, K. J., Peters, N. E., Burns, D. A., Hooper, R. P., … Kendall, C. (2002). The role of bedrock topography on subsurface storm flow. *Water Resources Research*, *38*(12), 1–16. doi:10.1029/2001wr000872

Fritz, K. M., Nadeau, T. L., Kelso, J. E., Beck, W. S., Mazor, R. D., Harrington, R. A., & Topping, B. J. (2020). Classifying streamflow duration: The scientific basis and an operational framework for method development. *Water (Switzerland)*, *12*(9), 1–34. doi:10.3390/w12092545

Fullerton, A. H., Torgersen, C. E., Lawler, J. J., Faux, R. N., Steel, E. A., Beechie, T. J., … Leibowitz, S. G. (2015). Rethinking the longitudinal stream temperature paradigm: Region-wide comparison of thermal infrared imagery reveals unexpected complexity of river temperatures. *Hydrological Processes*, *29*(22), 4719–4737. doi:10.1002/hyp.10506

Fullerton, A. H., Torgersen, C. E., Lawler, J. J., Steel, E. A., Ebersole, J. L., & Lee, S. Y. (2018). Longitudinal thermal heterogeneity in rivers and refugia for coldwater species: effects of scale and climate change. *Aquatic Sciences*, *80*(1), 1–15. doi:10.1007/s00027-017-0557-9

Gabrielli, C. P., McDonnell, J. J., & Jarvis, W. T. (2012). The role of bedrock groundwater in rainfall-runoff response at hillslope and catchment scales. *Journal of Hydrology*, *450–451*, 117–133. doi:10.1016/j.jhydrol.2012.05.023

Garner, G., Malcolm, I. A., Sadler, J. P., & Hannah, D. M. (2014). What causes cooling water temperature gradients in a forested stream reach? *Hydrology and Earth System Sciences*, *18*(12), 5361–5376. doi:10.5194/hess-18-5361-2014

Garner, G., Malcolm, I. A., Sadler, J. P., & Hannah, D. M. (2017). The role of riparian vegetation density, channel orientation and water velocity in determining river temperature dynamics. *Journal of Hydrology*, *553*, 471–485. doi:10.1016/j.jhydrol.2017.03.024

Gendaszek, A. S., Dunham, J. B., Torgersen, C. E., Hockman-Wert, D. P., Heck, M. P., Thorson, J., … Allai, T. (2020). Land-cover and climatic controls on water temperature, flow permanence, and fragmentation of Great Basin stream networks. *Water (Switzerland)*, *12*(7), 1–29. doi:10.3390/w12071962

Genereux, D. P., Hemond, H. F., & Mulholland, P. J. (1993). Spatial and temporal variability in streamflow generation on the West Fork of Walker Branch Watershed. *Journal of Hydrology*, *142*(1–4), 137–166. doi:10.1016/0022-1694(93)90009-X

Gerecht, K. (2012). *Anomalous stream temperature response to storms in a forested headwater stream in Central Pennsylvania*. Pennsylvania State University.

Gomi, T., Asano, Y., Uchida, T., Onda, Y., Sidle, R. C., Miyata, S., … Fukushima, T. (2010). Evaluation of storm runoff pathways in steep nested catchments draining a Japanese cypress forest in central Japan: a geochemical approach. *Hydrological*, *24*(November 2008), 550–566. doi:10.1002/hyp.7550

Gomi, T., Moore, R. D., & Dhakal, A. S. (2006). Headwater stream temperature response to clear-cut harvesting with different riparian treatments, coastal British Columbia, Canada. *Water Resources Research*, *42*(8), 1–11. doi:10.1029/2005WR004162

Gomi, T., Sidle, R. C., & Richardon, J. S. (2002). Understanding Processes and Downstream Linkages of Headwater Systems. *BioScience*, *52*(10), 905. doi:10.1641/0006-3568(2002)052[0905:upadlo]2.0.co;2

Gorsevski, P. V., Boll, J., Gomezdelcampo, E., & Brooks, E. S. (2008). Dynamic riparian buffer widths from potential non-point source pollution areas in forested watersheds. *Forest Ecology and Management*, *256*(4), 664–673. doi:10.1016/j.foreco.2008.05.019

Grabs, T., Seibert, J., Bishop, K., & Laudon, H. (2009). Modeling spatial patterns of saturated areas: A comparison of the topographic wetness index and a dynamic distributed model. *Journal of Hydrology*, *373*(1–2), 15–23. doi:10.1016/j.jhydrol.2009.03.031

Griebler, C., & Avramov, M. (2015). Groundwater ecosystem services: A review. *Freshwater Science*, *34*(1), 355–367. doi:10.1086/679903

Groom, J. D., Dent, L., Madsen, L. J., & Fleuret, J. (2011). Response of western Oregon (USA) stream temperatures to contemporary forest management. *Forest Ecology and Management*, *262*(8), 1618–1629. doi:10.1016/j.foreco.2011.07.012

Groom, J. D., Johnson, S. L., Seeds, J. D., & Ice, G. G. (2017). Evaluating links between forest harvest and stream temperature threshold exceedances: The value of spatial and temporal data. *Journal of the American Water Resources Association*, *53*(4), 761–773. doi:10.1111/1752-1688.12529

Groom, J. D., Madsen, L. J., Jones, J. E., & Giovanini, J. N. (2018). Informing changes to riparian forestry rules with a Bayesian hierarchical model. *Forest Ecology and Management*, *419–420*(March), 17–30. doi:10.1016/j.foreco.2018.03.014

Gu, C., Anderson, W. P., Colby, J. D., & Coffey, C. L. (2015). Air-stream temperature correlation in forested and urban headwater streams in the Southern Appalachians. *Hydrological Processes*, *29*(6), 1110–1118. doi:10.1002/hyp.10225

Guenther, S. M. (2007). *Impacts of Partial-Retention Harvesting With No Buffer on the Thermal Regime of a Headwater Stream and Its Riparian Zone*. University of British Columbia.

Guenther, S. M., Gomi, T., & Moore, R. D. (2014). Stream and bed temperature variability in a coastal headwater catchment: Influences of surface-subsurface interactions and partial-retention forest harvesting. *Hydrological Processes*, *28*(3), 1238–1249. doi:10.1002/hyp.9673

Halama, J. J., Kennedy, R. E., Graham, J. J., McKane, R. B., Barnhart, B. L., Djang, K. S., … Wingo, P. C. (2018). Penumbra: A spatially distributed, mechanistic model for simulating ground-level incident solar energy across heterogeneous landscapes. *PLoS ONE*, *13*(12), 1–21. doi:10.1371/journal.pone.0206439

Hale, V. C., & McDonnell, J. J. (2016). Effect of bedrock permeability on stream base flow mean transit time scaling relations: 1. A multiscale catchment intercomparison. *Water Resources Research*, *52*(2), 1358–1374. doi:10.1002/2014WR016124

Hale, V. C., McDonnell, J. J., Stewart, M. K., Solomon, D. K., Doolitte, J., Ice, G. G., & Pack, R. T. (2016). Effect of bedrock permeability on stream base flow mean transit time scaling relationships: 2. Process study of storage and release. *Water Resources Research*, *52*, 1375–1397. doi:10.1002/2015WR017660

Hangen, E., Lindenlaub, M., Leibundgut, C., & Von Wilpert, K. (2001). Investigating mechanisms of stormflow generation by natural tracers and hydrometric data: A small catchment study in the Black Forest, Germany. *Hydrological Processes*, *15*(2), 183–199. doi:10.1002/hyp.142

Hannah, D. M., Malcolm, I. A., Soulsby, C., & Youngson, A. F. (2008). A comparison of forest and moorland stream microclimate, heat exchanges and thermal dynamics. *Hydrological Processes*. doi:10.1002/hyp.7003

Harrington, J. S., Hayashi, M., & Kurylyk, B. L. (2017). Influence of a rock glacier spring on the stream energy budget and cold-water refuge in an alpine stream. *Hydrological Processes*, *31*(26), 4719–4733. doi:10.1002/hyp.11391

Hebert, C., Caissie, D., Satish, M. G., & El-Jabi, N. (2011). Study of stream temperature dynamics and corresponding heat fluxes within Miramichi River catchments (New Brunswick, Canada). *Hydrological Processes*, *25*(15), 2439–2455. doi:10.1002/hyp.8021

Herb, W. R., Janke, B., Mohseni, O., & Stefan, H. G. (2008). Thermal pollution of streams by runoff from paved surfaces. *Hydrological Processes*, *22*, 987–999. doi:10.1002/hyp.6986

Hester, E. T., & Doyle, M. W. (2011). Human impacts to river temperature and their effects on biological processes: A quantitative synthesis. *Journal of the American Water Resources Association*, *47*(3), 571–587. doi:10.1111/j.1752-1688.2011.00525.x

Hilderbrand, R. H., Kashiwagi, M. T., & Prochaska, A. P. (2014). Regional and local scale modeling of stream temperatures and spatio-temporal variation in thermal sensitivities. *Environmental Management*, *54*(1), 14–22. doi:10.1007/s00267-014-0272-4

Hofmeister, K. L., Cianfrani, C. M., & Hession, W. C. (2015). Complexities in the stream temperature regime of a small mixed-use watershed, Blacksburg, VA. *Ecological Engineering*, *78*, 101–111. doi:10.1016/j.ecoleng.2014.05.019

Isaak, D. J., Luce, C. H., Chandler, G. L., Horan, D. L., & Wollrab, S. P. (2018). Principal components of thermal regimes in mountain river networks. *Hydrology and Earth System Sciences*, *22*(12), 6225–6240. doi:10.5194/hess-22-6225-2018

Isaak, D. J., Young, M. K., Luce, C. H., Hostetler, S. W., Wenger, S. J., Peterson, E. E., … Nagel, D. E. (2016). Slow climate velocities of mountain streams portend their role as refugia for cold-water biodiversity. *Proceedings of the National Academy of Sciences of the United States of America*, *113*(16), 4374–4379. doi:10.1073/pnas.1522429113

Jackson, F. L., Fryer, R. J., Hannah, D. M., Millar, C. P., & Malcolm, I. A. (2018). A spatio-temporal statistical model of maximum daily river temperatures to inform the management of Scotland's Atlantic salmon rivers under climate change. *Science of the Total Environment*, *612*, 1543–1558. doi:10.1016/j.scitotenv.2017.09.010

Jaeger, K. L., Montgomery, D. R., & Bolton, S. M. (2007). Channel and perennial flow initiation in headwater streams: Management implications of variability in source-area size. *Environmental Management*, *40*(5), 775–786. doi:10.1007/s00267-005-0311-2

Janisch, J. E., Wondzell, S. M., & Ehinger, W. J. (2012). Headwater stream temperature: Interpreting response after logging, with and without riparian buffers, Washington, USA. *Forest Ecology and Management*, *270*, 302–313. doi:10.1016/j.foreco.2011.12.035

Jefferson, A., Grant, G., & Rose, T. (2006). Influence of volcanic history on groundwater patterns on the west slope of the Oregon High Cascades. *Water Resources Research*, *42*(12), 1–15. doi:10.1029/2005WR004812

Jencso, K. G., McGlynn, B. L., Gooseff, M. N., Wondzell, S. M., Bencala, K. E., & Marshall, L. A. (2009). Hydrologic connectivity between landscapes and streams: Transferring reach- and plot-scale understanding to the catchment scale. *Water Resources Research*, *45*(4), 1–16. doi:10.1029/2008WR007225

Johnson, B. R., Haas, A., & Fritz, K. M. (2010). Use of spatially explicit physicochemical data to measure downstream impacts of headwater stream disturbance. *Water Resources Research*, *46*(9), 1–15. doi:10.1029/2009WR008417

Johnson, M. F., Wilby, R. L., & Toone, J. A. (2014). Inferring air-water temperature relationships from river and catchment properties. *Hydrological Processes*, *28*(6), 2912–2928. doi:10.1002/hyp.9842

Johnson, S. L. (2003). Stream temperature: scaling of observations and issues for modelling. *Hydrological Processes*, *17*(2), 497–499. doi:10.1002/hyp.5091

Johnson, S. L. (2004). Factors influencing stream temperatures in small streams: Substrate effects and a shading experiment. *Canadian Journal of Fisheries and Aquatic Sciences*, *61*(6), 913–923. doi:10.1139/F04-040

Johnson, Z. C., Snyder, C. D., & Hitt, N. P. (2017). Landform features and seasonal precipitation predict shallow groundwater influence on temperature in headwater streams. *Water Resources Research*, 5788–5812. doi:10.1002/2017WR020455

Kanno, Y., Vokoun, J. C., & Letcher, B. H. (2014). Paired stream-air temperature measurements reveal fine-scale thermal heterogeneity within headwater brook trout stream networks. *River Research and Applications*, *30*, 745–755. doi:10.1002/rra.2677

Kasahara, T., & Wondzell, S. M. (2003). Geomorphic controls on hyporheic exchange flow in mountain streams. *Water Resources Research*, *39*(1), 1–14. doi:10.1029/2002wr001386

Kassambara, A. (2021). *R package "rstatix": Pipe-Friendly Framework for Basic Statistical Tests*. R package version 0.7.0.

Kelleher, C., Wagener, T., Gooseff, M., McGlynn, B., McGuire, K., & Marshall, L. (2012). Investigating controls on the thermal sensitivity of Pennsylvania streams. *Hydrological Processes*, *26*(5), 771–785. doi:10.1002/hyp.8186

Kelson, K. I., & Wells, S. G. (1989). Geologic influences on fluvial hydrology and bedload transport in small mountainous watersheds, Northern New Mexico, U.S.A. *Earth Surface Processes and Landforms*, *14*(8), 671–690. doi:10.1002/esp.3290140803

Keppeler, E. T., & Brown, D. (1998). Subsurface drainage processes and management impacts. In R. R. Ziemer (Ed.), *Proceedings of the Conference on Coastal Watersheds: The Caspar Creek Story, May 6, 1998, Ukiah, California* (pp. 25–34). Albany, CA: U.S. Forest Service Pacific Southwest Research Station, General Technical Report PSW GTR-168.

Keppeler, E. T., Ziemer, R. R., & Cafferata, P. H. (1994). Changes in soil moisture and pore pressure after harvesting a forested hillslope in northern California. In R. A. Marston & V. R. Hasfurther (Eds.), *Annual summer symposium of the American Water Resources Association: Effects of human-induced changes on hydrologic systems, 26-29 June 1994, Jackson Hole, Wyoming* (pp. 205–214). Bethesda, MD: American Water Resources Association.

Kibler, K. M., Skaugset, A., Ganio, L. M., & Huso, M. M. (2013). Effect of contemporary forest harvesting practices on headwater stream temperatures: Initial response of the Hinkle Creek catchment, Pacific Northwest, USA. *Forest Ecology and Management*, *310*, 680–691. doi:10.1016/j.foreco.2013.09.009

Kiffney, P. M., Richardson, J. S., & Bull, J. P. (2003). Responses of periphyton and insects to experimental manipulation of riparian buffer width along forest streams. *Journal of Applied Ecology*, *40*(6), 1060–1076. doi:10.1111/j.1365-2664.2003.00855.x

Klos, P. Z., & Link, T. E. (2018). Quantifying shortwave and longwave radiation inputs to headwater streams under differing canopy structures. *Forest Ecology and Management*, *407*(October 2017), 116–124. doi:10.1016/j.foreco.2017.10.046

Kobayashi, D., Ishii, Y., & Kodama, Y. (1999). Stream temperature, specific conductance and runoff process in mountain watersheds. *Hydrological Processes*, *13*(6), 865–876. doi:10.1002/(SICI)1099-1085(19990430)13:6<865::AID-HYP761>3.0.CO;2-O

Kreutzweiser, D. P., Sibley, P. K., Richardson, J. S., & Gordon, A. M. (2012). Introduction and a theoretical basis for using disturbance by forest management activities to sustain aquatic ecosystems. *Freshwater Science*, *31*(1), 224–231. doi:10.1899/11-114.1

Krosby, M., Theobald, D. M., Norheim, R., & McRae, B. H. (2018). Identifying riparian climate corridors to inform climate adaptation planning. *PLoS ONE*, *13*(11), 1–18. doi:10.1371/journal.pone.0205156

Kuglerová, L., Ågren, A., Jansson, R., & Laudon, H. (2014). Towards optimizing riparian buffer zones: Ecological and biogeochemical implications for forest management. *Forest Ecology and Management*, *334*, 74–84. doi:10.1016/j.foreco.2014.08.033

Lange, J., & Haensler, A. (2012). Runoff generation following a prolonged dry period. *Journal of Hydrology*, *464–465*, 157–164. doi:10.1016/j.jhydrol.2012.07.010

Larsen, L. G., & Woelfle-Erskine, C. (2018). Groundwater is key to salmonid persistence and recruitment in intermittent Mediterranean-climate streams. *Water Resources Research*, *54*(11), 8909–8930. doi:10.1029/2018WR023324

Larson, S. L., Larson, L. L., & Larson, P. A. (2002). Perspectives on water flow and the interpretation of FLIR images. *Journal of Range Management*, *55*(2), 106–111. doi:10.2307/4003344

Laudon, H., Kuglerová, L., Sponseller, R. A., Futter, M., Nordin, A., Bishop, K., … Ågren, A. M. (2016). The role of biogeochemical hotspots, landscape heterogeneity, and hydrological connectivity for minimizing forestry effects on water quality. *Ambio*, *45*, 152–162. doi:10.1007/s13280-015-0751-8

Leach, J. A., Lidberg, W., Kuglerová, L., Peralta-Tapia, A., Ågren, A., & Laudon, H. (2017). Evaluating topography-based predictions of shallow lateral groundwater discharge zones for a boreal lake-stream system. *Water Resources Research*, *53*, 5420–5437. doi:10.1002/2016WR019804

Leach, J. A., & Moore, D. (2017). Insights on stream temperature processes through development of a coupled hydrologic and stream temperature model for forested coastal headwater catchments. *Hydrological Processes*, *31*(18), 3160–3177. doi:10.1002/hyp.11190

Leach, J. A., & Moore, R. D. (2010). Above-stream microclimate and stream surface energy exchanges in a wildfire-disturbed riparian zone. *Hydrological Processes*, *24*(17), 2369–2381. doi:10.1002/hyp.7639

Leach, J. A., & Moore, R. D. (2011). Stream temperature dynamics in two hydrogeomorphically distinct reaches. *Hydrological Processes*, *25*(5), 679–690. doi:10.1002/hyp.7854

Leach, J. A., & Moore, R. D. (2014). Winter stream temperature in the rain-on-snow zone of the Pacific Northwest: Influences of hillslope runoff and transient snow cover. *Hydrology and Earth System Sciences*, *18*(2), 819–838. doi:10.5194/hess-18-819-2014

Leach, J. A., & Moore, R. D. (2015). Observations and modeling of hillslope throughflow temperatures in a coastal forested catchment. *Water Resources Research*, 3770–3795. doi:10.1002/2014WR016763

Leach, J. A., Olson, D. H., Anderson, P. D., & Eskelson, B. N. I. (2016). Spatial and seasonal variability of forested headwater stream temperatures in western Oregon, USA. *Aquatic Sciences*, *79*(2), 291–307. doi:10.1007/s00027-016-0497-9

Lee, P., Smyth, C., & Boutin, S. (2004). Quantitative review of riparian buffer width guidelines from Canada and the United States. *Journal of Environmental Management*, *70*(2), 165–180. doi:10.1016/j.jenvman.2003.11.009

Leibowitz, S. G., Comeleo, R. L., Wigington, P. J., Weaver, C. P., Morefield, P. E., Sproles, E. A., & Ebersole, J. L. (2014). Hydrologic landscape classification evaluates streamflow vulnerability to climate change in Oregon, USA. *Hydrology and Earth System Sciences*, *18*(9), 3367–3392. doi:10.5194/hess-18-3367-2014

Lewis, T. E., Lamphear, D. W., McCanne, D. R., Webb, A. S., Krieter, J. P., & Conroy, W. D. (2000). *Regional assessment of stream temperatures across northern California and their relationship to various landscape-level and site-specific attributes*. Humboldt State University Foundation Forest Science Project, Arcata, CA.

Lisi, P. J., Schindler, D. E., Cline, T. J., Scheuerell, M. D., & Walsh, P. B. (2015). Watershed geomorphology and snowmelt control stream thermal sensitivity to air temperature. *Geophysical Research Letters*, *42*, 3380–3388. doi:10.1002/2015GL064083

Liu, W., Birgand, F., Tian, S., & Chen, C. (2021). Event-scale hysteresis metrics to reveal processes and mechanisms controlling constituent export from watersheds: A review☆. *Water Research*, *200*, 117254. doi:10.1016/j.watres.2021.117254

Lloyd, C. E. M., Freer, J. E., Johnes, P. J., & Collins, A. L. (2016a). Technical Note: Testing an improved index for analysing storm discharge-concentration hysteresis. *Hydrology and Earth System Sciences*, *20*(2), 625–632. doi:10.5194/hess-20-625-2016

Lloyd, C. E. M., Freer, J. E., Johnes, P. J., & Collins, A. L. (2016b). Using hysteresis analysis of high-resolution water quality monitoring data, including uncertainty, to infer controls on nutrient and sediment transfer in catchments. *Science of the Total Environment*, *543*, 388–404. doi:10.1016/j.scitotenv.2015.11.028

Loperfido, J. V., Just, C. L., & Schnoor, J. L. (2009). High-frequency diel dissolved oxygen stream data modeled for variable temperature and scale. *Journal of Environmental Engineering*, *135*(12), 1250–1256. doi:10.1061/(ASCE)EE.1943-7870.0000102

Lowe, W. H., & Likens, G. E. (2005). Moving Headwater Streams to the Head of the Class. *BioScience*. doi:10.1641/0006-3568(2005)055[0196:mhstth]2.0.co;2

Lowry, C. S., Walker, J. F., Hunt, R. J., & Anderson, M. P. (2007). Identifying spatial variability of groundwater discharge in a wetland stream using a distributed temperature sensor. *Water Resources Research*, *43*(October), 1–9. doi:10.1029/2007WR006145

MacDonald, G. A. (1963). *Geology of the Manzanita Lake quadrangle, California.* U.S. Geological Survey, Geologic Quadrangle Map GQ-248, scale 1:62,500.

MacDonald, L. H., & Coe, D. (2007). Influence of headwater streams on downstream reaches in forested areas. *Forest Science*, *53*(2), 148–168.

MacDonald, R. J., Boon, S., & Byrne, J. M. (2014a). A process-based stream temperature modelling approach for mountain regions. *Journal of Hydrology*, *511*, 920–931. doi:10.1016/j.jhydrol.2014.02.009

MacDonald, R. J., Boon, S., Byrne, J. M., Robinson, M. D., & Rasmussen, J. B. (2014b). Potential future climate effects on mountain hydrology, stream temperature, and native salmonid life history. *Canadian Journal of Fisheries and Aquatic Sciences*, *71*(2), 189–202. doi:10.1139/cjfas-2013-0221

Macdonald, R. J., Boon, S., Byrne, J. M., & Silins, U. (2014). A comparison of surface and subsurface controls on summer temperature in a headwater stream. *Hydrological Processes*, *28*(4), 2338–2347. doi:10.1002/hyp.9756

Magnusson, J., Jonas, T., & Kirchner, J. W. (2012). Temperature dynamics of a proglacial stream: Identifying dominant energy balance components and inferring spatially integrated hydraulic geometry. *Water Resources Research*, *48*(6), 1–16. doi:10.1029/2011WR011378

Maheu, A., Poff, N. L., & St-Hilaire, A. (2016). A Classification of Stream Water Temperature Regimes in the Conterminous USA. *River Research and Applications*. doi:10.1002/rra.2906

Martin, D. J., Kroll, A. J., & Knoth, J. L. (2021). An evidence-based review of the effectiveness of riparian buffers to maintain stream temperature and stream-associated amphibian populations in the Pacific Northwest of Canada and the United States. *Forest Ecology and Management*, *491*(March), 119190. doi:10.1016/j.foreco.2021.119190

Mayer, T. D. (2012). Controls of summer stream temperature in the Pacific Northwest. *Journal of Hydrology*, *475*, 323–335. doi:10.1016/j.jhydrol.2012.10.012

McDonald, S. R. (1995). *LaTour Demonstration State Forest sustained yield plan*. The State of California Board of Forestry and Fire Protection, Sacramento, CA.

Mistick, E., & Johnson, M. S. (2020). High-frequency analysis of dissolved organic carbon storm responses in headwater streams of contrasting forest harvest history. *Journal of Hydrology*, *590*(July), 125371. doi:10.1016/j.jhydrol.2020.125371

Mohseni, O., & Stefan, H. G. (1999). Stream temperature/air temperature relationship: A physical interpretation. *Journal of Hydrology*, *218*(3–4), 128–141. doi:10.1016/S0022-1694(99)00034-7

Monk, W. A., Wilbur, N. M., Allen Curry, R., Gagnon, R., & Faux, R. N. (2013). Linking landscape variables to cold water refugia in rivers. *Journal of Environmental Management*, *118*, 170–176. doi:10.1016/j.jenvman.2012.12.024

Montgomery, D. R., & Buffington, J. M. (1997). Channel-reach morphology in mountain drainage basins. *Bulletin of the Geological Society of America*, *109*(5), 596–611. doi:10.1130/0016-7606(1997)109<0596:CRMIMD>2.3.CO;2

Moore, R. D., Spittlehouse, D. L., & Story, A. (2005a). Riparian microclimate and stream temperature response to forest harvesting: A review. *Journal of the American Water Resources Association*, *41*(4), 813–834. doi:10.1111/j.1752-1688.2005.tb04465.x

Moore, R. D., Sutherland, P., Gomi, T., & Dhakal, A. (2005b). Thermal regime of a headwater stream within a clear-cut, coastal British Columbia, Canada. *Hydrological Processes*, *19*(13), 2591–2608. doi:10.1002/hyp.5733

Moore, R. D., & Wondzell, S. M. (2005). Physical hydrology and the effects of forest harvesting in the Pacific Northwest: A review. *Journal of the American Water Resources Association*, *41*(4), 763–784. doi:10.1111/j.1752-1688.2005.tb04463.x

Morin, A., Lamoureux, W., & Busnarda, J. (1999). Empirical models predicting primary productivity from chlorophyll a and water temperature for stream periphyton and lake and ocean phytoplankton. *Journal of the North American Benthological Society*, *18*(3), 299–307. doi:10.2307/1468446

Morrice, J. A., Valett, H. M., Dahm, C. N., & Campana, M. E. (1997). Alluvial characteristics, groundwater-surface water exchange and hydrological retention in headwater streams. *Hydrological Processes*, *11*(3), 253–267. doi:10.1002/(SICI)1099-1085(19970315)11:3<253::AID-HYP439>3.0.CO;2-J

Morrill, J. C., Bales, R. C., & Conklin, M. H. (2005). Estimating stream temperature from air temperature: Implications for future water quality. *Journal of Environmental Engineering*, *131*(1), 139–146. doi:10.1061/(ASCE)0733-9372(2005)131:1(139)

Neres-Lima, V., Machado-Silva, F., Baptista, D. F., Oliveira, R. B. S., Andrade, P. M., Oliveira, A. F., … Moulton, T. P. (2017). Allochthonous and autochthonous carbon flows in food webs of tropical forest streams. *Freshwater Biology*, *62*(6), 1012–1023. doi:10.1111/fwb.12921

Newton, M., & Ice, G. G. (2016). Regulating riparian forests for aquatic productivity in the Pacific Northwest, USA: addressing a paradox. *Environmental Science and Pollution Research*, *23*(2), 1149–1157. doi:10.1007/s11356-015-5814-7

Nichols, A. L., Willis, A. D., Jeffres, C. A., & Deas, M. L. (2014). Water temperature patterns below large groundwater springs: Management implications for coho salmon in the shasta river, california. *River Research and Applications*, *30*, 442–455. doi:10.1002/rra.2655

Nickolas, L. B., Segura, C., & Brooks, J. R. (2017). The influence of lithology on surface water sources. *Hydrological Processes*, *31*(10), 1913–1925. doi:10.1002/hyp.11156

O'Briain, R., Shephard, S., & Coghlan, B. (2017). River reaches with impaired riparian tree cover and channel morphology have reduced thermal resilience. *Ecohydrology*, *10*(8), 1–9. doi:10.1002/eco.1890

O'Callaghan, J. F., & Mark, D. M. (1984). The extraction of drainage networks from digital elevation data. *Computer Vision, Graphics, and Image Processing*, *28*(3), 323–344. doi:10.1016/S0734-189X(84)80011-0

O'Driscoll, M. A., & DeWalle, D. R. (2006). Stream-air temperature relations to classify stream-ground water interactions in a karst setting, central Pennsylvania, USA. *Journal of Hydrology*, *329*(1–2), 140–153. doi:10.1016/j.jhydrol.2006.02.010

O'Sullivan, A. M., Devito, K. J., & Curry, R. A. (2019). The influence of landscape characteristics on the spatial variability of river temperatures. *Catena*, *177*, 70–83. doi:10.1016/j.catena.2019.02.006

Olson, D. H., Anderson, P. D., Frissell, C. A., Welsh, H. H., & Bradford, D. F. (2007). Biodiversity management approaches for stream-riparian areas: Perspectives for Pacific Northwest headwater forests, microclimates, and amphibians. *Forest Ecology and Management*, *246*(1 SPEC. ISS.), 81–107. doi:10.1016/j.foreco.2007.03.053

Olson, D. H., & Rugger, C. (2007). Preliminary study of the effects of headwater riparian reserves with upslope thinning on stream habitats and amphibians in western Oregon. *Forest Science*, *53*(2), 331–342. doi:10.1093/forestscience/53.2.331

Oware, E. K., & Peterson, E. W. (2020). Storm driven seasonal variation in the thermal response of the streambed water of a low-gradient stream. *Water (Switzerland)*, *12*(9), 40–44. doi:10.3390/w12092498

Ozaki, N., Fukushima, T., Harasawa, H., Kojiri, T., Kawashima, K., & Ono, M. (2003). Statistical analyses on the effects of air temperature fluctuations on river water qualities. *Hydrological Processes*, *17*(14), 2837–2853. doi:10.1002/hyp.1437

Pate, A. A., Segura, C., & Bladon, K. D. (2020). Streamflow permanence in headwater streams across four geomorphic provinces in Northern California. *Hydrological Processes*, *34*(23), 4487–4504. doi:10.1002/hyp.13889

Penna, D., van Meerveld, H. J., Oliviero, O., Zuecco, G., Assendelft, R. S., Dalla Fontana, G., & Borga, M. (2015). Seasonal changes in runoff generation in a small forested mountain catchment. *Hydrological Processes*, *29*(8), 2027–2042. doi:10.1002/hyp.10347

Peterson, E. W., & Sickbert, T. B. (2006). Stream water bypass through a meander neck, laterally extending the hyporheic zone. *Hydrogeology Journal*, *14*(8), 1443–1451. doi:10.1007/s10040-006-0050-3

Ploum, S. W., Leach, J. A., Kuglerová, L., & Laudon, H. (2018). Thermal detection of discrete riparian inflow points (DRIPs) during contrasting hydrological events. *Hydrological Processes*, *32*(19), 3049–3050. doi:10.1002/hyp.13184

Pollock, M. M., Beechie, T. J., Liermann, M., & Bigley, R. E. (2009). Stream temperature relationships to forest harvest in Western Washington. *Journal of the American Water Resources Association*, *45*(1), 141–156. doi:10.1111/j.1752-1688.2008.00266.x

Poole, G. C., & Berman, C. H. (2001). An ecological perspective on in-stream temperature: Natural heat dynamics and mechanisms of human-caused thermal degradation. *Environmental Management*, *27*(6), 787–802. doi:10.1007/s002670010188

Puntenney-Desmond, K. C., Bladon, K. D., & Silins, U. (2020). Runoff and sediment production from harvested hillslopes and the riparian area during high intensity rainfall events. *Journal of Hydrology*, *582*(October 2019), 124452. doi:10.1016/j.jhydrol.2019.124452

Radke, A. G., Godsey, S. E., Lohse, K. A., McCorkle, E. P., Perdrial, J., Seyfried, M. S., & Holbrook, W. S. (2019). Spatiotemporal heterogeneity of water flowpaths controls dissolved organic carbon sourcing in a snow-dominated, headwater catchment. *Frontiers in Ecology and Evolution*, *7*(FEB). doi:10.3389/fevo.2019.00046

Railsback, S. F., & Rose, K. A. (1999). Bioenergetics modeling of stream trout growth: temperature and food consumption effects. *Transactions of the American Fisheries Society*, *128*(2), 241–256. doi:10.1577/1548-8659(1999)128<0241:bmostg>2.0.co;2

Reiter, M., Bilby, R. E., Beech, S., & Heffner, J. (2015). Stream Temperature Patterns over 35 Years in a Managed Forest of Western Washington. *Journal of the American Water Resources Association*, *51*(5), 1418–1435. doi:10.1111/1752-1688.12324

Rex, J. F., Maloney, D. A., Krauskopf, P. N., Beaudry, P. G., & Beaudry, L. J. (2012). Variable-retention riparian harvesting effects on riparian air and water temperature of sub-boreal headwater streams in British Columbia. *Forest Ecology and Management*, *269*, 259–270. doi:10.1016/j.foreco.2011.12.023

Richardson, J. S. (2019). Biological diversity in headwater streams. *Water (Switzerland)*, *11*(2), 1–19. doi:10.3390/w11020366

Richardson, J. S., & Danehy, R. J. (2007). A Synthesis of the Ecology of Headwater Streams and their Riparian Zones in Temperate Forests. *Forest Science*, *53*(2), 131–147.

Richardson, J. S., Naiman, R. J., & Bisson, P. A. (2012). How did fixed-width buffers become standard practice for protecting freshwaters and their riparian areas from forest harvest practices? *Freshwater Science*, *31*(1), 232–238. doi:10.1899/11-031.1

Rinderer, M., Van Meerveld, H. J., & Seibert, J. (2014). Topographic controls ond shallow groundwater levels in a steep, prealpine catchment. *Water Resources Research*, *50*, 6067–6080. doi:10.1002/2013WR015009

Roon, D. A., Dunham, J. B., & Groom, J. D. (2021). Shade, light, and stream temperature responses to riparian thinning in second- growth redwood forests of northern California. *PLoS ONE*, *16*(2), 1–25. doi:10.1371/journal.pone.0246822

Rykken, J. J., Chan, S. S., & Moldenke, A. R. (2007). Headwater riparian microclimate patterns under alternative forest management treatments. *Forest Science*, *53*(2), 270–280. doi:10.1093/forestscience/53.2.270

Sass, G. Z., Creed, I. F., Riddell, J., & Bayley, S. E. (2014). Regional-scale mapping of groundwater discharge zones using thermal satellite imagery. *Hydrological Processes*, *28*(23), 5662–5673. doi:10.1002/hyp.10068

Schlosser, I. J. (1991). *Stream Fish Ecology : A Landscape Perspective*. *41*(10), 704–712.

Segura, C., Caldwell, P., Sun, G., Mcnulty, S., & Zhang, Y. (2015). A model to predict stream water temperature across the conterminous USA. *Hydrological Processes*, *29*(9), 2178–2195. doi:10.1002/hyp.10357

Segura, C., Noone, D., Warren, D., Jones, J. A., Tenny, J., & Ganio, L. M. (2019). Climate, landforms, and geology affect baseflow sources in a mountain catchment. *Water Resources Research*, *55*(7), 5238–5254. doi:10.1029/2018WR023551

Selker, J., van de Giesen, N. C., Westhoff, M., Luxemburg, W., & Parlange, M. B. (2006). Fiber optics opens window on stream dynamics. *Geophysical Research Letters*, *33*(24), 27–30. doi:10.1029/2006GL027979

Shanley, J. B., & Peters, N. E. (1988). Preliminary observations of streamflow generatio during storms in a forested Piedmont watershed using temperature as a tracer. *Journal of Contaminant Hydrology*, *3*, 349–365. doi:10.1016/0169-7722(88)90040-X

Shreve, R. L. (1969). Stream Lengths and Basin Areas in Topologically Random Channel Networks. *Journal of Geology*, *77*(4), 397–414.

Sidle, R. C., Tsuboyama, Y., Noguchi, S., Hosoda, I., Fujieda, M., & Shimizu, T. (2000). Stormflow generation in steep forested headwaters: A linked hydrogeomorphic paradigm. *Hydrological Processes*, *14*(3), 369–385. doi:10.1002/(SICI)1099-1085(20000228)14:3<369::AID-HYP943>3.0.CO;2-P

Simmons, J. A., Anderson, M., Dress, W., Hanna, C., Hornbach, D. J., Janmaat, A., … Vasseur, L. (2014). A comparison of the temperature regime of short stream segments under forested and non-forested riparian zones at eleven sites across North America. *River Research and Applications*, *31*(8), 964–974. doi:10.1002/rra.2796

Sklash, M. G., & Farvolden, R. N. (1979). The role of groundwater in storm runoff. *Journal of Hydrology*, *43*(1–4), 45–65. doi:10.1016/0022-1694(79)90164-1

Sloat, M. R., & Osterback, A. M. K. (2013). Maximum stream temperature and the occurrence, abundance, and behavior of steelhead trout (Oncorhynchus mykiss) in a southern California stream. *Canadian Journal of Fisheries and Aquatic Sciences*, *70*(1), 64–73. doi:10.1139/cjfas-2012-0228

Snyder, C. D., Hitt, N. P., & Young, J. A. (2015). Accounting for groundwater in stream fish thermal habitat responses to climate change. *Ecological Applications*, *25*(5), 1397–1419. doi:10.5061/dryad.th6g8

Soil Survey Staff, NRCS, U. (2016). *Coppercreek and Sasquatch Series: Official Soil Series Descriptions.* Retrieved from https://soilseries.sc.egov.usda.gov/OSD_Docs/C/COPPERCREEK.html#:~:text=The Coppercreek series consists of,of 9 to 75 percent.

Somers, K. A., Bernhardt, E. S., Grace, J. B., Hassett, B. A., Sudduth, E. B., Wang, S., & Urban, D. L. (2013). Streams in the urban heat island: Spatial and temporal variability in temperature. *Freshwater Science*, *32*(1), 309–326. doi:10.1899/12-046.1

Somers, K. A., Bernhardt, E. S., Mcglynn, B. L., & Urban, D. L. (2016). Downstream Dissipation of Storm Flow Heat Pulses: A Case Study and its Landscape-Level Implications. *Journal of the American Water Resources Association*, *52*(2), 281–297. doi:10.1111/1752-1688.12382

Sowder, C., & Steel, E. A. (2012). A note on the collection and cleaning of water temperature data. *Water (Switzerland)*, *4*(3), 597–606. doi:10.3390/w4030597

Spearman, C. (1904). The proof and measurement of association between two things. *International Journal of Epidemiology*, *39*(5), 1137–1150. doi:10.1093/ije/dyq191

Steel, E. A., Beechie, T. J., Torgersen, C. E., & Fullerton, A. H. (2017). Envisioning, Quantifying, and Managing Thermal Regimes on River Networks. *BioScience*, *67*(6), 506–522. doi:10.1093/biosci/bix047

Stefan, H. G., & Preud'homme, E. B. (1993). Stream temperature estimation from air temperature. *Journal of the American Water Resources Association*, *29*(1), 27–45. doi:10.1111/j.1752-1688.1993.tb01502.x

Story, A., Moore, R. D., & Macdonald, J. S. (2003). Stream temperatures in two shaded reaches below cutblocks and logging roads: Downstream cooling linked to subsurface hydrology. *Canadian Journal of Forest Research*, *33*(8), 1383–1396. doi:10.1139/x03-087

Subehi, L., Fukushima, T., Onda, Y., Mizugaki, S., Gomi, T., Kosugi, K., … Terajima, T. (2010). Analysis of stream water temperature changes during rainfall events in forested watersheds. *Limnology*, *11*(2), 115–124. doi:10.1007/s10201-009-0296-2

Surfleet, C., & Louen, J. (2018). The influence of hyporheic exchange on water temperatures in a headwater stream. *Water (Switzerland)*, *10*(11). doi:10.3390/w10111615

Swartz, A., Roon, D., Reiter, M., & Warren, D. (2020). Stream temperature responses to experimental riparian canopy gaps along forested headwaters in western Oregon. *Forest Ecology and Management*, *474*(June), 1–12. doi:10.1016/j.foreco.2020.118354

Sweeney, B. W., & Newbold, J. D. (2014). Streamside forest buffer width needed to protect stream water quality, habitat, and organisms: A literature review. *Journal of the American Water Resources Association*, *50*(3), 560–584. doi:10.1111/jawr.12203

Tague, C., Farrell, M., Grant, G., Lewis, S., & Rey, S. (2007). Hydrogeologic controls on summer stream temperatures in the McKenzie River basin, Oregon. *Hydrological Processes*, *21*(24), 3288–3300. doi:10.1002/hyp.6538

Tague, C., Grant, G., Farrell, M., Choate, J., & Jefferson, A. (2008). Deep groundwater mediates streamflow response to climate warming in the Oregon Cascades. *Climatic Change*, *86*(1–2), 189–210. doi:10.1007/s10584-007-9294-8

Tarboton, D. G. (1997). A new method for the determination of flow directions and upslope areas in grid digital elevation models. *Water Resources Research*, *33*(2), 309–319. doi:10.1029/96WR03137

Thomas, C. D., Cameron, A., Green, R. E., Bakkenes, M., Beaumont, L. J., Collingham, Y. C., … Williams, S. E. (2004). Extinction risk from climate change. *Nature*, *427*(6970), 145–148.

Tiwari, T., Lundström, J., Kuglerová, L., Laudon, H., Öhman, K., & Ågren, A. M. (2016). Cost of riparian buffer zones: A comparison of hydrologically adapted site-specific riparian buffers with traditional fixed widths. *Water Resources Research*. doi:10.1002/2015WR018014

Torgersen, C. E., Price, D. M., Li, H. W., & McIntosh, B. A. (1999). Multiscale thermal refugia and stream habitat associations of chinook salmon in northeastern Oregon. *Ecological Applications*, *9*(1), 301–319. doi:10.1890/1051-0761(1999)009[0301:MTRASH]2.0.CO;2

Tromp-Van Meerveld, H. J., & McDonnell, J. J. (2006). Threshold relations in subsurface stormflow: 1. A 147-storm analysis of the Panola hillslope. *Water Resources Research*, *42*(2). doi:10.1029/2004WR003778

Trumbo, B. A., Nislow, K. H., Stallings, J., Hudy, M., Smith, E. P., Kim, D. Y., … Dolloff, C. A. (2014). Ranking site vulnerability to increasing temperatures in Southern Appalachian brook trout streams in Virginia: An exposure-sensitivity approach. *Transactions of the American Fisheries Society*, *143*(1), 173–187. doi:10.1080/00028487.2013.835282

Uchida, T., Kosugi, K., & Mizuyama, T. (2002). Effects of pipe flow and bedrock groundwater on runoff generation in a steep headwater catchment in Ashiu, Central Japan. *Water Resources Research*, *38*(7), 24-1-24–14. doi:10.1029/2001wr000261

van Meerveld, H. J. I., Sauquet, E., Gallart, F., Sefton, C., Seibert, J., & Bishop, K. (2020). Aqua temporaria incognita. *Hydrological Processes*, *2018*(November), 1–8. doi:10.1002/hyp.13979

Van Meerveld, H. J., Seibert, J., & Peters, N. E. (2015). Hillslope-riparian-stream connectivity and flow directions at the Panola Mountain Research Watershed. *Hydrological Processes*, *29*, 3556–3574. doi:10.1002/hyp.10508

Vander Vorste, R., Obedzinski, M., Nossaman Pierce, S., Carlson, S. M., & Grantham, T. E. (2020). Refuges and ecological traps: extreme drought threatens persistence of an endangered fish in intermittent streams. *Global Change Biology*, (May 2019), 1–12. doi:10.1111/gcb.15116

Vannote, R. L., Minshall, G. W., Cummins, K. W., Sedell, J. R., & Cushing, C. E. (1980). The river continuum concept. *Canadian Journal of Fisheries and Aquatic Sciences*, *37*(1), 130–137. doi:10.1139/f80-017

Vaughan, M. C. H., Bowden, W. B., Shanley, J. B., Vermilyea, A., Sleeper, R., Gold, A. J., … Schroth, A. W. (2017). High-frequency dissolved organic carbon and nitrate measurements reveal differences in storm hysteresis and loading in relation to land cover and seasonality. *Water Resources Research*. doi:10.1002/2017WR020491

Wagner, M. J., Bladon, K. D., Silins, U., Williams, C. H. S., Martens, A. M., Boon, S., … Anderson, A. (2014). Catchment-scale stream temperature response to land disturbance by wildfire governed by surface-subsurface energy exchange and atmospheric controls. *Journal of Hydrology*, *517*, 328–338. doi:10.1016/j.jhydrol.2014.05.006

Walker, C. M., King, R. S., Whigham, D. F., & Baird, S. J. (2012). Landscape and wetland influences on headwater stream chemistry in the Kenai Lowlands, Alaska. *Wetlands*, *32*(2), 301–310. doi:10.1007/s13157-011-0260-x

Wang, L., & Liu, H. (2006). An efficient method for identifying and filling surface depressions in digital elevation models for hydrologic analysis and modelling. *International Journal of Geographical Information Science*, *20*(2), 193–213. doi:10.1080/13658810500433453

Wawrzyniak, V., Piégay, H., Allemand, P., Vaudor, L., Goma, R., & Grandjean, P. (2016). Effects of geomorphology and groundwater level on the spatio-temporal variability of riverine cold water patches assessed using thermal infrared (TIR) remote sensing. *Remote Sensing of Environment*, *175*, 337–348. doi:10.1016/j.rse.2015.12.050

Webb, B. W., Hannah, D. M., Moore, R. D., Brown, L. E., & Nobilis, F. (2008). Recent advances in stream and river temperature research. *Hydrological Processes*, *22*(7), 902–918. doi:10.1002/hyp.6994

Webb, B. W., & Zhang, Y. (1997). Spatial and seasonal variability in the components of the river heat budget. *Hydrological Processes*, *11*, 79–101. doi:10.1002/(SICI)1099-1085(199701)11:1<79::AID-HYP404>3.0.CO;2-N

Wei, T., Simko, V., Levy, M., Xie, Y., Jin, Y., & Zemla, J. (2017). *R package "corrplot": Visualization of a Correlation Matrix*. Retrieved from https://github.com/taiyun/corrplot%0Ahttps://github.com/taiyun/corrplot/issues

Welsh, H. H., Hodgson, G. R., Harvey, B. C., & Roche, M. F. (2001). Distribution of juvenile coho salmon in relation to water temperatures in tributaries of the Mattole River, California. *North American Journal of Fisheries Management*, *21*(3), 464–470. doi:10.1577/1548-8675(2001)021<0464:dojcsi>2.0.co;2

Westhoff, J. T., & Paukert, C. P. (2014). Climate change simulations predict altered biotic response in a thermally heterogeneous stream system. *PLoS ONE*, *9*(10), 1–15. doi:10.1371/journal.pone.0111438

Wilby, R. L., Johnson, M. F., & Toone, J. A. (2014). Nocturnal river water temperatures: Spatial and temporal variations. *Science of the Total Environment*, *482–483*(1), 157–173. doi:10.1016/j.scitotenv.2014.02.123

Wilby, R. L., Johnson, M. F., & Toone, J. A. (2015). Thermal shockwaves in an upland river. *Weather*, *70*(3), 92–100. doi:10.1002/wea.2435

Winfree, M. M., Hood, E., Stuefer, S. L., Schindler, D. E., Cline, T. J., Arp, C. D., & Pyare, S. (2018). Landcover and geomorphology influence streamwater temperature sensitivity in salmon bearing watersheds in Southeast Alaska. *Environmental Research Letters*, *13*(6), 1–10. doi:10.1088/1748-9326/aac4c0

Winter, T. C. (2001). The concept of hydrologic landscapes. *Journal of the American Water Resources Association*, *37*(2), 335–349. doi:10.1111/j.1752-1688.2001.tb00973.x

Wipfli, M. S., Richardson, J. S., & Naiman, R. J. (2007). Ecological linkages between headwaters and downstream ecosystems: Transport of organic matter, invertebrates, and wood down headwater channels. *Journal of the American Water Resources Association*, *43*(1), 72–85. doi:10.1111/j.1752-1688.2007.00007.x

Woltemade, C. J. (2017). Stream Temperature Spatial Variability Reflects Geomorphology, Hydrology, and Microclimate: Navarro River Watershed, California. *Professional Geographer*, *69*(2), 177–190. doi:10.1080/00330124.2016.1193032

Wondzell, S. M., Diabat, M., & Haggerty, R. (2019). What Matters Most: Are Future Stream Temperatures More Sensitive to Changing Air Temperatures, Discharge, or Riparian Vegetation? *Journal of the American Water Resources Association*, *55*(1), 116–132. doi:10.1111/1752-1688.12707

Wondzell, S. M., & Gooseff, M. N. (2013). Geomorphic Controls on Hyporheic Exchange Across Scales: Watersheds to Particles. In J. Shroder & E. Wohl (Eds.), *Treatise on Geomorphology* (Vol. 9, pp. 203–218). doi:10.1016/B978-0-12-374739-6.00238-4

Woodward, J. S., Lamphear, D. W., & House, M. R. (2011). *General Technical Report PSW-GTR-238: Delineation of Preventative Landslide Buffers Along Steep Streamside Slopes in Northern California*.

Xu, C. L., Letcher, B. H., & Nislow, K. H. (2010). Size-dependent survival of brook trout Salvelinus fontinalis in summer: Effects of water temperature and stream flow. *Journal of Fish Biology*, *76*(10), 2342–2369. doi:10.1111/j.1095-8649.2010.02619.x

Zemke, J. J., Enderling, M., Klein, A., & Skubski, M. (2019). The influence of soil compaction on runoff formation. A case study focusing on skid trails at forested andosol sites. *Geosciences (Switzerland)*, *9*(5). doi:10.3390/geosciences9050204

Zimmer, M. A., & McGlynn, B. L. (2017). Ephemeral and intermittent runoff generation processes in a low relief, highly weathered catchment. *Water Resources Research*, *53*(8), 7055–7077. doi:10.1002/2016WR019742

Zimmer, M. A., & McGlynn, B. L. (2018). Lateral, Vertical, and Longitudinal Source Area Connectivity Drive Runoff and Carbon Export Across Watershed Scales. *Water Resources Research*, *54*(3), 1576–1598. doi:10.1002/2017WR021718

Appendix

Table A1. Individual stream temperature statistics with all parameters in units of °C.

Region	Stream	Type	Avg. Daily Mean	Avg. Daily SD	Avg. Daily Max	Avg. Daily Min	Mean Diel Range
Cascade Range	BEA	T_a	14.7	5.8	27.7	8.4	19.3
		T_s	6.3	0.5	7.5	5.7	1.8
	BUL	T_a	15.1	5.9	26.3	7.9	18.5
		T_s	8.0	1.0	10.1	6.8	3.2
	SUG	T_a	14.4	4.3	23.0	9.2	13.8
		T_s	8.8	0.7	10.0	7.9	2.1
Coast Range	HEN	T_a	13.1	2.6	18.1	9.8	8.3
		T_s	12.0	0.3	12.6	11.6	1.0
	IVE	T_a	13.1	2.8	18.6	9.7	8.9
		T_s	11.9	0.2	12.2	11.6	0.7
	RIC	T_a	13.2	2.3	17.1	10.1	6.9
		T_s	11.9	0.3	12.3	11.4	0.9
	WIL	T_a	13.1	2.2	16.9	10.2	6.7
		T_s	12.2	0.3	12.6	11.8	0.8
	XRA	T_a	13.0	2.5	17.8	9.8	8.1
		T_s	12.0	0.3	12.6	11.6	1.0

Table A2. Site-level stream temperature statistics for the 8 study streams. Missing values denote stream temperature sensors that were dry or lost during the study period.

Region	Stream	Average Daily (°C)	Fractional Distance Upstream											
			1	**0.91**	**0.82**	**0.73**	**0.64**	**0.55**	**0.45**	**0.36**	**0.27**	**0.18**	**0.09**	**0**
Cascade Range	BEA	Mean	5.36	7.05	7.17	7.37	8.10	8.23	4.66	4.89	4.96	5.17	5.31	5.47
		Max	6.38	8.74	7.72	8.14	9.46	9.62	5.27	5.87	6.10	6.61	6.99	7.28
		Min	5.08	6.32	6.77	6.78	7.36	7.40	4.48	4.56	4.57	4.66	4.71	4.78
		Range	1.30	2.42	0.95	1.36	2.10	2.22	0.79	1.31	1.53	1.95	2.28	2.49
	BUL	Mean	9.46	9.20	9.52	9.49	9.94	10.51	-	12.13	5.09	5.98	6.92	6.41
		Max	13.44	11.93	11.99	12.51	11.71	11.81	-	15.25	6.34	7.86	8.52	7.94
		Min	7.49	7.81	8.08	7.94	8.68	9.47	-	9.76	4.75	5.24	6.11	5.55
		Range	5.95	4.12	3.91	4.57	3.04	2.34	-	5.49	1.60	2.62	2.41	2.40
	SUG	Mean	9.46	9.66	-	7.55	5.51	8.43	9.20	9.23	7.94	8.81	8.09	8.73
		Max	11.79	11.24	-	10.80	5.83	9.10	10.67	9.75	11.34	9.98	9.66	9.37
		Min	7.96	8.38	-	5.94	5.28	8.02	8.35	8.71	6.19	7.94	6.58	8.17
		Range	3.84	2.86	-	4.86	0.55	1.08	2.32	1.04	5.14	2.04	3.08	1.19
Coast Range	HEN	Mean	-	-	12.14	12.05	12.26	11.59	12.00	11.99	12.11	11.53	-	-
		Max	-	-	12.57	13.27	12.55	11.83	13.49	12.20	12.79	12.26	-	-
		Min	-	-	11.76	11.67	11.95	11.37	10.72	11.80	11.81	10.97	-	-
		Range	-	-	0.81	1.60	0.60	0.46	2.76	0.39	0.98	1.29		
	IVE	Mean	12.19	-	11.97	11.71	11.51	11.76	11.80	-	11.49	11.96	12.02	11.98
		Max	12.97	-	12.16	12.25	12.16	12.07	12.26	-	11.96	12.08	12.45	12.27
		Min	11.35	-	11.77	11.40	11.34	11.42	11.39	-	11.00	11.82	11.53	11.68
		Range	1.62	-	0.39	0.85	0.82	0.64	0.88	-	0.97	0.25	0.92	0.59
	RIC	Mean	11.77	11.61	-	-	11.71	11.52	11.78	11.89	12.21	12.03	11.97	12.16
		Max	11.97	11.78	-	-	11.77	11.67	12.01	12.41	13.40	12.71	12.47	12.84
		Min	11.56	11.40	-	-	11.63	11.33	11.52	11.39	11.01	11.26	11.42	11.49

Table A2. Continued

	Range	0.41	0.38	-	-	0.15	0.35	0.49	1.02	2.38	1.45	1.05	1.35
WIL	Mean	-	11.71	-	11.95	12.18	-	11.54	12.24	11.98	12.56	12.36	12.33
	Max	-	12.34	-	12.67	12.76	-	11.57	12.65	12.19	12.75	13.08	12.53
	Min	-	11.11	-	11.26	11.71	-	11.51	11.76	11.75	12.37	11.64	12.09
	Range	-	1.23	-	1.41	1.06	-	0.06	0.89	0.44	0.38	1.44	0.44
XRA	Mean	-	11.79	-	11.81	11.84	11.08	12.02	12.16	12.67	11.75	12.21	12.25
	Max	-	12.69	-	12.18	12.32	11.89	12.34	12.66	13.01	12.08	12.68	13.04
	Min	-	11.36	-	11.48	11.49	10.24	11.94	11.80	12.29	11.42	11.72	11.54
	Range	-	1.33	-	0.70	0.83	1.66	0.40	0.86	0.71	0.65	0.96	1.51

Table A3. Linear regression model output (y-intercept, slope, and R^2 value) for each stream temperature monitoring location along each measured stream.

Region	Stream	Regression parameter	Fractional Distance Upstream										
			1	**0.91**	**0.82**	**0.73**	**0.64**	**0.55**	**0.45**	**0.36**	**0.27**	**0.18**	**0.09**	**0**
Cascade Range	BEA	Intercept	4.46	5.56	4.73	4.18	4.01	3.73	3.80	4.07	3.79	4.06	4.01	3.96
		Slope	0.05	0.10	0.16	0.22	0.29	0.31	0.06	0.06	0.08	0.08	0.09	0.11
		R^2	0.39	0.11	0.35	0.48	0.53	0.63	0.80	0.64	0.85	0.59	0.62	0.64
	BUL	Intercept	5.41	5.82	6.31	4.49	4.12	3.83	-	3.23	4.43	4.80	5.02	5.05
		Slope	0.27	0.22	0.23	0.30	0.39	0.43	-	0.63	0.04	0.08	0.13	0.10
		R^2	0.53	0.70	0.54	0.81	0.68	0.71	-	0.60	0.84	0.49	0.48	0.63
	SUG	Intercept	4.69	5.22	-	-	4.20	4.47	0.05	3.38	4.54	2.97	4.80	4.35
		Slope	0.32	0.30	-	-	0.10	0.27	0.59	0.40	0.28	0.45	0.29	0.34
		R^2	0.71	0.50	-	-	0.46	0.30	0.63	0.58	0.63	0.57	0.53	0.59
Coast Range	HEN	Intercept	-	-	9.45	7.73	7.39	9.36	2.9	7.8	6.46	8.19	-	-
		Slope	-	-	0.2	0.32	0.36	0.18	0.77	0.33	0.44	0.27	-	-
		R^2	-	-	0.44	0.51	0.54	0.45	0.93	0.58	0.68	0.68	-	-
	IVE	Intercept	6.87	-	9.81	9.02	9.67	8.75	8.07	-	7.12	9.49	7.50	7.30
		Slope	0.43	-	0.16	0.21	0.15	0.22	0.27	-	0.35	0.19	0.34	0.36
		R^2	0.73	-	0.42	0.78	0.54	0.61	0.65	-	0.60	0.32	0.64	0.69
	RIC	Intercept	8.68	7.82	-	-	-	8.91	7.77	6.99	5.14	4.26	5.59	5.18
		Slope	0.24	0.29	-	-	-	0.20	0.31	0.37	0.54	0.59	0.48	0.53
		R^2	0.28	0.40	-	-	-	0.36	0.46	0.53	0.70	0.75	0.71	0.73
	WIL	Intercept	-	7.23	-	7.54	7.90	-	10.28	7.34	7.63	11.18	7.71	8.96
		Slope	-	0.35	-	0.35	0.32	-	0.10	0.37	0.33	0.10	0.35	0.26
		R^2	-	0.62	-	0.65	0.56	-	0.29	0.56	0.52	0.11	0.63	0.40
	XRA	Intercept	-	7.69	-	7.84	6.84	6.70	-	-	9.10	7.74	5.69	5.80
		Slope	-	0.32	-	0.31	0.39	0.38	-	-	0.26	0.32	0.50	0.49
		R^2	-	0.65	-	0.59	0.73	0.78	-	-	0.35	0.74	0.69	0.75

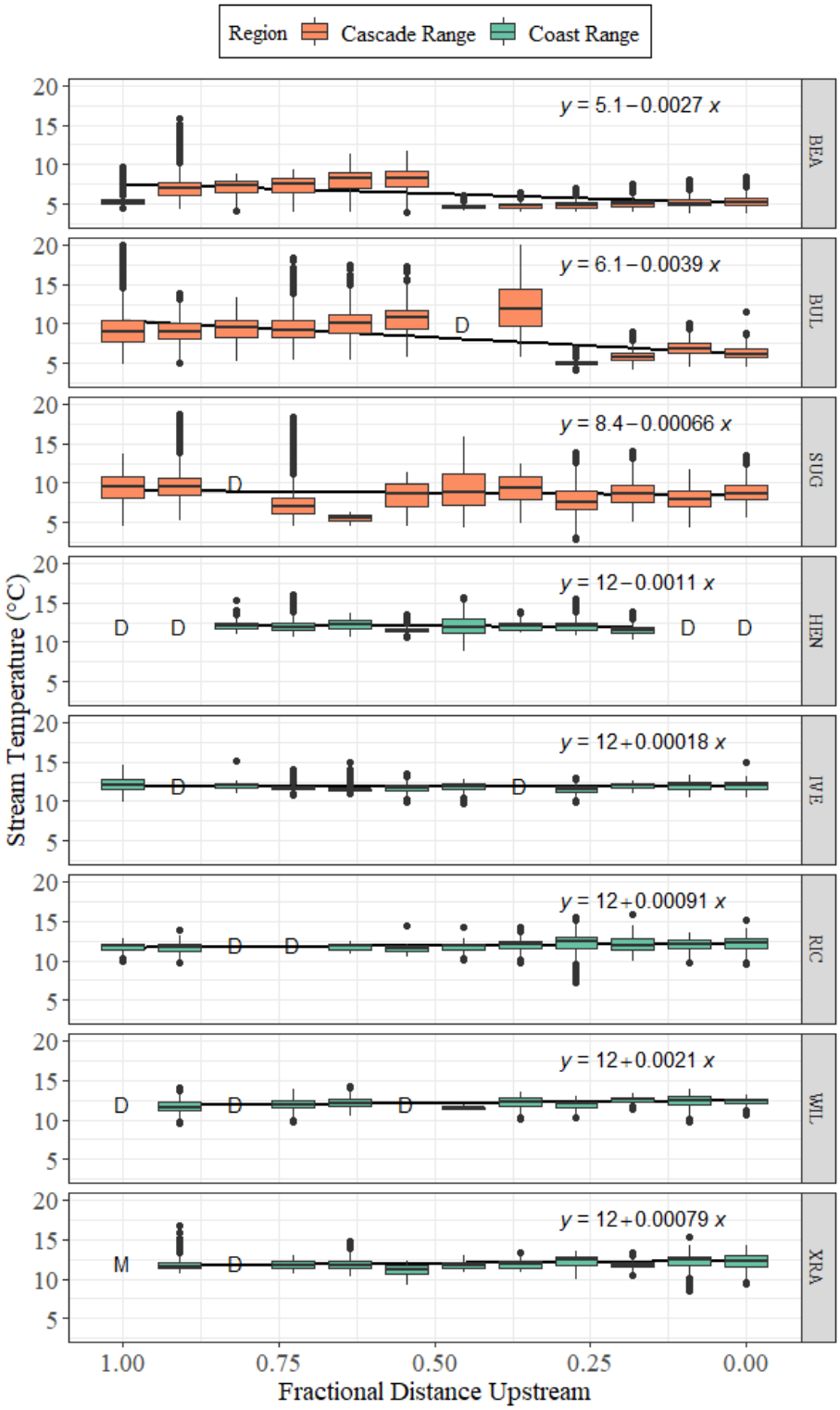

Figure A1. Longitudinal distribution of daily mean summer stream temperatures measured along each stream with the longitudinal linear regression equation predicting average daily mean stream temperature from downstream distance (m) shown to indicate downstream warming or cooling.

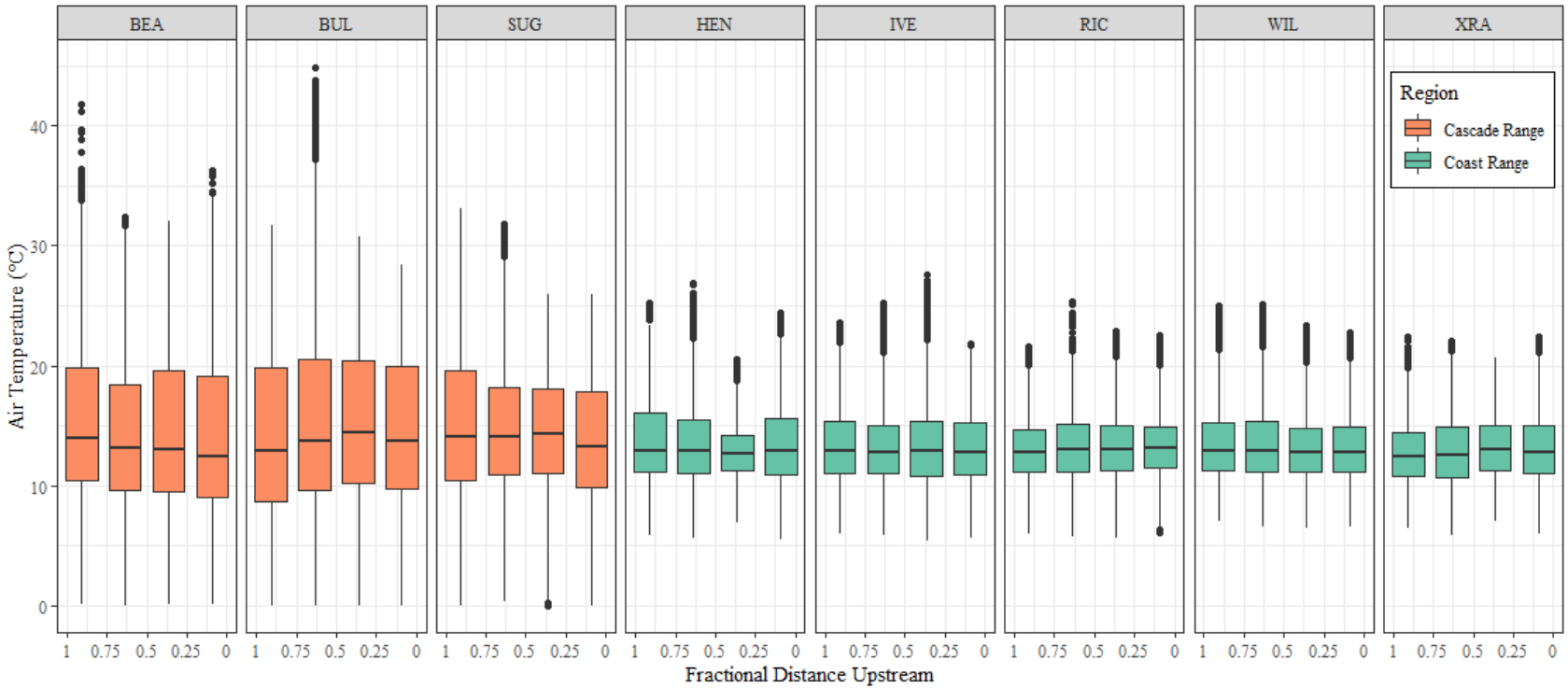

Figure A2. Distributions of air temperature during summer 2018 along streams in the Cascade Range and Coast Range. The boxplot central tendency line is the median, shaded boxes represent the interquartile range (IQR), whiskers represent the largest value up to 1.5-times the IQR, and the black dots indicate outliers beyond 1.5-times the IQR.

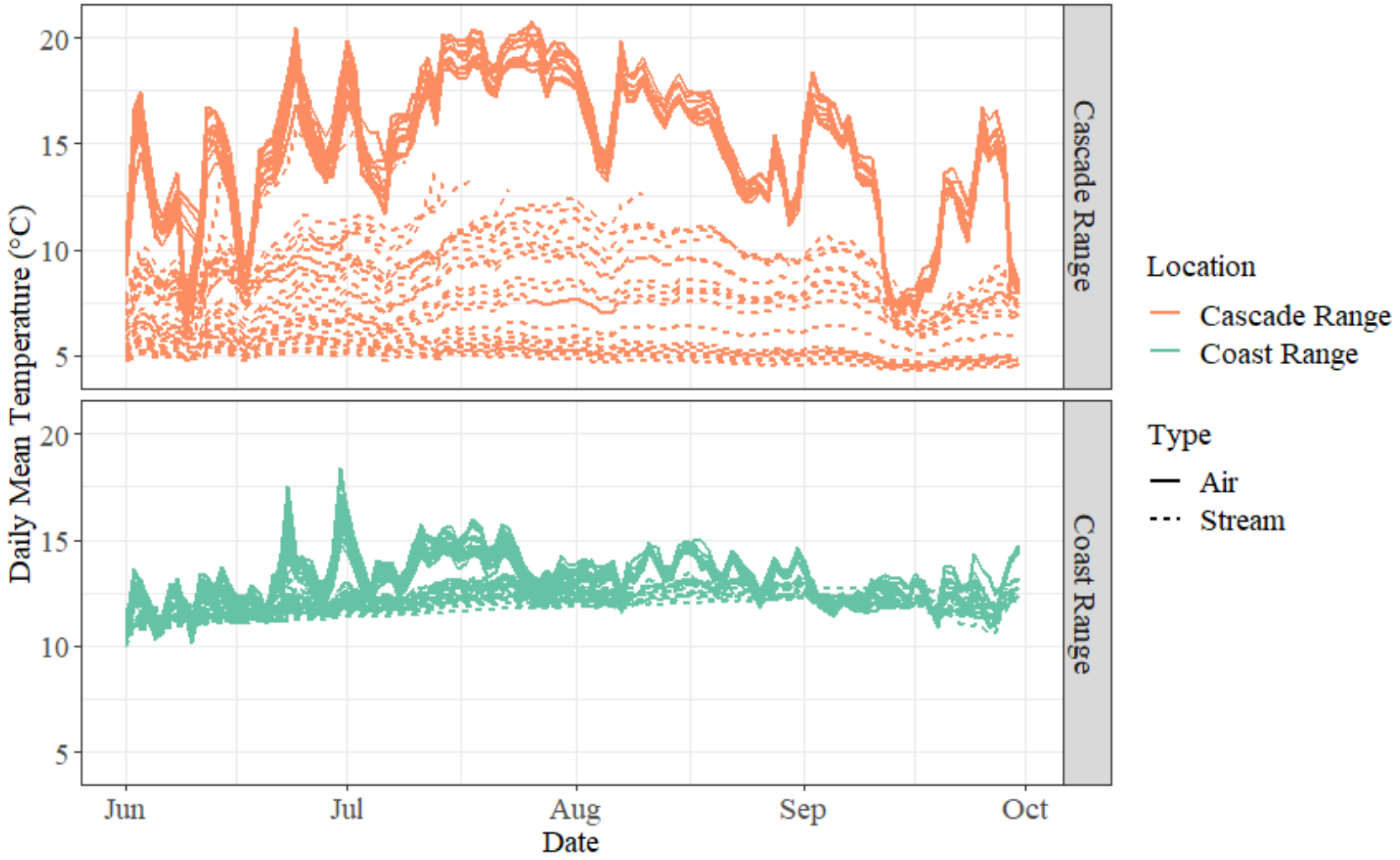

Figure A3. Timeseries trends for air (solid line) and stream (dashed line) daily mean temperatures (°C) over summer 2018. Each line represents an individual stream or air temperature monitoring location.

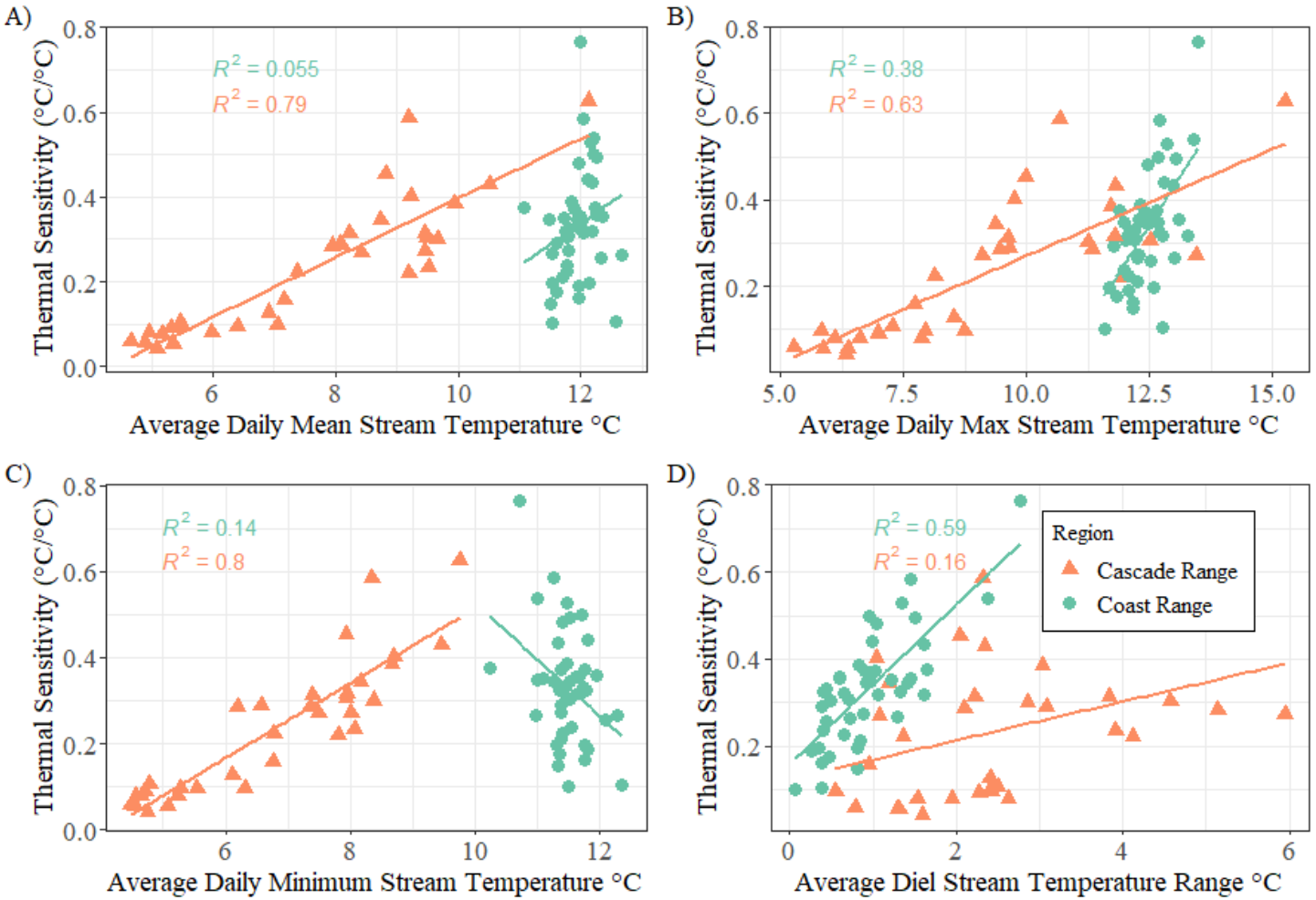

Figure A4. Regression relationships between average summer temperature metrics ((A) daily mean, (B) daily max, (C) daily minimum, (D) diel range) and site-level thermal sensitivity values for Cascade Range (triangles) and Coast Range (circles) streams. R^2 values in the top left corner of each plot indicate the fit of the linear regression line.

Comparison of Hysteresis Metrics Using Stage Versus Discharge

An analysis was done to see whether or not hysteresis indices calculated using a time series of discharge different significantly from those using a time series of stream stage. We used paired t-testing to assess for differences in mean values using both methods. Results of this analysis indicate that the true difference in mean values of both the hysteresis index (p = 0.20, 95% CI: -0.016 – 0.077) and flushing index (p = 0.11, 95% CI: -0.12 – 0.013) were not significantly different than 0 between measurement methods (using stage versus discharge). These results indicate that using measurements of stage rather than discharge likely have a small effect on the outcome of our results.

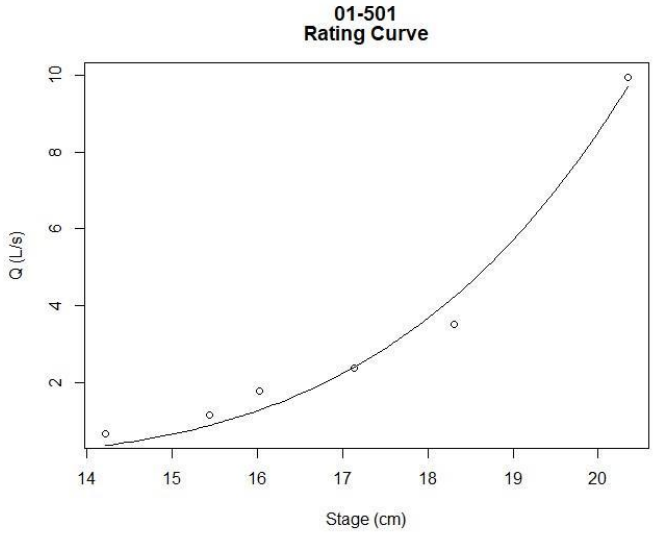

Figure A5. Fitted rating curve for stream 1 for data collected via salt dilution gauging up to 2021-04-07. The resulting rating curve equation is Q = 0.0006139 * (stage - 9.37808) ^ (4.03648), where Q is flow (L/s) and stage is in cm.

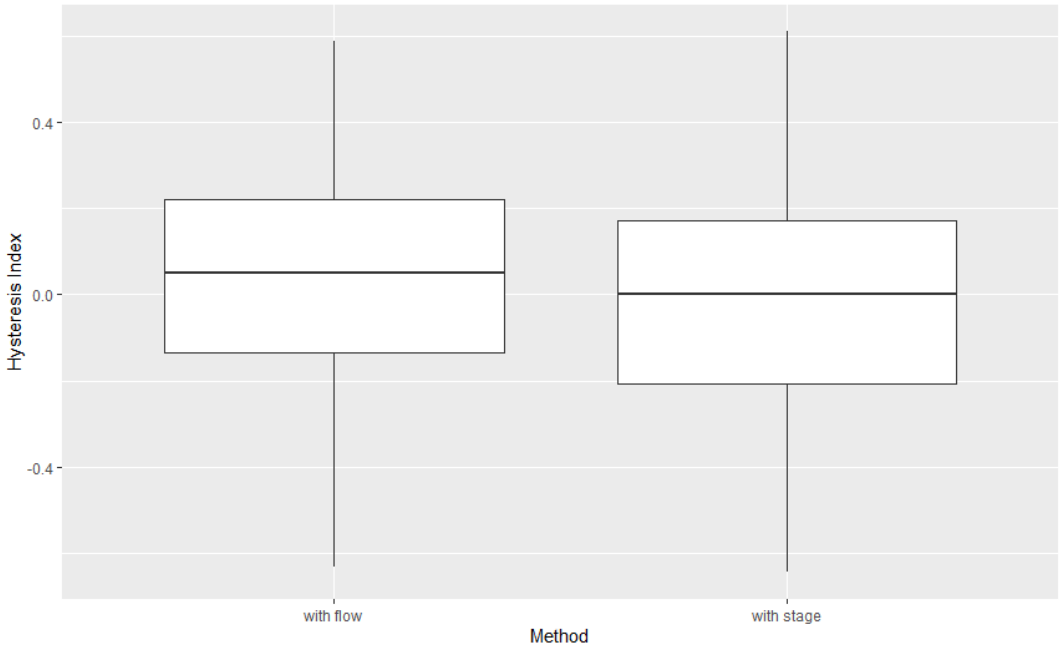

Figure A6. Distribution of Hysteresis Index values measured with a timeseries of flow (left) calculated using the rating curve in Fig. A4, versus using a timeseries of stage (right).

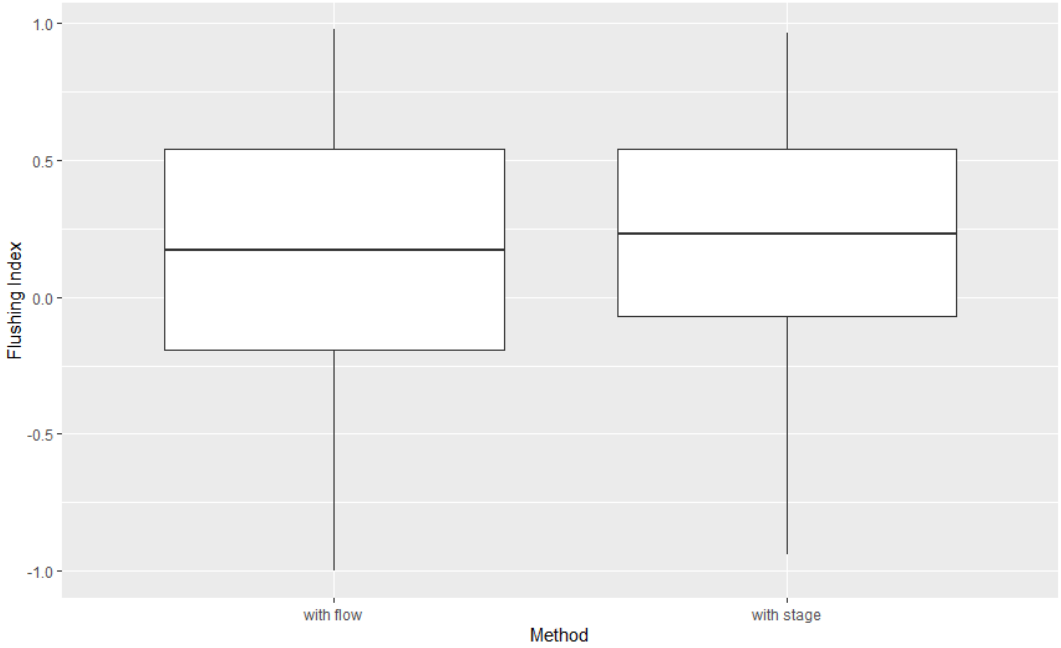

Figure A7. Distribution of Flushing Index values measured with a timeseries of flow (left) calculated using the rating curve in Fig. A4, versus using a timeseries of stage (right).

Table A4. Storm characteristics for the 23 analyzed events across both weather stations (North and South).

Storm Date	Season	Total depth (mm)		Duration (h)		Average Intensity (mm/h)		Max Intensity (mm/1-hr)		14-day Antecedent Rainfall (mm)	
		North	South	North	South	North	South	North	South	North	South
9/15/2019	Summer	43.4	24.0	25.3	14.3	1.7	1.7	10.2	7.0	7.8	2.8
9/17/2019	Summer	67.0	48.0	32.0	36.0	2.1	1.3	12.6	8.6	51.4	30.6
10/16/2019	Fall	38.4	35.4	21.5	24.0	1.8	1.5	9.0	9.0	0.0	0.0
10/19/2019	Fall	26.6	22.2	10.0	14.8	2.7	1.5	10.2	8.0	46.8	41.8
11/19/2019	Fall	11.2	15.6	17.0	16.5	0.7	0.9	2.6	3.6	3.0	2.8
11/26/2019	Fall	47.2	51.4	28.5	11.8	1.7	4.4	11.0	12.6	14.2	18.6
12/7/2019	Fall	33.6	37.0	28.0	32.3	1.2	1.1	5.6	6.2	67.2	112.2
12/21/2019	Fall	54.4	59.0	37.3	31.8	1.5	1.9	5.2	4.6	145.2	179.8
12/29/2019	Winter	19.8	23.4	6.8	5.8	2.9	4.1	8.8	8.8	76.4	92.4
1/5/2020	Winter	10.6	10.6	10.8	8.8	1.0	1.2	4.0	5.6	84.4	95.0
1/7/2020	Winter	64.2	44.4	39.3	45.3	1.6	1.0	9.2	6.4	72.0	75.6
1/12/2020	Winter	71.2	79.2	76.8	65.5	0.9	1.2	7.0	6.8	158.4	144.2
1/16/2020	Winter	64.8	48.0	36.8	36.8	1.8	1.3	9.8	4.2	193.0	187.4
1/21/2020	Winter	26.4	26.2	11.3	12.5	2.3	2.1	9.0	8.4	226.8	207.4
1/23/2020	Winter	23.6	20.2	12.5	17.5	1.9	1.2	11.2	5.2	189.8	192.2
2/16/2020	Winter	23.6	13.2	13.3	15.8	1.8	0.8	4.2	2.6	5.2	8.6
4/4/2020	Spring	50.4	53.2	30.5	29.8	1.7	1.8	4.4	6.4	71.6	89.2
4/22/2020	Spring	19.8	12.2	20.5	21.5	1.0	0.6	3.4	3.2	0.4	0.2
5/2/2020	Spring	31.4	24.8	13.0	6.5	2.4	3.8	14.2	8.0	21.6	14.4
5/12/2020	Spring	19.2	33.2	15.5	20.5	1.2	1.6	5.2	9.4	38.8	33.0
5/13/2020	Spring	25.4	26.6	33.5	29.3	0.8	0.9	5.0	5.0	58.0	66.2
5/17/2020	Spring	45.2	38.6	33.3	38.0	1.4	1.0	9.6	6.6	71.2	82.2
5/30/2020	Spring	31.4	33.2	20.0	15.8	1.6	2.1	5.4	6.4	66.4	57.8

Table A5. Predictor variables included in the correlation matrix to assess influences on hysteresis behavior.

Predictor	Description	Units	Type
ql_initial	Intial stream stage	m	**Hydrological**
ql_peak	Peak stream stage	m	**Hydrological**
ql_response	Difference between peak and initial stream stage	m	**Hydrological**
tempC_initial	Initial stream temperature	°C	**Meteorological**
stream_air_tempdif_initial	Difference between stream and air temperature at event start	°C	**Meteorological**
antecedent_14day	14-day antecedent rainfall	mm	**Meteorological**
air_tempC_initial	Initial air temperature	°C	**Meteorological**
avgintensity	Average rainfall intensity	mm/hr	**Meteorological**
max1hr_intens	Maximum 1-hour rainfall intensity	mm/hr	**Meteorological**
mean_daily_solrad	Mean daily solar radiation	W/m2/day	**Meteorological**
antecedent_7day	7-day antecedent rainfall	mm	**Meteorological**
avg_air_temp	Average air temperature	°C	**Meteorological**
three_day_solrad	Three-day average solar radiation prior to storm	W/m2/day	**Meteorological**
depth_mm	Storm depth	mm	**Meteorological**
air_tempC_at_peak	Air Temperature at hydrograph peak	°C	**Meteorological**
dur_hours	Storm duration	hr	**Meteorological**
air_tempC_risinglimb_response	Air temperature change during rising limb	°C	**Meteorological**
reach_wide_stream_slope	Average stream channel slope	%	**Topographic**
avg_FWS	Average flow weighted slope at each monitoring location	%	**Topographic**
fws_point_uaa	Flow weighted slope at each monitoring location scaled by lateral UAA	%	**Topographic**
average_watershed_slope	Stream average watershed slope	°	**Topographic**
mean_slope_deg	Mean slope of upslope are draining to each monitoring location	°	**Topographic**
lateral_uaa_ha	Lateral upslope accumulated area draining to each monitoring location	ha	**Topographic**

Table A5. continued

average_active_width_ft	Wetted width at each monitoring location	ft	**Topographic**
drainage_area_ac	Drainage area of catchment	ac	**Topographic**
avg_UAA_m2	Average upslope accumulated area measured at each monitoring location	ha	**Topographic**
avg_TWI	Average topographic wetness index of upslope area draining to each monitoring location	-	**Topographic**
twi_point	Topographic wetness index point value at each monitoring location	-	**Topographic**
sensor_elevation	Stream temperature sensor elevation	m	**Topographic**
ele	Stream average elevation	m	**Topographic**

Figure A8. All storm hydrographs for stream 1, with those selected for hysteresis analysis colored as blue solid lines. Dotted lines indicate event hydrographs that failed to recede to at least half the maximum stage value achieved during the event, and were excluded from analysis. Events with hydrographs as red solid lines were excluded because these events did not included data from at least 6 of the 10 streams.

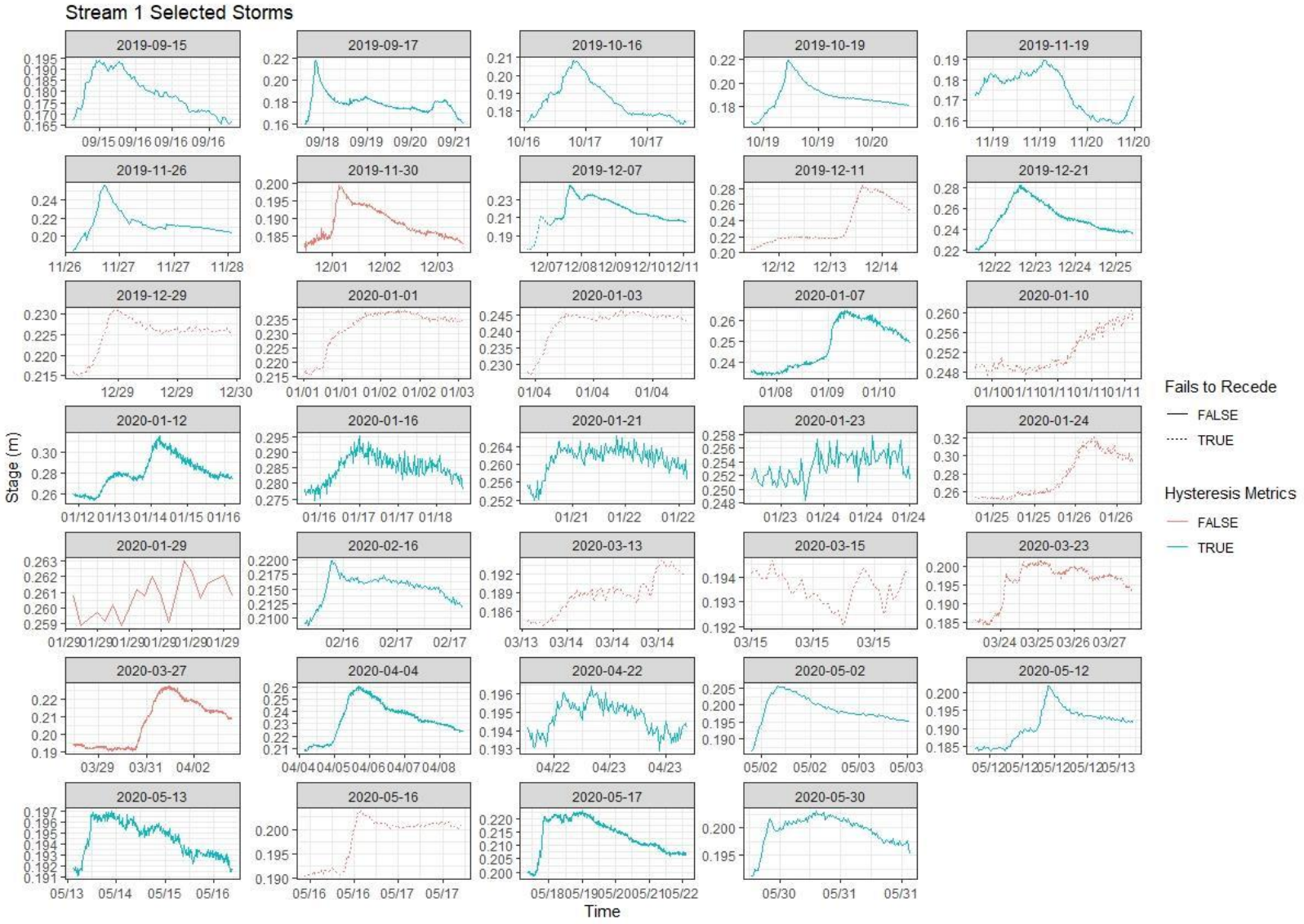

Figure A8. (Continued)

Figure A9. All storm hydrographs for stream 2, with those selected for hysteresis analysis colored as blue solid lines. Dotted lines indicate event hydrographs that failed to recede to at least half the maximum stage value achieved during the event, and were excluded from analysis. Events with hydrographs as red solid lines were excluded because these events did not included data from at least 6 of the 10 streams.

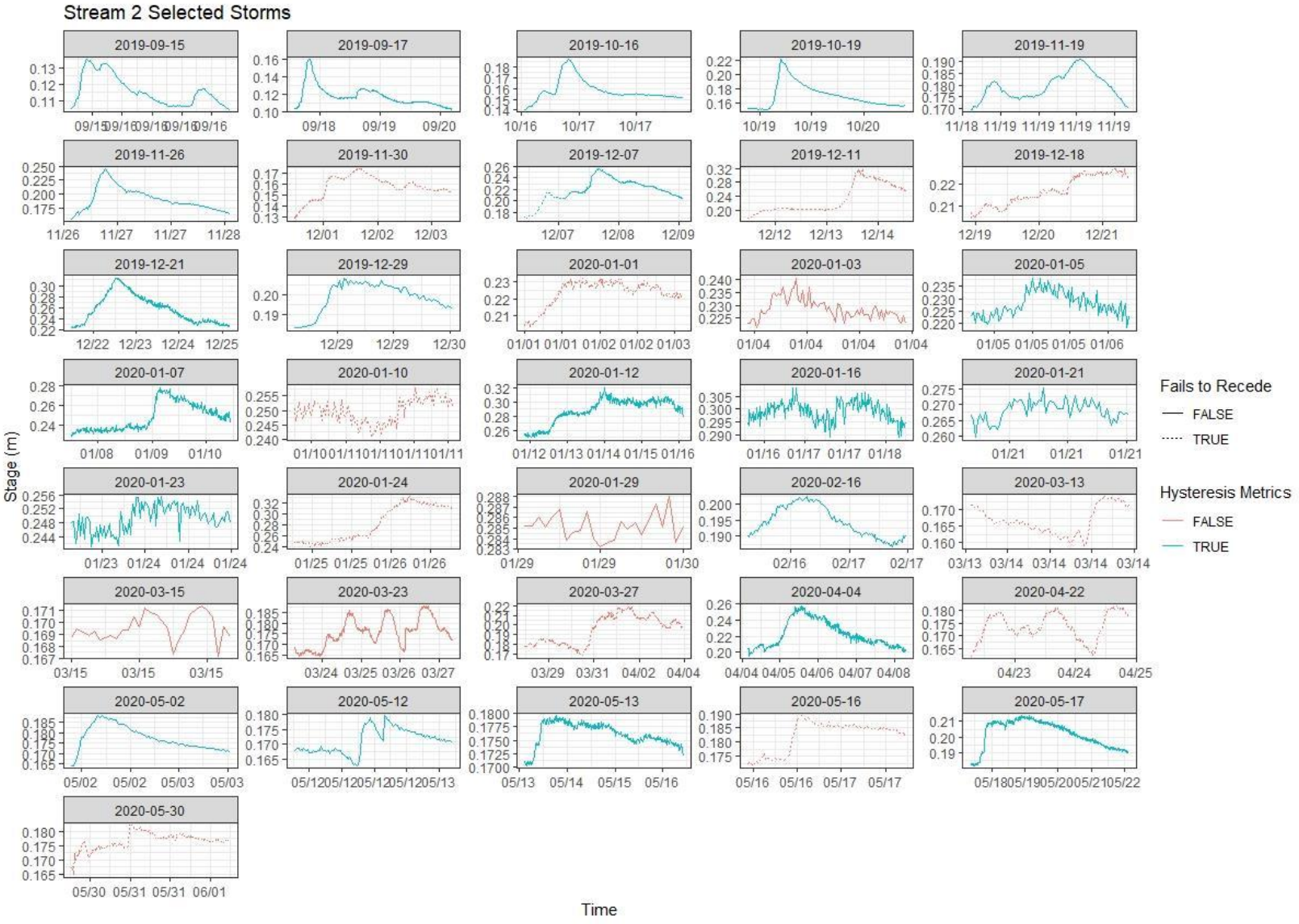

Figure A9. (Continued)

Figure A10. All storm hydrographs for stream 3, with those selected for hysteresis analysis colored as blue solid lines. Dotted lines indicate event hydrographs that failed to recede to at least half the maximum stage value achieved during the event, and were excluded from analysis. Events with hydrographs as red solid lines were excluded because these events did not included data from at least 6 of the 10 streams.

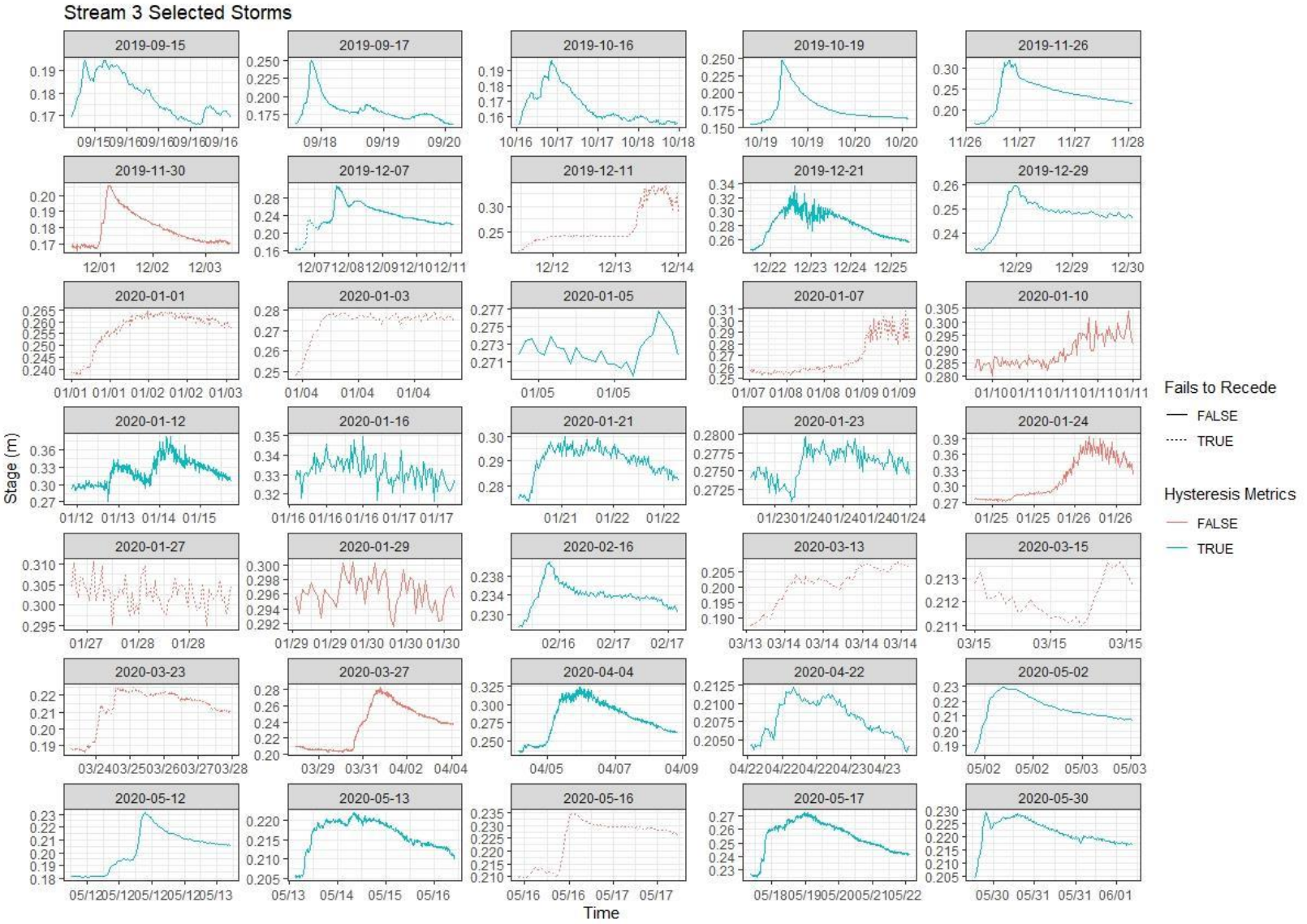

Figure A10. (Continued)

Figure A11. All storm hydrographs for stream 4, with those selected for hysteresis analysis colored as blue solid lines. Dotted lines indicate event hydrographs that failed to recede to at least half the maximum stage value achieved during the event, and were excluded from analysis. Events with hydrographs as red solid lines were excluded because these events did not included data from at least 6 of the 10 streams.

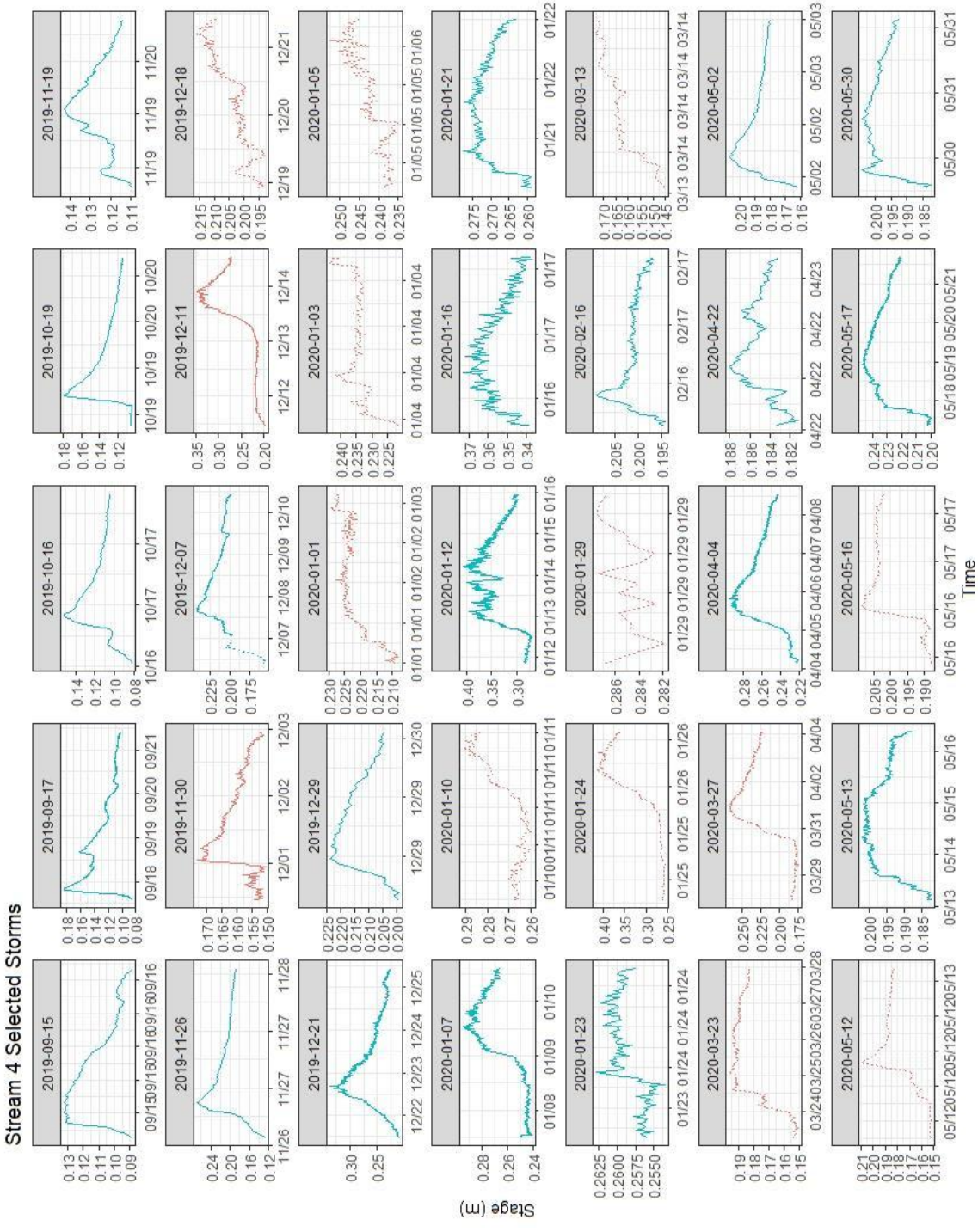

Figure A11. (Continued)

Figure A12. All storm hydrographs for stream 5, with those selected for hysteresis analysis colored as blue solid lines. Dotted lines indicate event hydrographs that failed to recede to at least half the maximum stage value achieved during the event, and were excluded from analysis. Events with hydrographs as red solid lines were excluded because these events did not included data from at least 6 of the 10 streams.

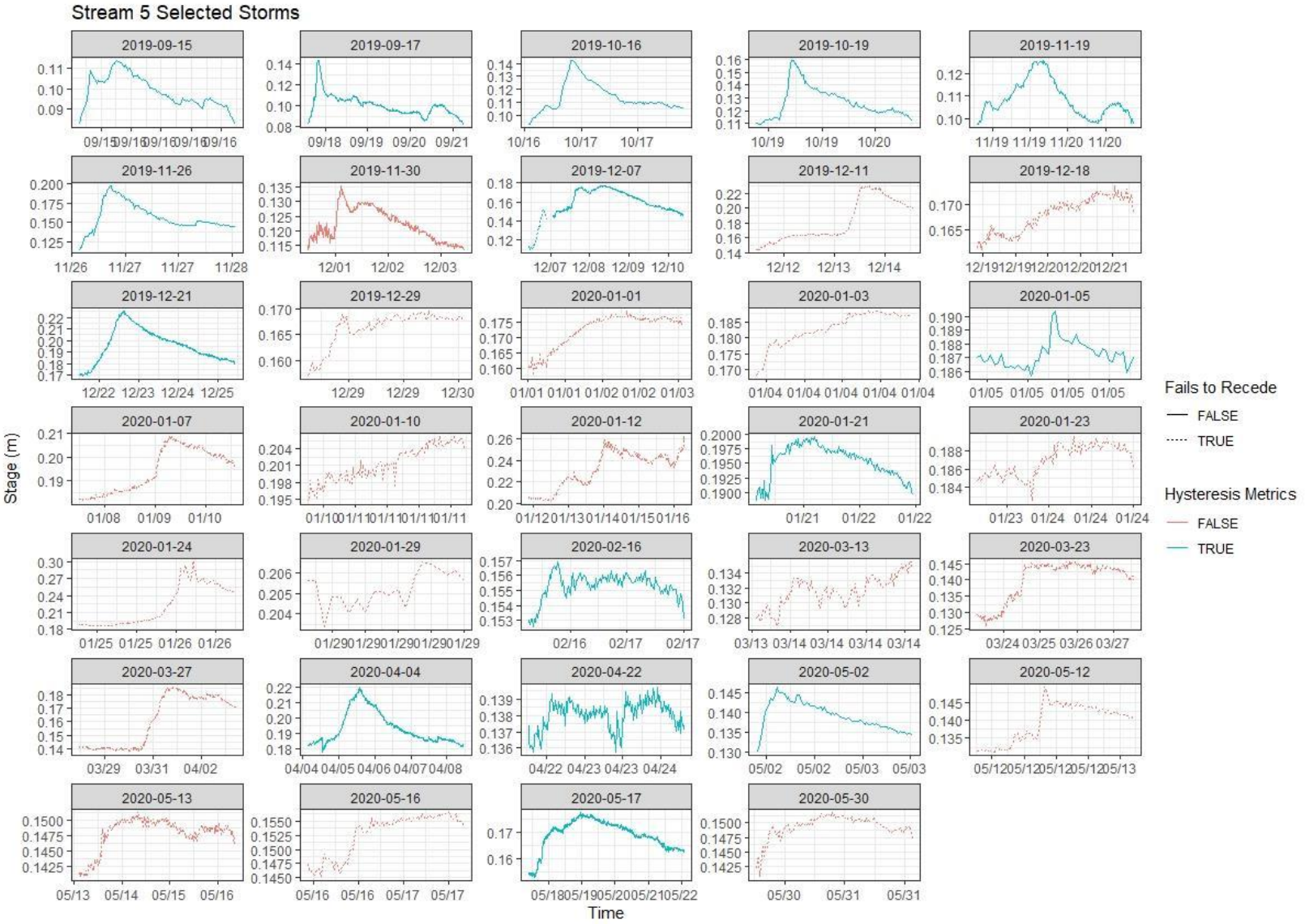

Figure A12. (Continued)

Figure A13. All storm hydrographs for stream 11, with those selected for hysteresis analysis colored as blue solid lines. Dotted lines indicate event hydrographs that failed to recede to at least half the maximum stage value achieved during the event, and were excluded from analysis. Events with hydrographs as red solid lines were excluded because these events did not included data from at least 6 of the 10 streams.

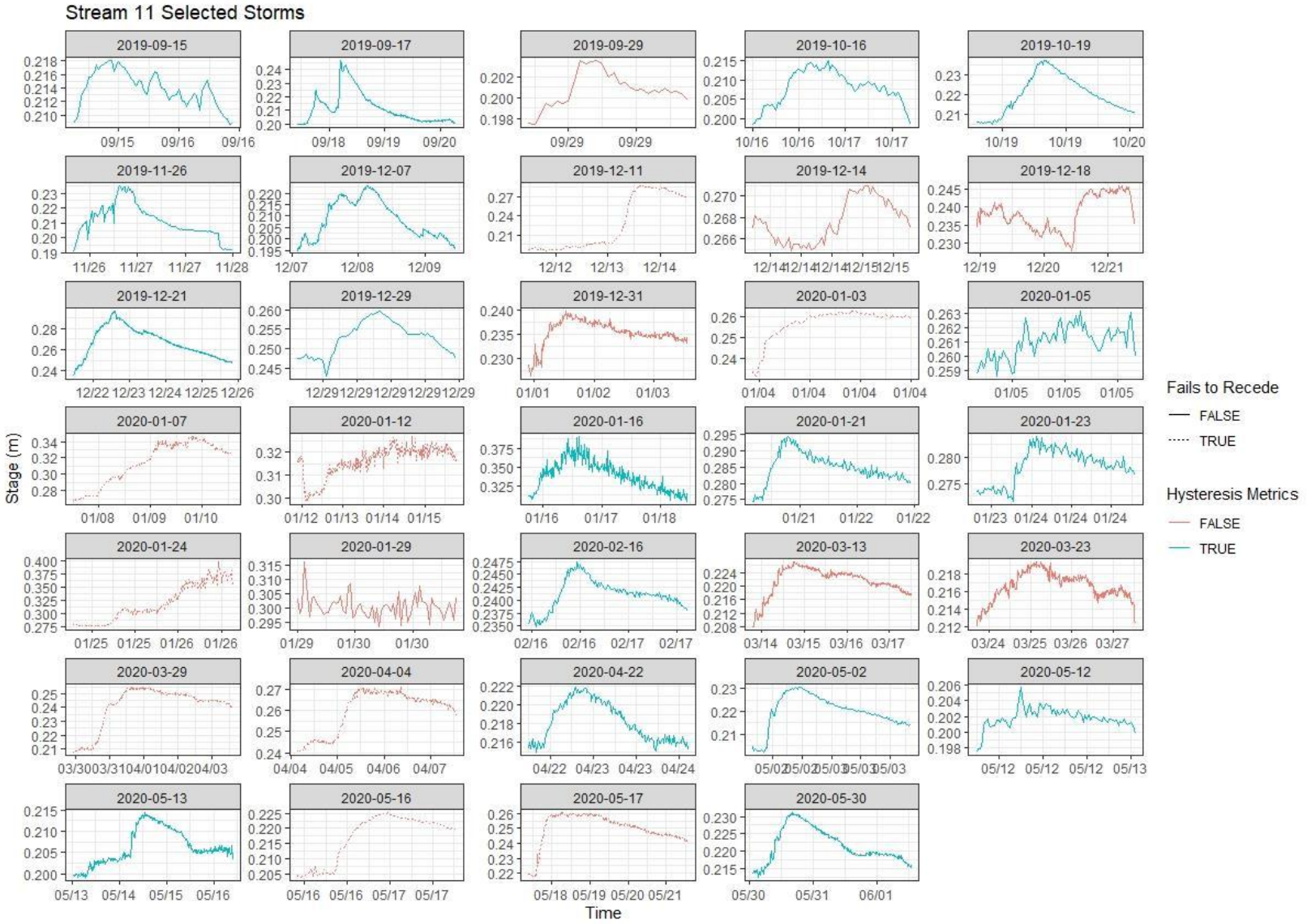

Figure A13. (Continued)

Figure A14. All storm hydrographs for stream 13, with those selected for hysteresis analysis colored as blue solid lines. Dotted lines indicate event hydrographs that failed to recede to at least half the maximum stage value achieved during the event, and were excluded from analysis. Events with hydrographs as red solid lines were excluded because these events did not included data from at least 6 of the 10 streams.

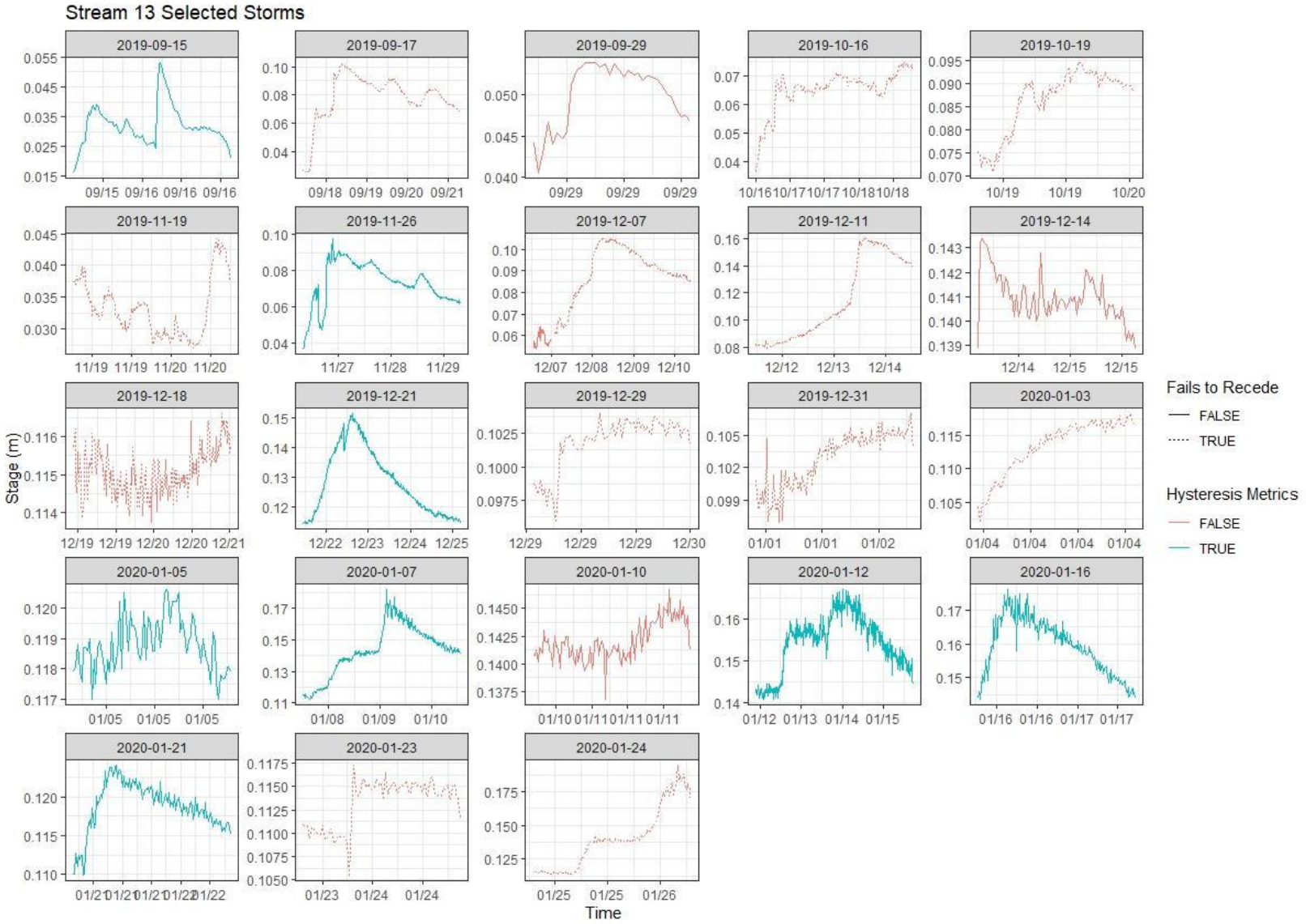

Figure A14. (Continued)

Figure A15. All storm hydrographs for stream 14, with those selected for hysteresis analysis colored as blue solid lines. Dotted lines indicate event hydrographs that failed to recede to at least half the maximum stage value achieved during the event, and were excluded from analysis. Events with hydrographs as red solid lines were excluded because these events did not included data from at least 6 of the 10 streams.

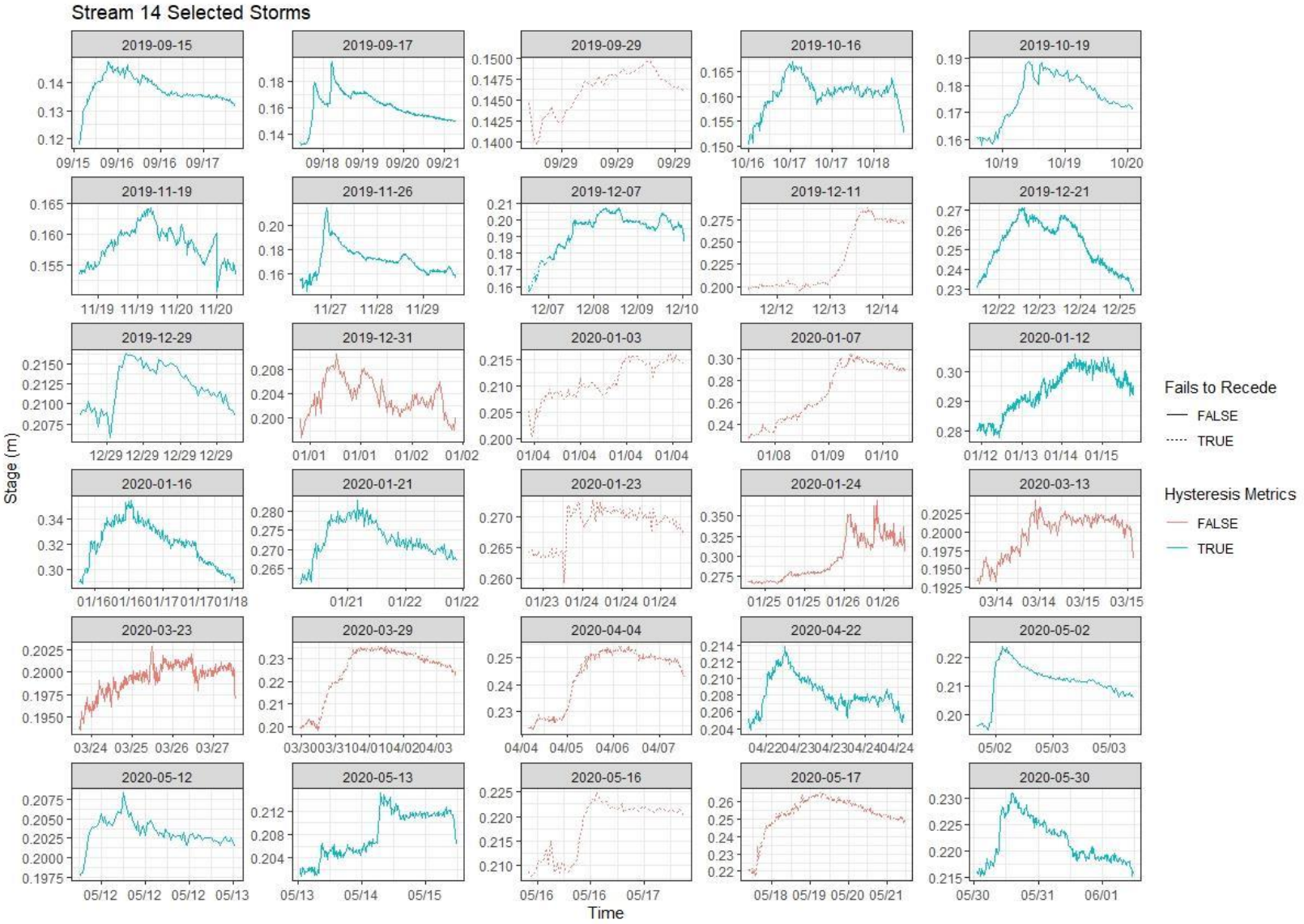

Figure A15. (Continued)

Figure A16. All storm hydrographs for stream 15, with those selected for hysteresis analysis colored as blue solid lines. Dotted lines indicate event hydrographs that failed to recede to at least half the maximum stage value achieved during the event, and were excluded from analysis. Events with hydrographs as red solid lines were excluded because these events did not included data from at least 6 of the 10 streams.

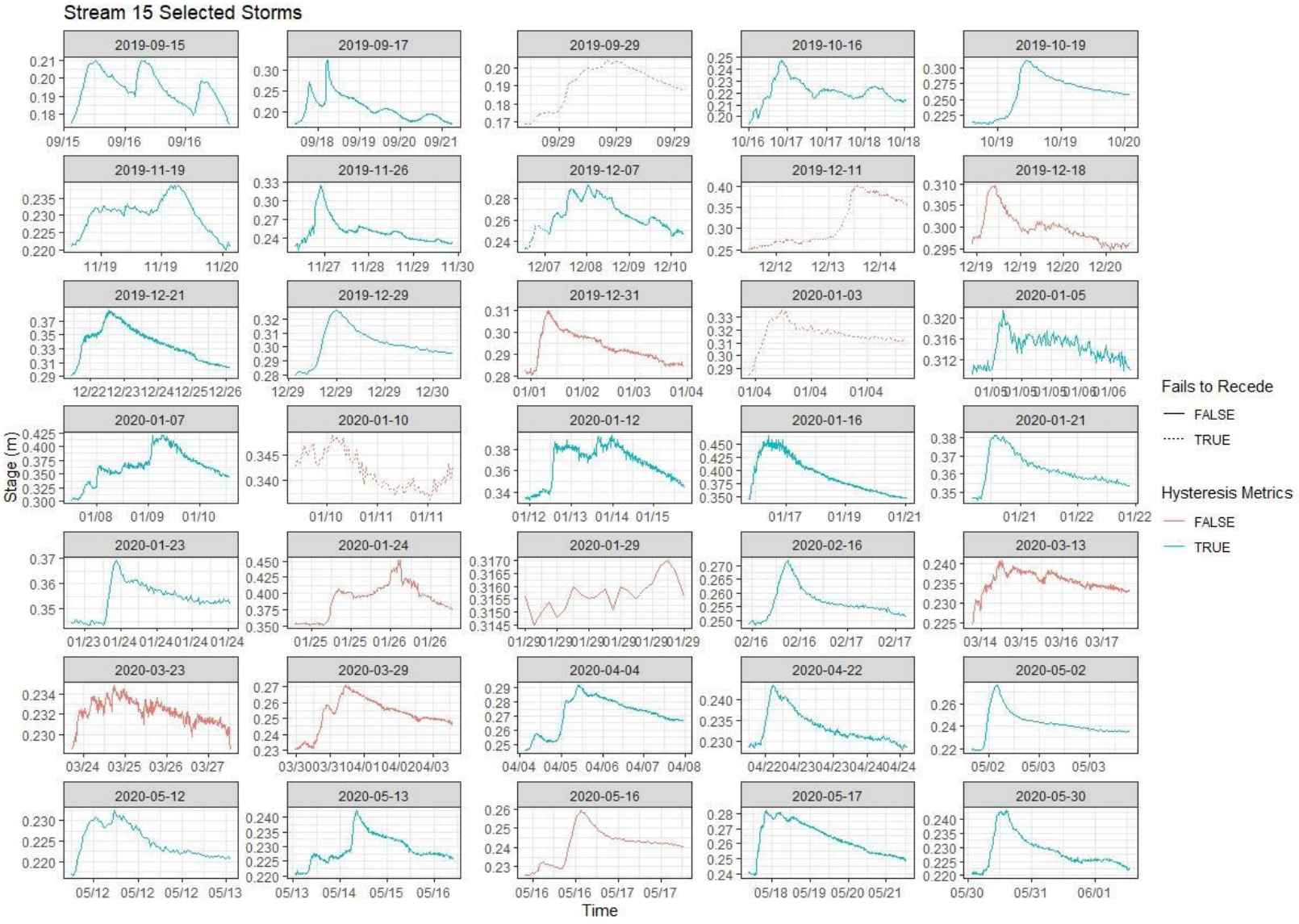

Figure A16. (Continued)

Figure A17. All storm hydrographs for stream 18, with those selected for hysteresis analysis colored as blue solid lines. Dotted lines indicate event hydrographs that failed to recede to at least half the maximum stage value achieved during the event, and were excluded from analysis. Events with hydrographs as red solid lines were excluded because these events did not included data from at least 6 of the 10 streams.

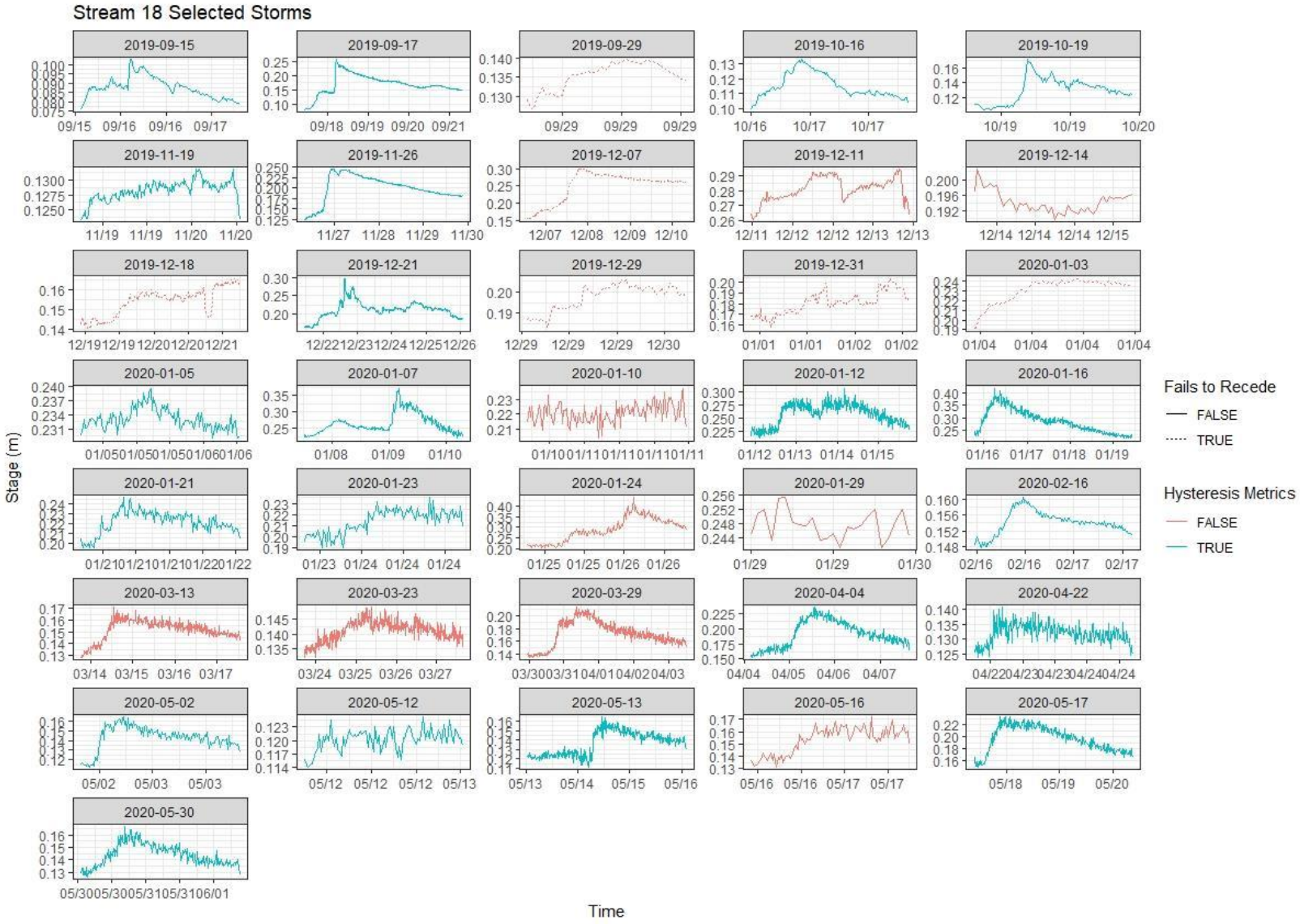

Figure A17. (Continued)

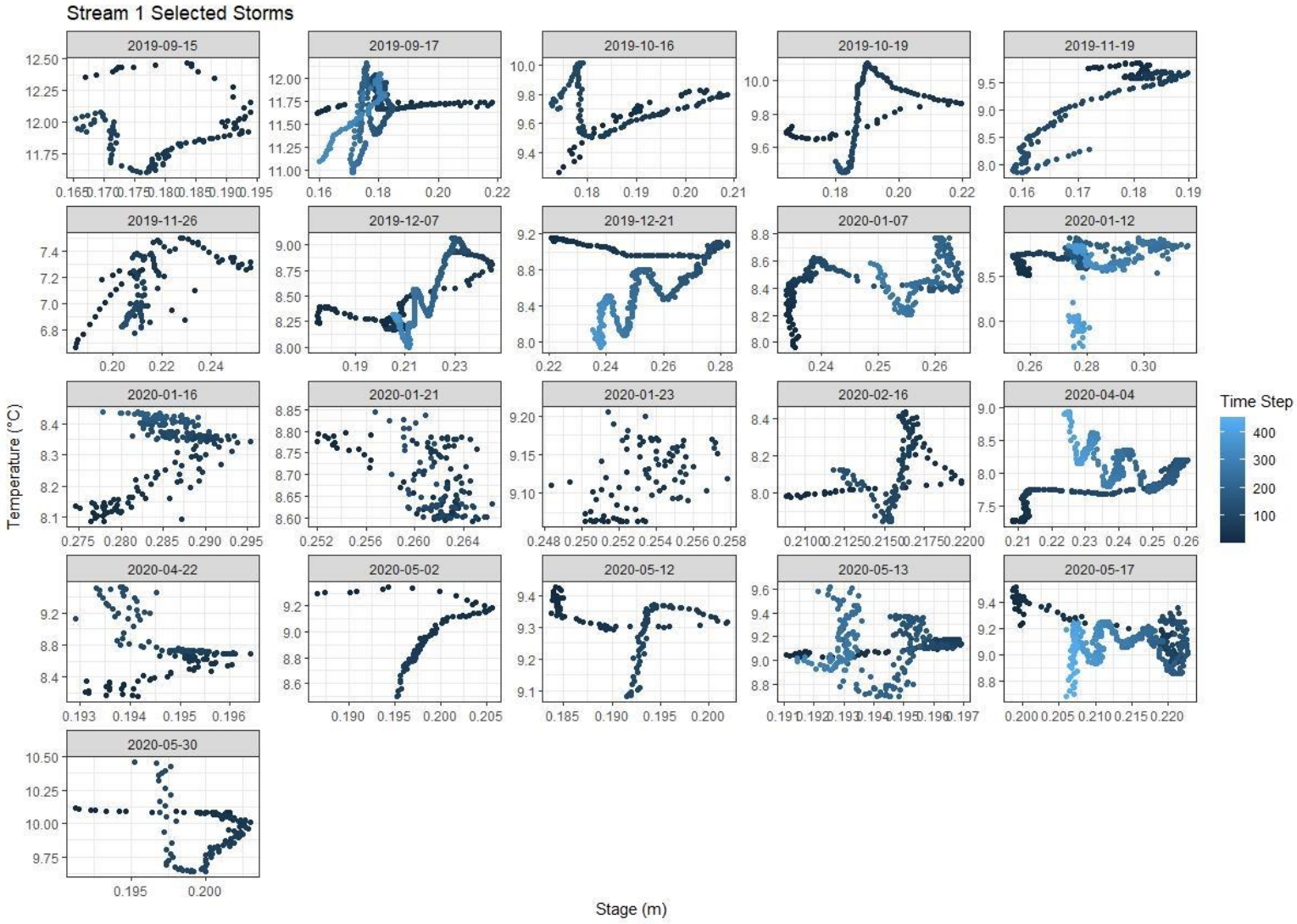

Figure A18. All stream temperature-stream stage hysteresis relationships for stream 1, with the color bar denoting the beginning (dark blue) and end (light blue) of each event.

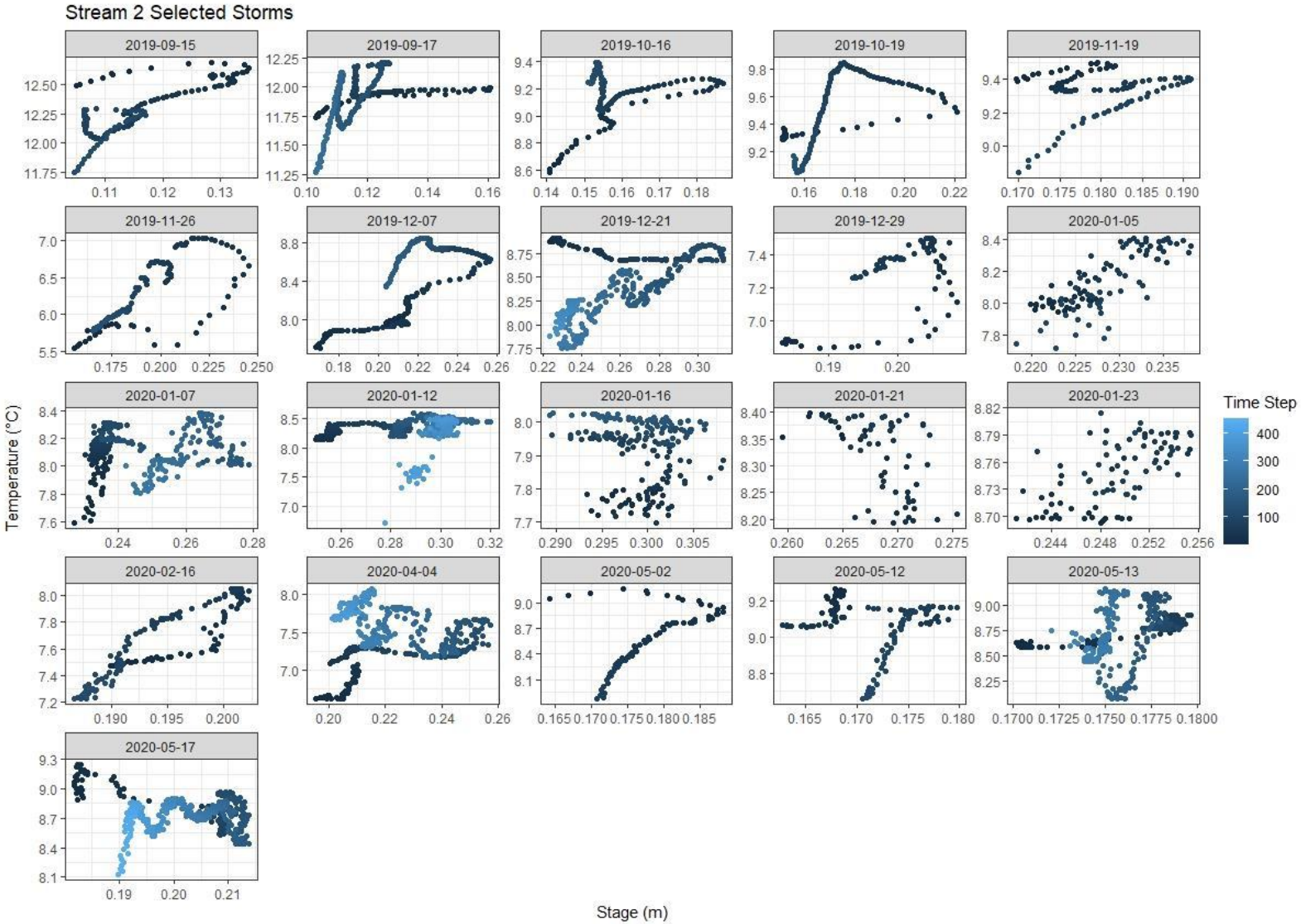

Figure A19. All stream temperature-stream stage hysteresis relationships for stream 2, with the color bar denoting the beginning (dark blue) and end (light blue) of each event.

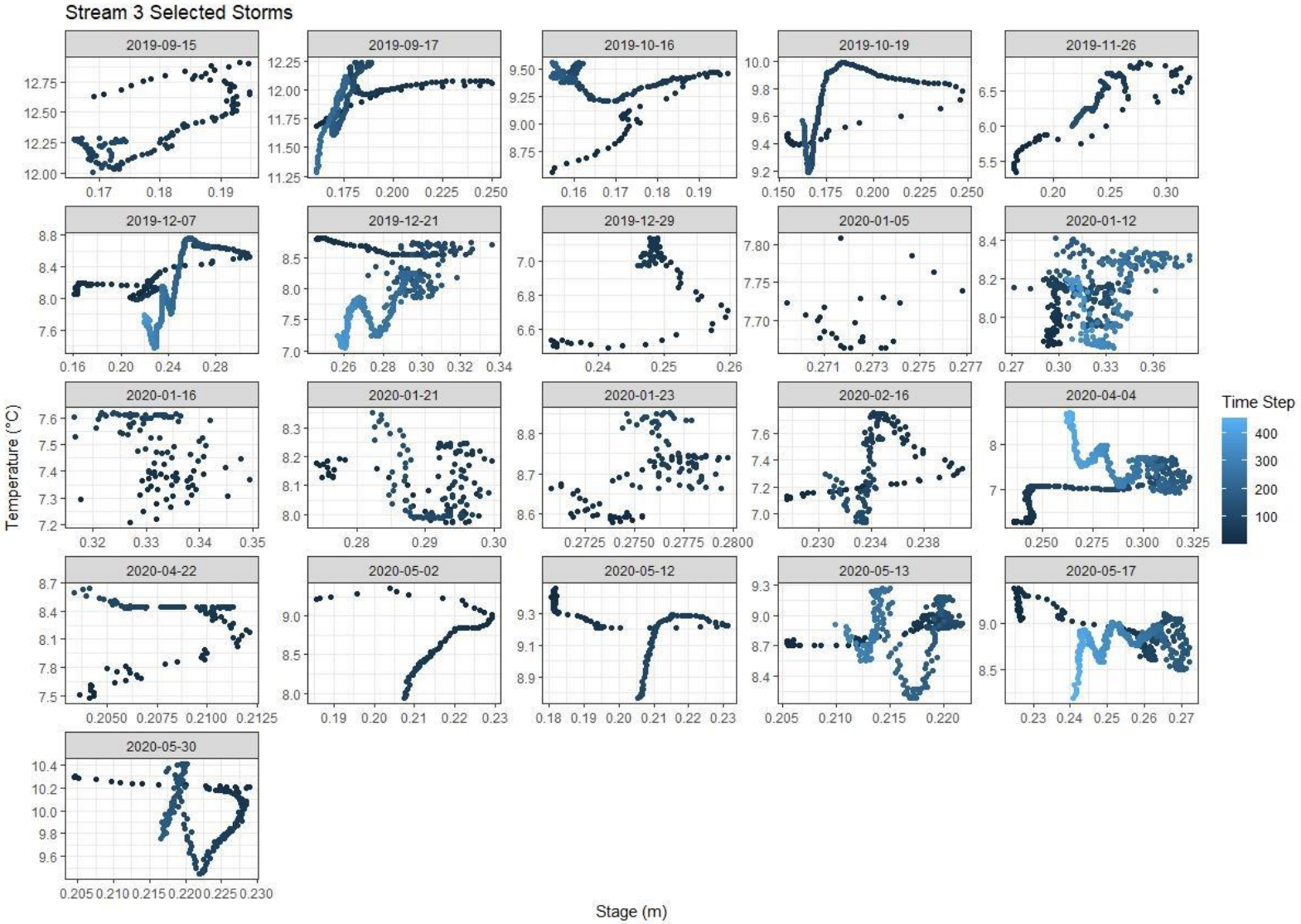

Figure A20. All stream temperature-stream stage hysteresis relationships for stream 3, with the color bar denoting the beginning (dark blue) and end (light blue) of each event.

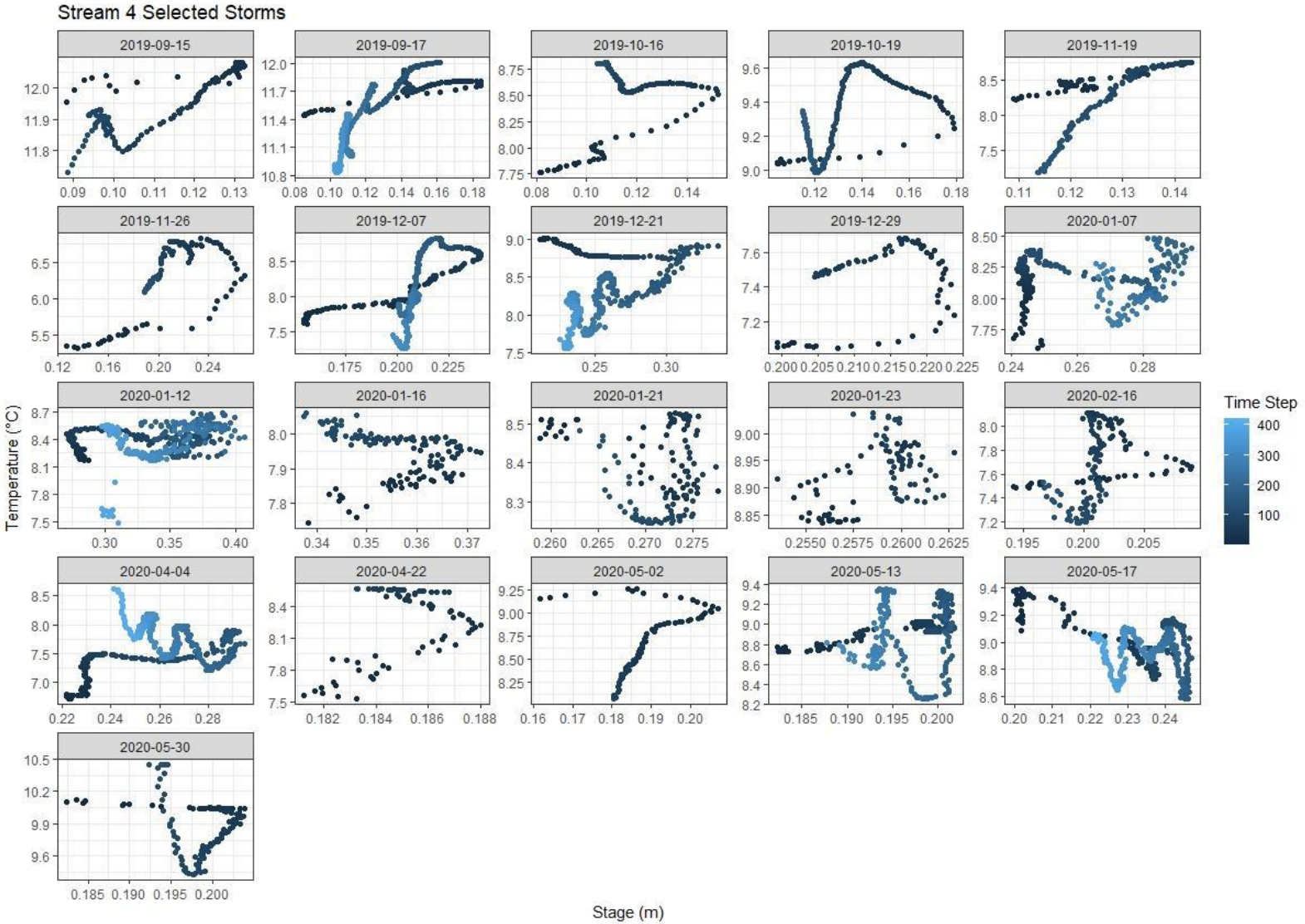

Figure A21. All stream temperature-stream stage hysteresis relationships for stream 4, with the color bar denoting the beginning (dark blue) and end (light blue) of each event.

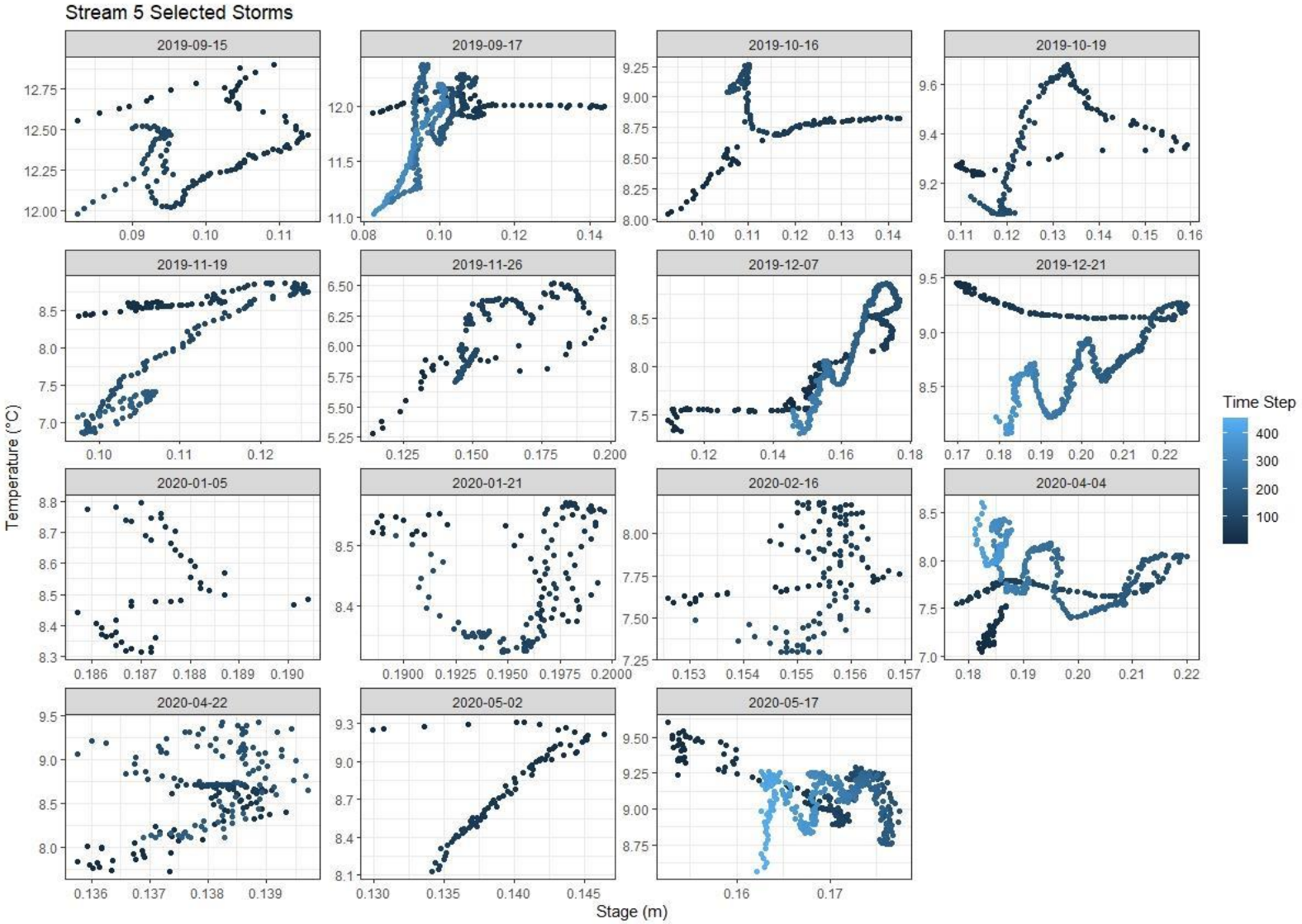

Figure A22. All stream temperature-stream stage hysteresis relationships for stream 5, with the color bar denoting the beginning (dark blue) and end (light blue) of each event.

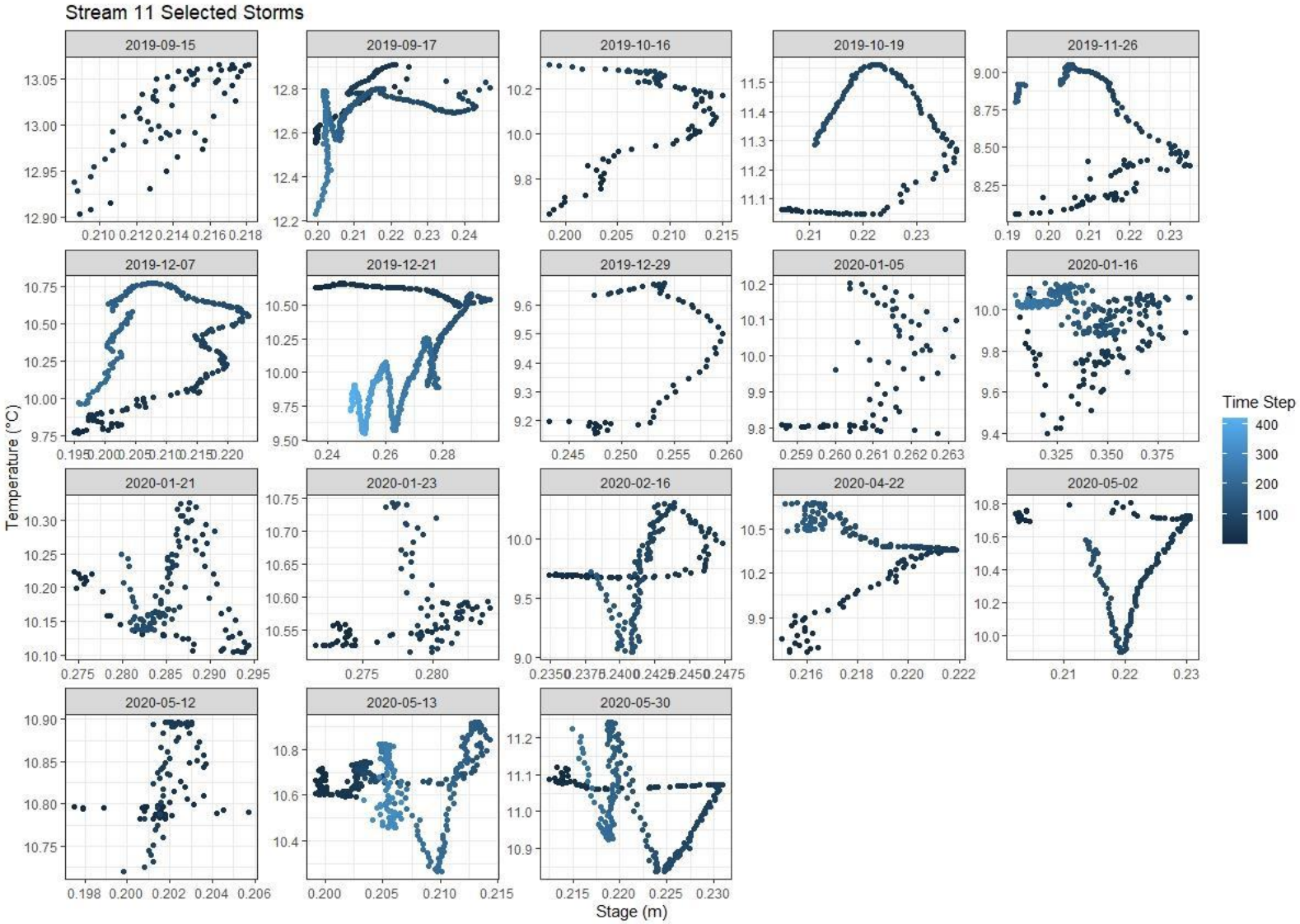

Figure A23. All stream temperature-stream stage hysteresis relationships for stream 11, with the color bar denoting the beginning (dark blue) and end (light blue) of each event.

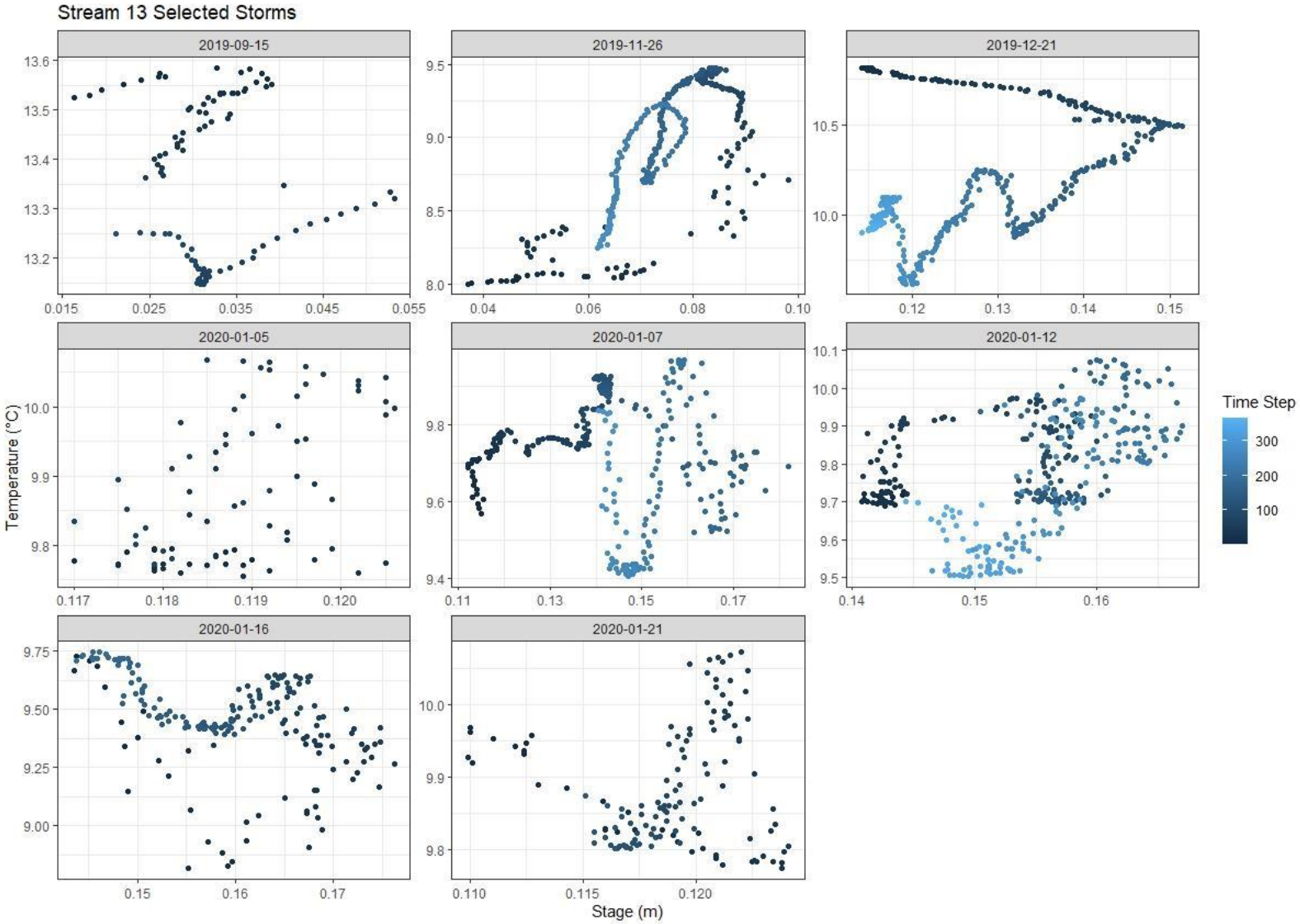

Figure A24. All stream temperature-stream stage hysteresis relationships for stream 13, with the color bar denoting the beginning (dark blue) and end (light blue) of each event.

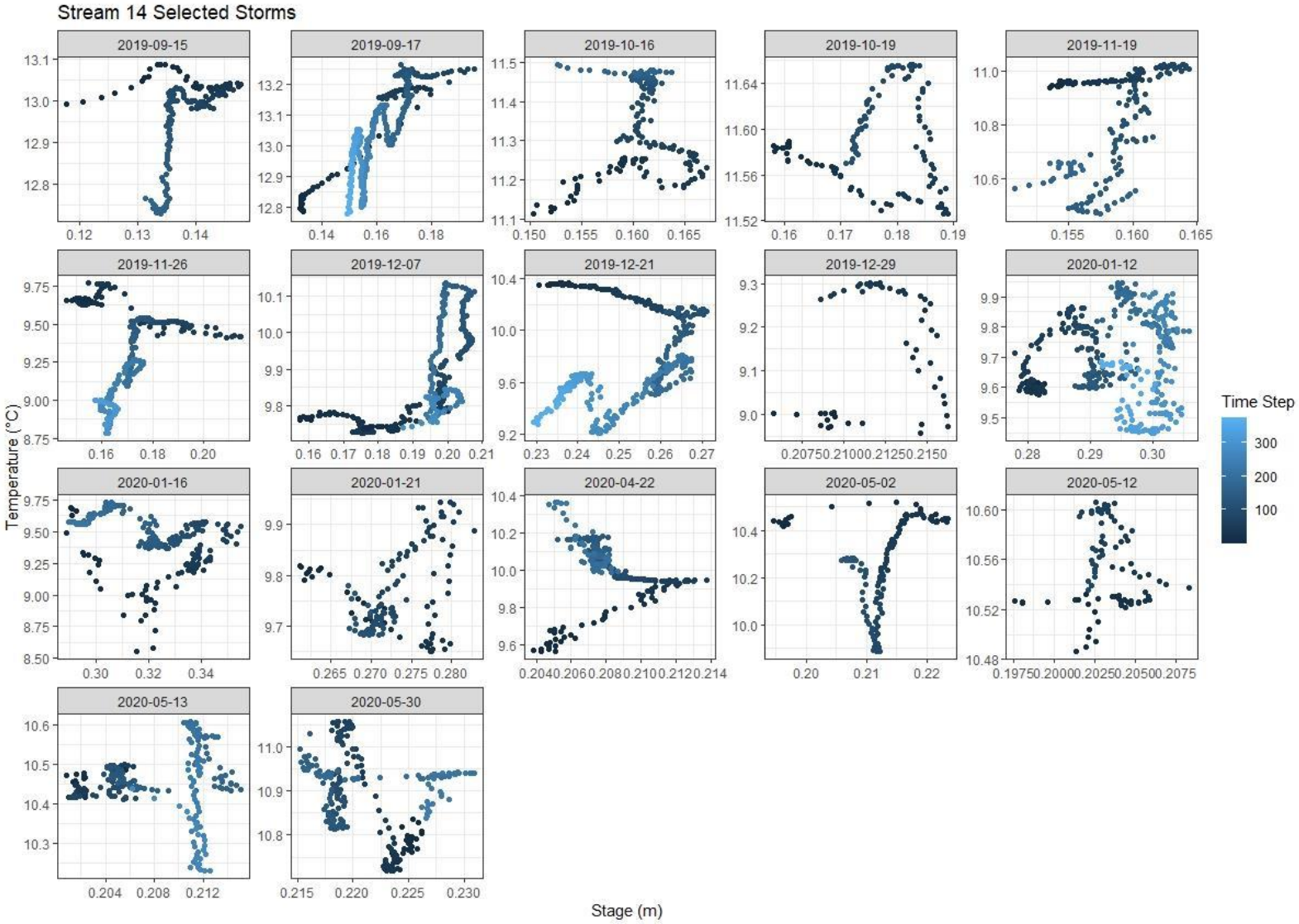

Figure A25. All stream temperature-stream stage hysteresis relationships for stream 14, with the color bar denoting the beginning (dark blue) and end (light blue) of each event.

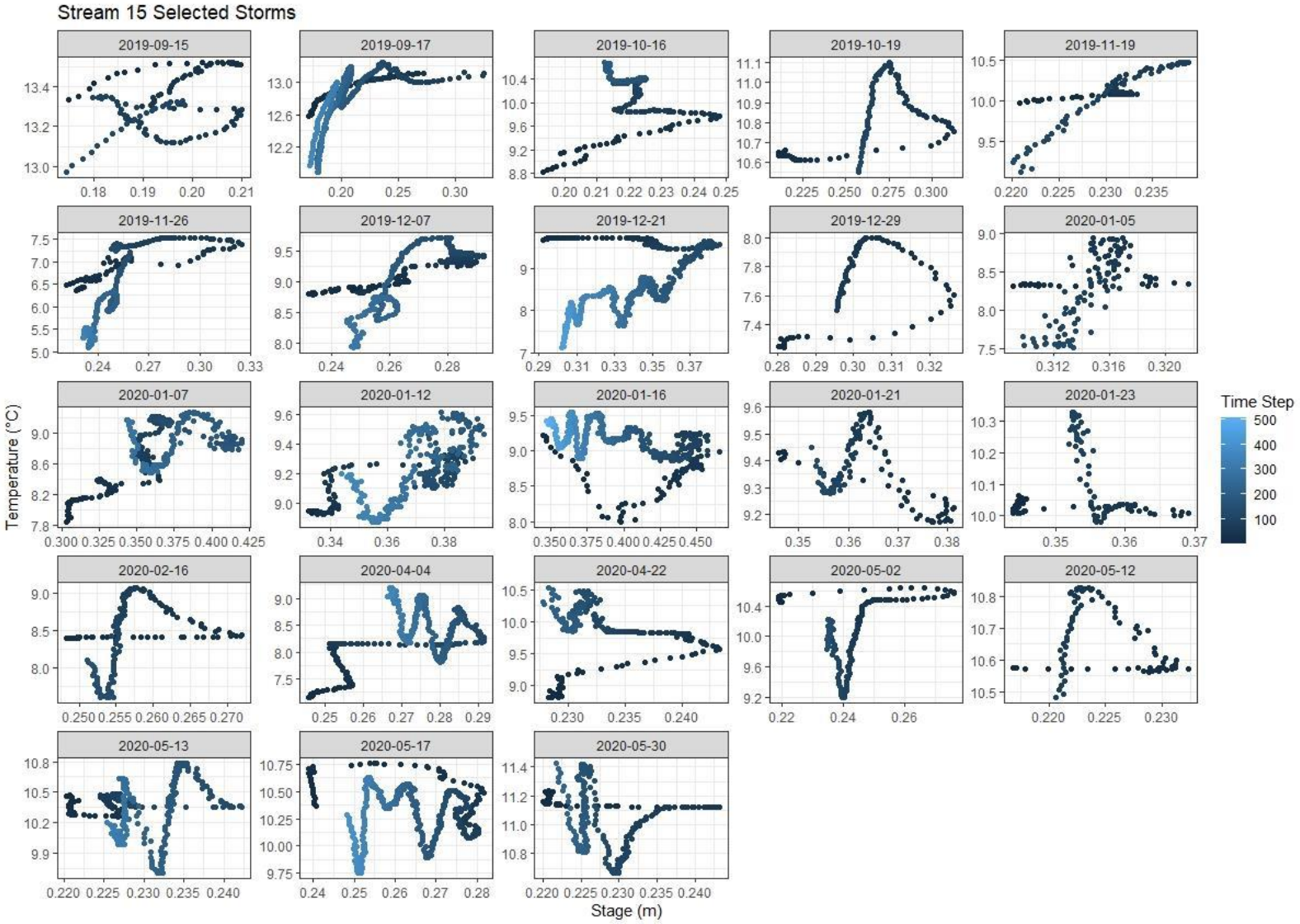

Figure A26. All stream temperature-stream stage hysteresis relationships for stream 15, with the color bar denoting the beginning (dark blue) and end (light blue) of each event.

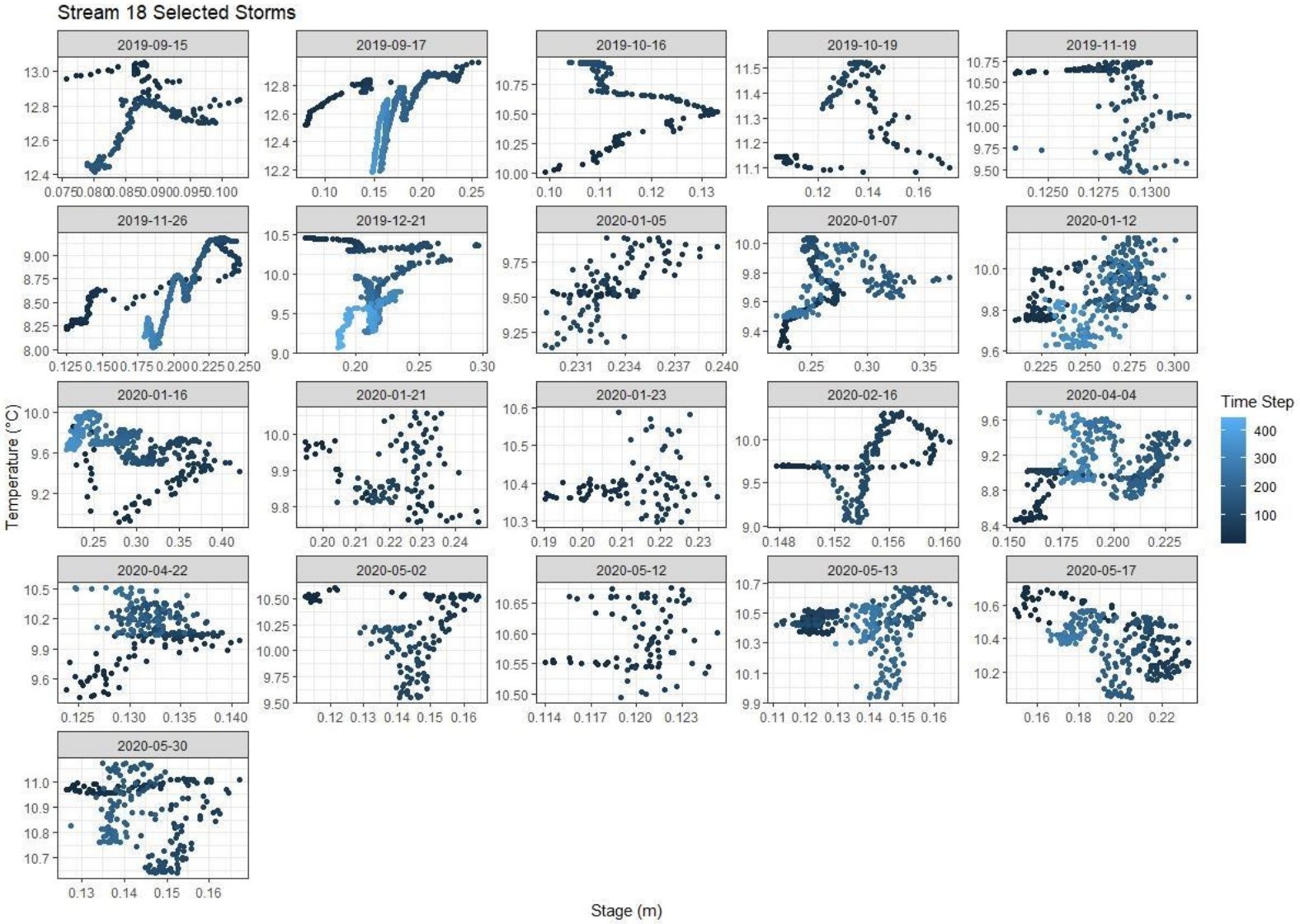

Figure A27. All stream temperature-stream stage hysteresis relationships for stream 18, with the color bar denoting the beginning (dark blue) and end (light blue) of each event.